UNIVERSITY OF CALIFORNIA, SAN DIEGO

Wave-Induced Motion of Ramp-Interconnected Craft

A Thesis submitted in partial satisfaction of the requirements
for the degree Master of Science

in

Engineering Science (Mechanical Engineering)

by

Stephen Holt Oonk

Committee in charge:

Professor Miroslav Krstic, Chair
Professor Thomas Bewley
Professor Raymond de Callafon

2008

The Thesis of Stephen Holt Oonk is approved and it is acceptable in quality form for publication on microfilm and electronically:

Chair

University of California, San Diego

2008

TABLE OF CONTENTS

LIST OF FIGURES

LIST OF TABLES

LIST OF GRAPHS

ABSTRACT OF THE THESIS

Wave-Induced Motion of Ramp-Interconnected Craft

by

Stephen Holt Oonk

Master of Science in Engineering Science (Mechanical Engineering)

University of California, San Diego, 2008

Professor Miroslav Krstic, Chair

The behavior of a system consisting of two ships connected by a ramp subject to external forcing from ocean waves is a relevant issue when considering the possible transportation of cargo. The resulting motions of the interconnected dynamical system can be extremely complex due to the nonlinear nature of the problem. As such, the development of a mathematical model is bypassed in favor of a computer-based method using MATLAB, Simulink, and

SimMechanics. In order to maintain a reasonable level of complexity, this method rests on several assumptions and simplifications such as the modeling of the ocean waves as sinusoidal surface forces. The effects of altering the ramp length and the ocean wave incidence angle on the motions of the system are explored, where special attention is given to the angles formed between the ramp and the ships, as they are quantities that need to be minimized. Surface plots are generated which highlight the dependence of these angles on the length of the ramp and wave orientation, and it is concluded that for longer ramp lengths and wavefront angles of about 62° from the ship-ramp-ship axis, the angles are reduced. A penalty function is then created based on the knowledge that increasing the ramp length results in a prohibitive weight and fails to decrease the roll component of the angles. With this penalty included, the surface plots assume a more convex shape with well-defined minima. The method of extremum seeking is then given, and its applicability to this system is discussed.

CHAPTER 1: BACKGROUND

The motion of a system consisting of two ships connected by a ramp in a bow-to-stern configuration subject to external forcing from ocean waves can be simulated using SimMechanics and Simulink provided by MATLAB. The mathematical formulation of the equations of motion of a single marine vehicle has already been thoroughly investigated in various papers and textbooks such as that by Fossen [3]. Unfortunately, the level of complexity that results from the addition of another ship connected by a ramp renders the mathematical approach undesirable as up to 24 state equations would result. Instead, the SimMechanics toolbox of Simulink can be utilized to model the system without having to deal with the mathematical calculations that would usually be required.

Figure 1.1 illustrates the bow-to-stern configuration of the two ships connected by a ramp that is implemented in the computer program.

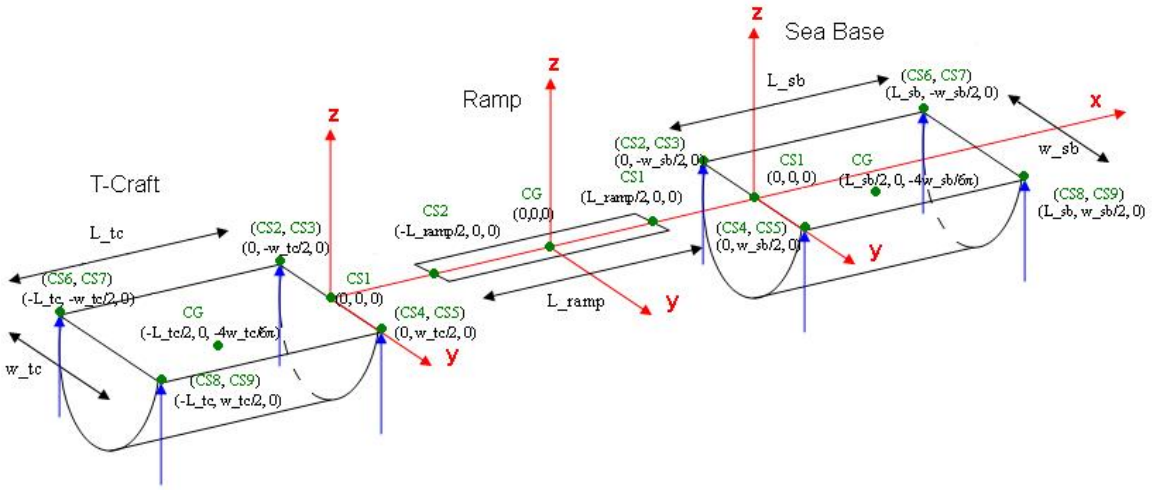

Figure 1.1: SimMechanics representation of the Sea Base connected to the T-Craft by a ramp in a bow-to-stern configuration. The local coordinate systems are represented in red, and the points to be forced by an ocean wave are represented by the blue vectors.

The larger of the two vessels will from here on be referred to as a Sea Base (an LMSR: Large, Medium-Speed Roll-On/Roll-Off Ship) whereas the smaller vessel will be referred to as a T-Craft. In SimMechanics, the points on Figure 1.1 labeled by the acronym CS (Coordinate System) are locations on the rigid bodies which may be actuated, sensed, connected to a joint, etc. For instance, the CS points labeled 1 and 2 on the ramp and the CS points labeled 1 on the ships form locations where joints are inserted. The geometries of the ships and ramp are given below in Figures 1.2 and 1.3 along with the formulas for the moments of inertias. For simplicity, the geometry of the two ships is simplified to that of half cylinders, and the ramp is modeled as a rectangular prism of very small height.

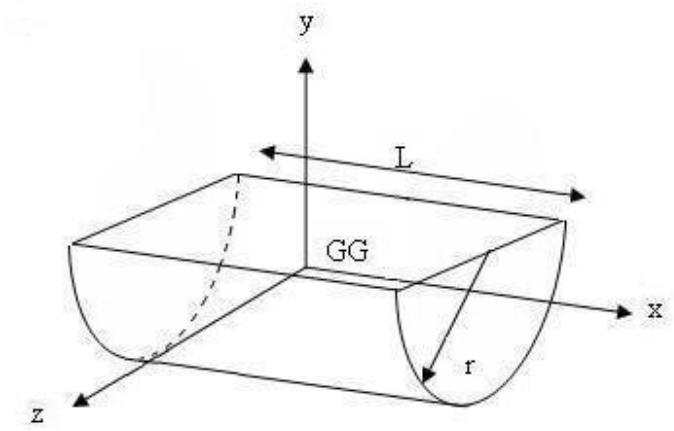

Moments of inertia through center of gravity:

$$I_{XX} = \left(\frac{1}{2} - \frac{16}{9\pi^2}\right) mr^2$$

$$I_{YY} = \frac{1}{4} mr^2 + \frac{1}{12} mL^2$$

$$I_{ZZ} = \left(\frac{1}{4} - \frac{16}{9\pi^2}\right) mr^2 + \frac{1}{12} mL^2$$

Figure 1.2: Geometry of the T-Craft and Sea Base and corresponding moments of inertia

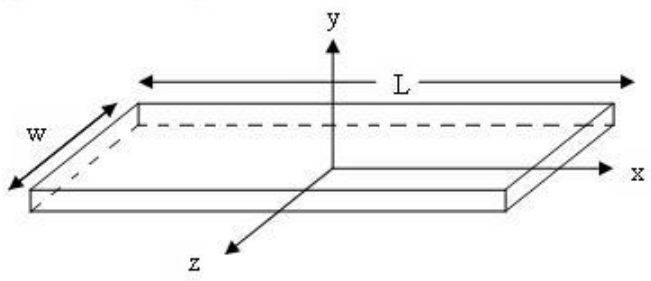

Moments of inertia through center of gravity (*negligable thickness*):

$$I_{XX} = \frac{1}{12} mw^2$$

$$I_{YY} = \frac{1}{4} m\left(w^2 + L^2\right)$$

$$I_{ZZ} = \frac{1}{12} mL^2$$

Figure 1.3: Geometry of the ramp and corresponding moments of inertia

In order to simulate the forces due to buoyancy F = ρgV and gravity F = mg that act upon the ships, each CS point on the ships is connected to a spring and damper in parallel whose constants can be wisely chosen to make the most physical sense possible. As a consequence, no hydrodynamic modeling is used in the simulations at hand. This idea that a heaving, floating body can be modeled as a second order dynamical system is proposed by Biran [2], where the equation of motion is similar to that of a simple spring, mass, and damper:

$$m\ddot{x} + b\dot{x} + kx = F_0 \cos(\omega t) \tag{1.1}$$

where x is the state variable governing the motion of the mass, ω the exciting frequency, b the damping coefficient, and k the spring constant. For a heaving body subject to ocean waves, Biran gives the following equation of motion:

$$\begin{aligned} &(m + A_{33})\ddot{x} + b\dot{x} + kx = F \\ &k = \rho g A_W \\ &F = \rho g A_W \xi_0 \cos(\omega t) \end{aligned} \tag{1.2}$$

where A_W is defined as the waterplane area (a horizontal slice through the hull at the water level) and A_{33} is an added mass term. It is obvious upon comparison of Equation (1.1) that this is exactly the same equation of motion except with $m = (m+A_{33})$, $k = \rho g A_W$, and $F_0 = \rho g A_W \xi_0$. Therefore, in the simplified model, the ships connected by a ramp can be described as a spring-mass-damper system where the springs emulate the restoring nature of gravity and buoyancy. As a consequence of using the spring-mass-damper of Equation (1.2) to represent the system, the exciting ocean waves must be modeled purely as forces.

The CS points on the ships are externally actuated by vertical (along the z axis) sinusoidal forces which are designated by the blue vectors in Figure 1.1. These points of external forcing can be collectively used to simulate an approaching wavefront at any desired orientation. The particular method that is used to accomplish this is discussed in the next chapter. Figure 1.4 shows the T-Craft, ramp, and Sea Base system with an incoming wavefront at various orientations. These cases all induce different types of motions on the system, and as such, will be thoroughly investigated throughout this report. It should be noted that it is assumed for simplicity that the waves are purely surface disturbances, and thus act along a two dimensional plane (x-y plane in Figure 1.1). The validity, as well as the feasibility of removing such assumptions will be discussed in greater detail in Chapter 3.

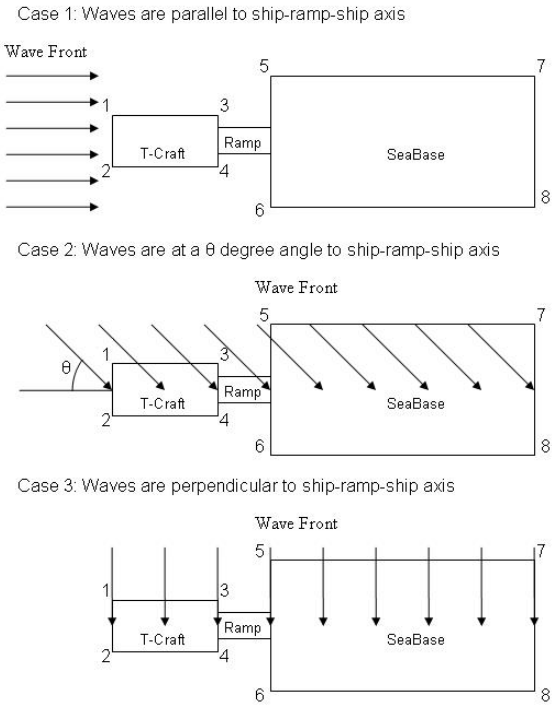

Figure 1.4: Different cases of wavefront orientations in the simulation. The points marked by numbers represent actuation points in the computer simulation.

CHAPTER 2: MODELING OF THE WAVEFRONT

2.1 Mathematical Description of the Wave Model

Generally when a ship is out at sea, there are three major types of environmental disturbances that it may encounter: waves, wind, and ocean currents. The mathematical representations of these disturbances, usually based on empirical data, are explored in the textbook by Fossen [3]. For simplicity, the ocean currents and the direct contribution of wind will be neglected here, whereas the waves (which are generated from wind) will still be considered.

Before discussing the mathematical description of the ocean waves, some terminology must first be introduced. In the analysis of signals, it is well known that signal spectra represent the different frequency contents of a signal. In order to capture this fact, a signal's power spectrum is usually defined as:

$$\Phi_s(\omega) = \sum_{\tau=-\infty}^{\infty} R_s(\tau) e^{-i\tau\omega} \tag{2.1}$$

where $R_s(\tau)$ is the covariance function of a signal s(t), and is usually given as:

$$R_s(\tau) = \lim_{N\to\infty} \frac{1}{N} \sum_{t=1}^{N} s(t)s(t-\tau) \tag{2.2}$$

An interesting application of a power spectrum as defined in Equation (2.1) is in determining how a signal's properties will change as it is filtered through a linear system. Theorem 2.2 in the textbook by Ljung [4] states that if w(t) is a quasi-stationary signal (the expectations E{w(t)} and E{w(t)w(t - τ)} are bounded) with a

spectrum $\Phi_w(\omega)$, and G(q) is a stable transfer function with s(t) being defined as:

$$s(t) = G(q)w(t) \tag{2.3}$$

Then the signal s(t) is also quasi-stationary, and the spectrum of s(t) is given by:

$$\Phi_s(\omega) = \left|G(e^{i\omega})\right|^2 \Phi_w(\omega) \tag{2.4}$$

Wind-generated waves can also be described as a signal with a certain power spectrum, or a wave spectral density function, S(ω). In [3], Fossen notes that typically the ocean wave elevation may be represented as the sum of a number of individual components:

$$\zeta(x,t) = \sum_{i=1}^{N} A_i \cos(\omega_i t - k_i x + \varphi_i) + \sum_{i=1}^{N} \frac{1}{2} k_i A_i^2 \cos 2(\omega_i t - k_i x + \varphi_i) + O(A_i^3) \tag{2.5}$$

where φ_i is a random, uniformly distributed phase angle, and k_i is the wave number. Each component contributes a certain frequency, ω_i to a small portion of the total spectral density. Therefore, when all components are considered, a wind-generated wave's signal spectrum exhibits a range of frequencies, typically with one peak frequency.

There are a multitude of empirical-based equations that represent the signal spectra of waves for a range of conditions. An in-depth analysis of the various formulations is not included here. Instead, it is sufficient to recognize that one of the simpler methods of representing the wave spectrum is to use a linear approximation of S(ω) given by the following wave model:

$$y(s) = G(s)w(s) \tag{2.6}$$

where y(s) is the output from the wave and w(s) is a zero-mean Gaussian white

noise process with a spectrum $\Phi_w(\omega) = 1$. Due to the similarity of this equation with Equation (2.3), Theorem 2.2 by Ljung can now invoked to yield a similar expression as that in Equation (2.4):

$$\Phi_y(\omega) = \left|G(j\omega)\right|^2 \Phi_w(\omega) = \left|G(j\omega)\right|^2 \tag{2.7}$$

The work of Saelid, Jenssen, and Balchen, as discussed in [3], yielded a wave model that uses the following second order transfer function to represent G(s):

$$G(s) = \frac{K_w s}{s^2 + 2\zeta\omega_0 s + \omega_0^2} \tag{2.8}$$

where σ_w is a constant for the wave intensity, ζ is a damping coefficient, and ω_0 is the primary frequency. The gain K_w is often defined as $K_w = 2\zeta\omega_0\sigma_w$, and thus:

$$G(s) = \frac{2\zeta\omega_0\sigma_\omega s}{s^2 + 2\zeta\omega_0 s + \omega_0^2} \tag{2.9}$$

This transfer function is a rough approximation of the empirical-based Pierson-Moskowitz (PM) spectrum which is based on a fully developed sea. Substituting Equation (2.9) into Equation (2.6) yields the second order approximation of the wind-generated wave signal:

$$y(s) = \frac{2\zeta\omega_0\sigma_\omega s}{s^2 + 2\zeta\omega_0 s + \omega_0^2} w(s) \tag{2.10}$$

For this simple system, the plant G(s) essentially acts as a second-order filter of white noise, and the wave is considered to be the output. Using Equation (2.7), and still assuming that $\Phi_w(\omega) = 1$, the signal spectrum of the wave is given as:

$$\Phi_y(\omega) = \left|\frac{2(\zeta\omega_0\sigma_\omega)j\omega}{(\omega_0^2 - \omega^2) + 2\zeta\omega_0 j\omega}\right|^2 = \frac{4(\zeta\omega_0\sigma_\omega)^2\omega^2}{(\omega_0^2 - \omega^2)^2 + 4(\zeta\omega_0\omega)^2} \tag{2.11}$$

Equations (2.10) and (2.11) completely describe this commonly used approximation of a wind-generated wave along with its frequency contents. One interesting aspect of this wave model is that it very nearly resembles a sine wave, but with additional noise superimposed. Graph 2.1 compares the second order transfer function approximation directly with a sine wave. The dominating frequency, ω_0 is equal for both cases. Except for a few locations, the second order approximation overlaps with the sinusoidal approximation quite well (minus the high frequency contents, small phase shifts, and some amplitude variations).

Graph 2.1: Different ways of describing a wind-generated ocean wave

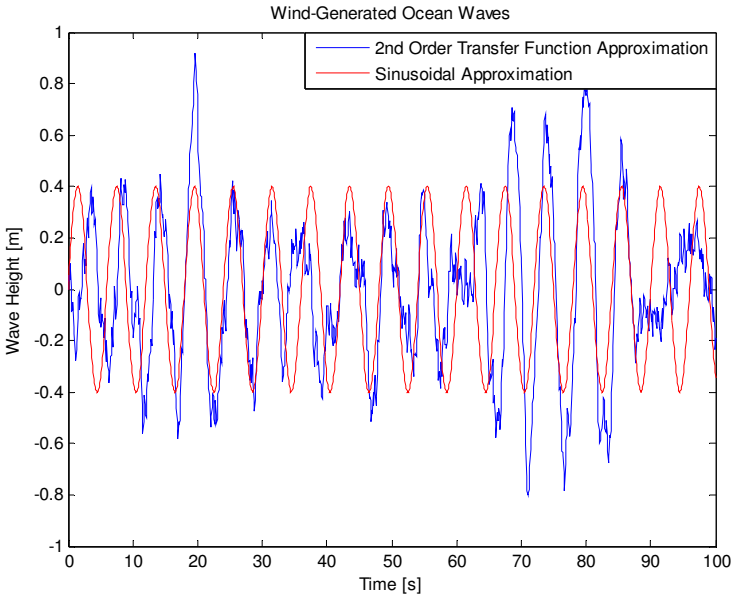

Keeping in mind the conclusions formed about Graph 2.1, in this report yet another wave model approximation is introduced. Here it is proposed that the general sinusoidal nature and additional high frequency contents in the second order transfer function approximation can be modeled as a sine wave with additive noise. As such, the wave model will take an even more simple form:

$$y(t) = A\sin(\omega_0 t + \varphi) + w(t) \tag{2.12}$$

where ω_0 is the wave frequency, w(t) is a zero-mean Gaussian white noise process, φ represents a possible phase shift, and A is an amplitude. Note that setting $A = \rho g A_W \xi_0$, $\varphi = \pi/2$, and considering the wave output y(t) as a force yields the same expression for the wave force given in Equation (1.2) except for the addition of a noise process. Graph 2.2 shows the standard second order transfer function approximation and the wave model provided by Equation (2.12). It is apparent that describing the wave as a sinusoid with additive noise is similar to the transfer function approximation of Equation (2.10). The high frequency components are emulated quite well; however, the lower frequency components (observed in the oscillations between 90 to 100 seconds) are missed entirely.

Graph 2.2: Describing an ocean wave as a sinusoid with additive noise

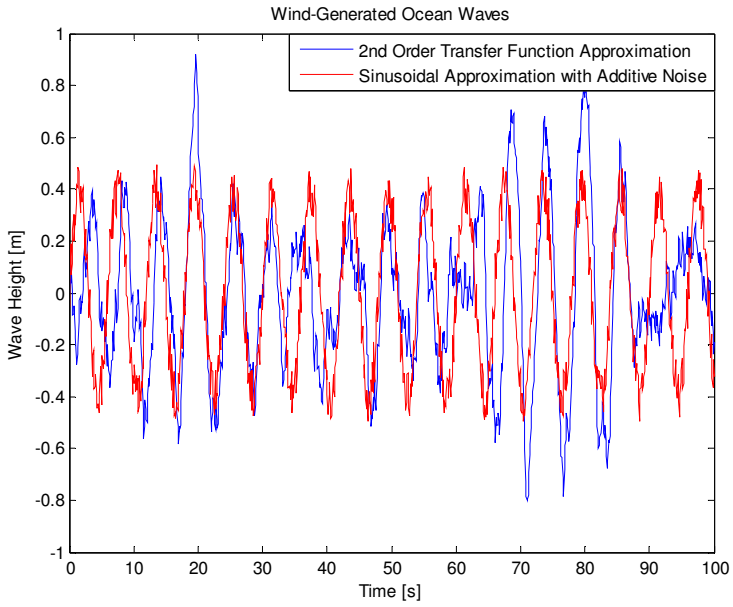

For the sake of simplicity, the wave model described by Equation (2.12) will be used instead of the traditional approach offered by Equation (2.10). This will facilitate the implementation of the wavefront based on phase shifts described in the next section, as a phase shift is already provided in Equation (2.12).

2.2 Representation of Approaching Wavefront

An approaching wavefront on the x-y plane that is about to collide with the Sea Base and T-Craft can be approximated by vertically (z axis) actuating the ships with the wave force at points designated by the numbers 1-8 in Figure 2.1.

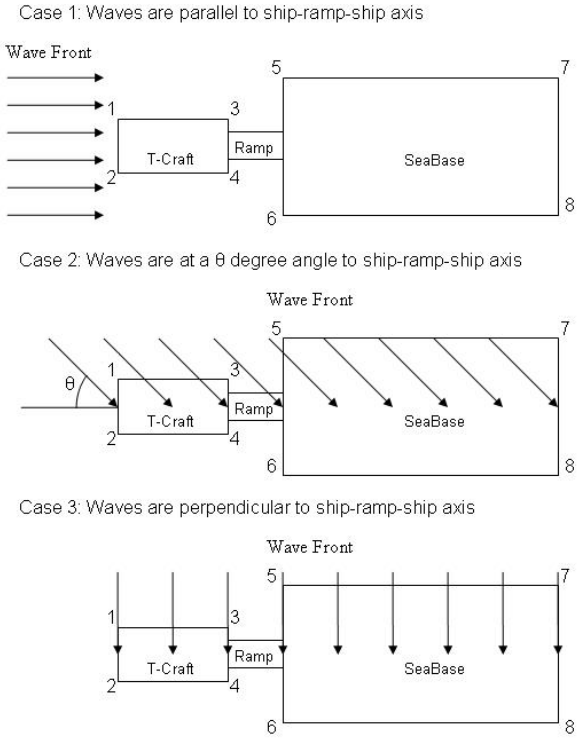

Figure 2.1: Figure 1.4 shown again for ease of analysis

The motivation behind this method of implementing the ocean wave is based on simple intuition. Consider a line of particles that is always parallel to the wavefront such that as the wave progresses, the line of particles moves along with the wave. Due to the geometry of the system as well as the orientation of the wavefront, these particles will collide with the ships at different times. For example, if the waves are aligned parallel to the ship-ramp-ship axis, the particles would first reach points 1 and 2, then points 3 and 4, and so on.

In this case, one could choose a phase shift of zero for the points 1 and 2, meaning that the ocean wave (a sine wave with superimposed noise) will immediately act upon those points. However, the particles will hit points 3 and 4 at a later time, which by Figure 2.1, will be dependent on the length of the T-Craft. This means that in order to simulate the same line of particles hitting the points at a different time, the sine wave component of the ocean wave at those points should have a phase shift. This phase shift is proportional to the distance the wave particles have to travel, multiplied by $2\pi/\lambda$, where lambda stands for the wavelength of the ocean wave and is used as a normalizing factor. The choice of the constant 2π is motivated by the fact that if the distance needed to travel divided by the wavelength is an integer, there is a 360 degree phase shift (meaning no phase shift at all). This makes physical sense since given a steady bombardment of waves that are parallel to a ship's axis, if the distance is divisible by the wavelength, (for example, if the ship's length is equal to the wavelength) the ship should move up and down in the waves without any tilting.

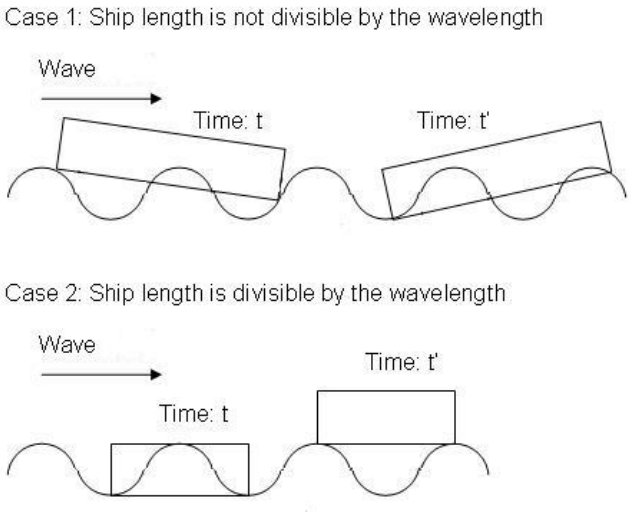

Figure 2.2: Graphical illustration of a continuous wavefront

By using the formula $Phase = \frac{Length}{\lambda} 2\pi$ where length stands for the distance that a particle on a line parallel to the wavefront has to travel, and λ is the wavelength, the appropriate phases for the sine wave components of the ocean waves can be found. Due to the symmetry about the x axis of the system, the angle θ in Figure 2.1 will only be considered in this report as it varies from 0° to 180°. The derivations in this chapter will only cover the angles of θ from 0° (Case 1) to 90° (Case 3). The phase shifts for angles from 90° to 180° are provided in the appendix. It should be noted that this type of mathematical construction only holds in the case that the ship displacements (in all 6 degrees of freedom: heave, sway, surge, roll, pitch, and yaw) due to the waves are relatively small. Large displacements of the ships will cause the lengths in the phase formulas to be different than those that will now be derived.

Case 1: Waves are parallel to ship-ramp-ship axis (θ = 0°):

Case 1 is particularly trivial in the phase shifts for the sine waves are directly proportional to the T-Craft, Sea Base, and ramp lengths. These phase shifts correspond to the first scenario in Figure 2.1 and are given as follows:

Points 1 and 2 Phase Shift: 0

Points 3 and 4 Phase Shift: $\frac{L_{tc}}{\lambda} 2\pi$

Points 5 and 6 Phase Shift: $\frac{L_{tc} + L_{ramp}}{\lambda} 2\pi$

Points 7 and 8 Phase Shift: $\frac{L_{tc} + L_{ramp} + L_{sb}}{\lambda} 2\pi$

Case 3: Waves are perpendicular to ship-ramp-ship axis (θ = 90°):

The possibility that the waves are aligned perpendicular to the ship-ramp-ship axis is explored in Case 3. This situation is only slightly more complicated than Case 1 in that an intermediate distance, $\frac{w_{sb}}{2} - \frac{w_{tc}}{2}$ is necessary since the T-Craft and Sea Base generally have different widths (i.e. $w_{sb} \neq w_{tc}$). The phase shifts are motivated by the third scenario in Figure 2.1 and are given below:

Points 5 and 7 Phase Shift: 0

Points 6 and 8 Phase Shift: $\frac{w_{sb}}{\lambda} 2\pi$

Points 1 and 3 Phase Shift: $\frac{\frac{w_{sb}}{2} - \frac{w_{tc}}{2}}{\lambda} 2\pi$

Points 2 and 4 Phase Shift: $\frac{\left(\frac{w_{sb}}{2} - \frac{w_{tc}}{2}\right) + w_{tc}}{\lambda} 2\pi$

Case 2: Waves are at a θ degree angle to ship-ramp-ship axis:

The formulation of the phase shifts for this possibility is far more complicated in that considerable trigonometry must be used. Consider first the simplification in that the ships have no width (or equal widths) as in Figure 2.3. The incoming waves meet the ship-ramp-ship axis designated by points 1-4 at an angle θ. The angle between the wavefront and the ship-ramp-ship axis is given as φ and can be defined in terms of θ. The length of the arrow vectors in Figure 2.3 determine the phase shifts. Given a line of particles parallel to the wavefront (as previously mentioned), and following the line as the waves approach the

ships, points on the line will reach different locations at different times due to the angle θ. The lengths of the arrow vectors basically determine how long it will take for that line to reach certain locations.

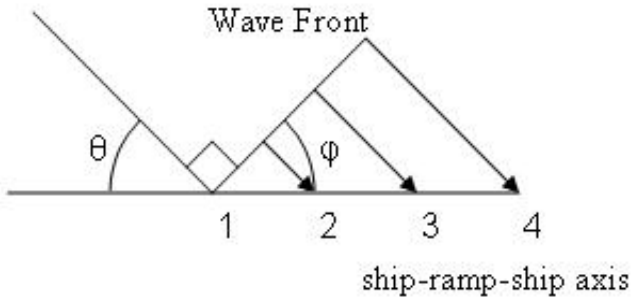

Figure 2.3: Wavefront approaching ship-ramp-ship axis for the simplified case of the ships and ramps having an no width (or equal widths)

Realizing that the distance from 1 to 2 is the length of the T-Craft, 2 to 3 is that of the ramp, and 3 to 4 is that of the Sea Base, the magnitudes of the arrow vectors can be represented in terms of sinφ and the known lengths of the ships and ramp. Using the general formula of $Phase = \frac{Length}{\lambda} 2\pi$ results in the following phase shifts (where it should be noted that in the event that φ is equal to π/2, or equivalently θ = 0, we arrive at the formulas given in Case 1):

Point 1 Phase Shift: 0

Point 2 Phase Shift: $\frac{L_{tc} \sin\varphi}{\lambda} 2\pi$

Point 3 Phase Shift: $\frac{\left(L_{tc} + L_{ramp}\right)\sin\varphi}{\lambda} 2\pi$

Point 4 Phase Shift: $\frac{\left(L_{tc} + L_{ramp} + L_{sb}\right)\sin\varphi}{\lambda} 2\pi$

In the actual simulation, the widths of the ships must be taken into account such that when φ is equal to 90 degrees (θ = 0°) we arrive at the formulas given in Case 1, and when φ is 0 degrees (θ = 90°), the expressions for Case 3 are produced. Figure 2.4 provided below takes variable widths into consideration, and shows the arrow vectors that determine when a point on the wavefront line will meet a certain location on the ships.

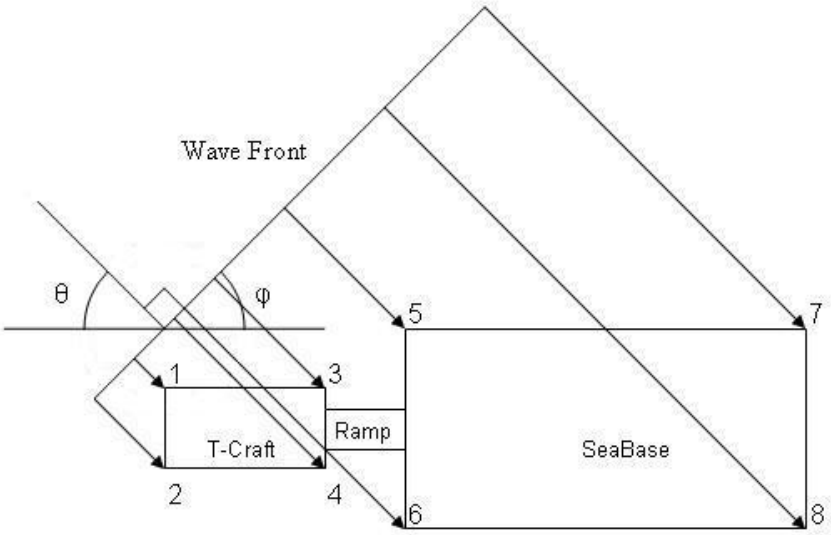

Figure 2.4: Wavefront approaching ship-ramp-ship axis at an angle

The phase shifts are once again formed by using the formula $Phase = \frac{Length}{\lambda} 2\pi$, where the length stands for the magnitude of the arrow vectors given in Figure 2.4. The auxiliary angle φ is used for ease of derivation and is defined as:

$$\varphi = \pi - \left(\theta + \frac{\pi}{2} \right) \tag{2.13}$$

Simplifying this expression yields a compact representation of θ in terms of φ:

$$\theta = \frac{\pi}{2} - \varphi \tag{2.14}$$

By considering the geometry of the system in Figure 2.4 and the relationship given by Equation (2.14), the following points have fairly obvious phase shifts:

Point 1 Phase Shift: $\frac{\left(\frac{w_{sb}}{2}-\frac{w_{tc}}{2}\right)\sin\left(\frac{\pi}{2}-\varphi\right)}{\lambda}2\pi$

Point 2 Phase Shift: $\frac{\left(w_{tc}+\frac{w_{sb}}{2}-\frac{w_{tc}}{2}\right)\sin\left(\frac{\pi}{2}-\varphi\right)}{\lambda}2\pi$

Point 5 Phase Shift: $\frac{\left(L_{tc}+L_{ramp}\right)\sin\varphi}{\lambda}2\pi$

Point 7 Phase Shift: $\frac{\left(L_{tc}+L_{ramp}+L_{sb}\right)\sin\varphi}{\lambda}2\pi$

When φ = π/2, the wavefront is parallel to the ship-ramp-ship axis, and the phase shifts for points 1, 2, 5, and 7 simplify to those given for Case 1. Furthermore, when φ = 0, the phase shifts for these points reduce to those listed for Case 3.

Now consider the more difficult problem posed by point 3. In order to find the necessary phase shift, the unknown length x in Figure 2.5 must be solved for.

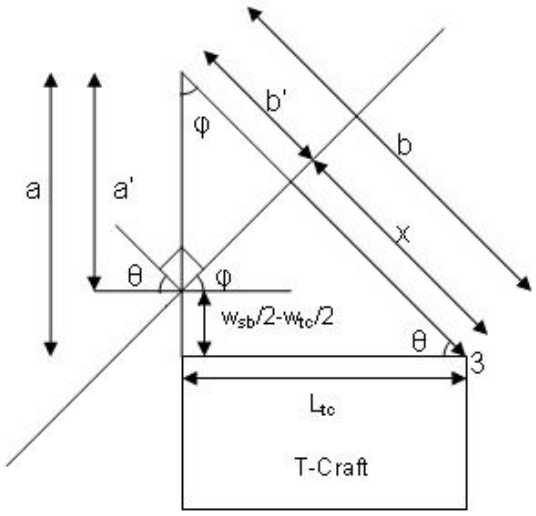

Figure 2.5: Trigonometry to find length of arrow vector to point 3

This unknown quantity represents the length of the arrow vector in Figure 2.4 that connects the wavefront with point 3. The solution of x can be used to build the appropriate phase shift formula. In order to solve for x, various intermediate variables must first be found. The length of b expressed in terms of L_{tc} is:

$$b = \frac{L_{tc}}{\cos\theta} \tag{2.15}$$

Likewise, the lengths of a and a' can quickly be determined to be equal to:

$$a = L_{tc}\tan\theta \qquad a' = L_{tc}\tan\theta - \left(\frac{w_{sb}}{2} - \frac{w_{tc}}{2}\right) \tag{2.16}$$

Noting that the length of b' can be expressed in terms of a' in Equation (2.16):

$$b' = a'\cos\varphi = \left[L_{tc}\tan\theta - \left(\frac{w_{sb}}{2} - \frac{w_{tc}}{2}\right)\right]\cos\varphi \tag{2.17}$$

It is clear from Figure 2.5 that x = b - b', therefore, simply subtracting Equation (2.17) from Equation (2.15) yields the formula for x in terms of known quantities:

$$x = \frac{L_{tc}}{\cos\left(\frac{\pi}{2} - \varphi\right)} - \left[L_{tc}\frac{\cos\varphi}{\sin\varphi} - \left(\frac{w_{sb}}{2} - \frac{w_{tc}}{2}\right)\right]\cos\varphi \tag{2.18}$$

The final expression for the phase shift for point 3 is given as:

Point 3 Phase Shift for $\varphi \in \left(0, \frac{\pi}{2}\right]$:

$$\frac{\dfrac{L_{tc}}{\cos\left(\frac{\pi}{2} - \varphi\right)} - \left[L_{tc}\dfrac{\cos\varphi}{\sin\varphi} - \left(\dfrac{w_{sb}}{2} - \dfrac{w_{tc}}{2}\right)\right]\cos\varphi}{\lambda} 2\pi$$

Phase Shift for $\varphi = 0$: $\dfrac{\frac{w_{sb}}{2} - \frac{w_{tc}}{2}}{\lambda} 2\pi$

When φ = 90 degrees the above expression reduces to the formula in Case 1 for point 3. Unfortunately, as φ approaches 0 degrees we arrive at a technicality due to division by 0. As the angle φ approaches 0, it is apparent from Figure 2.5 that the length b' becomes extremely large (in order to complete the upper triangle with the hypotenuse a'). This means that b also becomes extremely large. However, x remains finite sized because we are subtracting two very large quantities (b - b') to arrive at a smaller quantity. In the limit that φ approaches 0 degrees we cannot use the formula for x to arrive at the appropriate phase shift. This is because b = ∞ and b' = ∞ and x = b - b' = ∞ - ∞ is not well defined. However, we know from physical intuition that the length of the arrow vector in this case will still be finite sized. Thus, a separate formula for the phase shift is given in the case when φ = 0°. These formulas are identical to those found in Case 3, but they are also derived in the next section using L'Hôptial's rule.

Now consider a similar problem posed by point 4. In order to find the phase shift, the unknown length x must once again be solved using Figure 2.6.

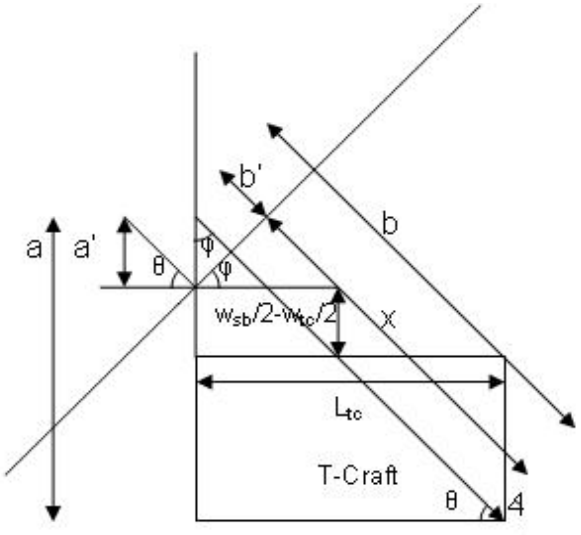

Figure 2.6: Trigonometry to find length of arrow vector to point 4

In order to express the magnitude of x in terms of known quantities, a, a', b, and b' must all be solved for first. As before, b is related to L_{tc} by a cosine term in:

$$b = \frac{L_{tc}}{\cos\theta} \tag{2.19}$$

The expression for the variable a remains the same; however, an additional w_{tc} term is added to a' as follows:

$$a = L_{tc}\tan\theta \qquad a' = L_{tc}\tan\theta - \left(\frac{w_{sb}}{2} - \frac{w_{tc}}{2} + w_{tc}\right) \tag{2.20}$$

Once again, substitution of Equation (2.20) into the expression for b' yields:

$$b' = a'\cos\varphi = \left[L_{tc}\tan\theta - \left(\frac{w_{sb}}{2} - \frac{w_{tc}}{2} + w_{tc}\right)\right]\cos\varphi \tag{2.21}$$

Subtracting Equation (2.21) from Equation (2.19) finally yields the unknown x:

$$x = \frac{L_{tc}}{\cos\left(\frac{\pi}{2} - \varphi\right)} - \left[L_{tc}\frac{\cos\varphi}{\sin\varphi} - \left(\frac{w_{sb}}{2} - \frac{w_{tc}}{2} + w_{tc}\right)\right]\cos\varphi \tag{2.22}$$

The necessary phase shift for point 4 is obtained by inserting the expression for x in Equation (2.22) into the standard phase formula $Phase = \frac{Length}{\lambda}2\pi$:

Point 4 Phase Shift for $\varphi \in \left(0, \frac{\pi}{2}\right]$:

$$\frac{\frac{L_{tc}}{\cos\left(\frac{\pi}{2} - \varphi\right)} - \left[L_{tc}\frac{\cos\varphi}{\sin\varphi} - \left(\frac{w_{sb}}{2} - \frac{w_{tc}}{2} + w_{tc}\right)\right]\cos\varphi}{\lambda}2\pi$$

Phase Shift for $\varphi = 0$: $\frac{\frac{w_{sb}}{2} - \frac{w_{tc}}{2} + w_{tc}}{\lambda}2\pi$

Just as with the case for point 3, the second condition for when φ = 0 is necessary in order to avoid division by zero. Also, when φ = 90 degrees, it is apparent that we arrive at the formula for point 4 given in Case 1.

Continuing onto the remaining points of the Sea Base, the phase shift required for point 6 can be found by solving for the length x in Figure 2.7:

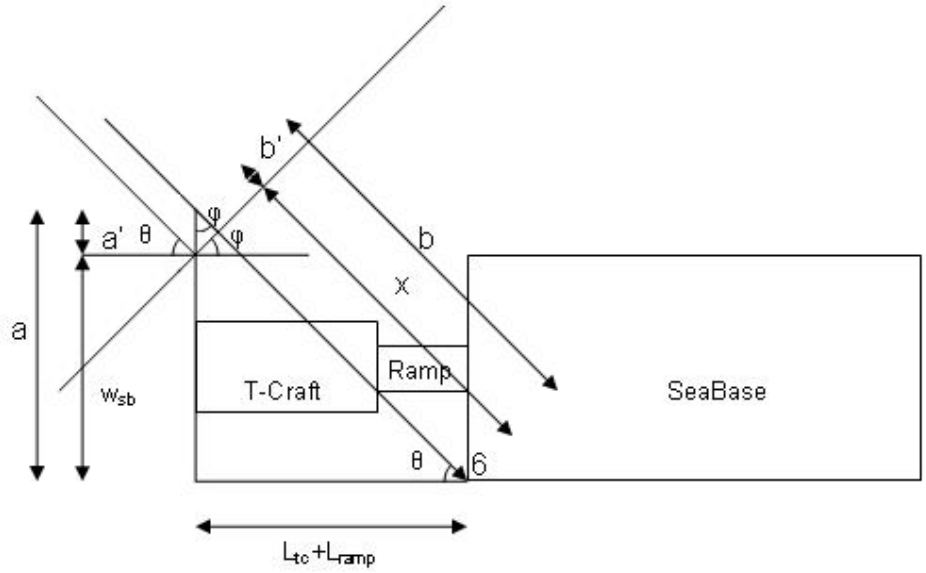

Figure 2.7: Trigonometry to find length of arrow vector to point 6

The expression for b is now slightly different in that it includes the ramp length:

$$b = \frac{L_{tc} + L_{ramp}}{\cos\theta} \tag{2.23}$$

The variables a and a' now incorporate an additional term in L_{ramp}, and only w_{sb} is subtracted in a' as given below:

$$a = \left(L_{tc} + L_{ramp}\right)\tan\theta \qquad a' = \left(L_{tc} + L_{ramp}\right)\tan\theta - w_{sb} \tag{2.24}$$

As always, b' is defined as the magnitude of a' multiplied by a cosine term:

$$b' = a'\cos\varphi = \left[\left(L_{tc} + L_{ramp}\right)\tan\theta - w_{sb}\right]\cos\varphi \tag{2.25}$$

Subtraction of Equation (2.25) from Equation (2.23) then yields our solution of x:

$$x = \frac{L_{tc} + L_{ramp}}{\cos\left(\frac{\pi}{2} - \varphi\right)} - \left[\left(L_{tc} + L_{ramp}\right)\frac{\cos\varphi}{\sin\varphi} - w_{sb}\right]\cos\varphi \qquad (2.26)$$

Using Equation (2.26) in the phase formula generates the required phase shift:

Point 6 Phase Shift for $\varphi \in \left(0, \frac{\pi}{2}\right]$:

$$\frac{\dfrac{L_{tc} + L_{ramp}}{\cos\left(\frac{\pi}{2} - \varphi\right)} - \left[\left(L_{tc} + L_{ramp}\right)\dfrac{\cos\varphi}{\sin\varphi} - w_{sb}\right]\cos\varphi}{\lambda} 2\pi$$

Phase Shift for $\varphi = 0$: $\dfrac{w_{sb}}{\lambda} 2\pi$

Lastly, consider the determination of the phase shift for point 8 on the Sea Base and solve for the unknown length x with the aid of Figure 2.8:

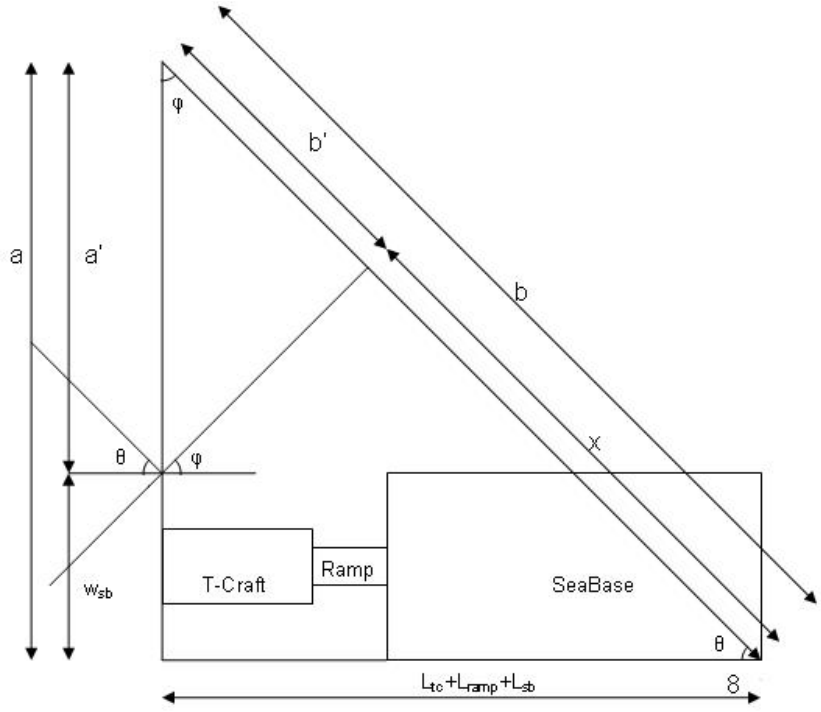

Figure 2.8: Trigonometry to find length of arrow vector to point 8

The value of b is now modified to include the lengths of both ships and the ramp:

$$b = \frac{L_{tc} + L_{ramp} + L_{sb}}{\cos\theta} \tag{2.27}$$

Likewise, the variables a and a' also contain all of the lengths at hand:

$$a = \left(L_{tc} + L_{ramp} + L_{sb}\right)\tan\theta \qquad a' = \left(L_{tc} + L_{ramp} + L_{sb}\right)\tan\theta - w_{sb} \tag{2.28}$$

The expression for b is then found using Equation (2.28):

$$b' = a'\cos\varphi = \left[\left(L_{tc} + L_{ramp} + L_{sb}\right)\tan\theta - w_{sb}\right]\cos\varphi \tag{2.29}$$

Applying the fact that x = b – b' yields the value of the unknown x:

$$x = \frac{L_{tc} + L_{ramp} + L_{sb}}{\cos\left(\frac{\pi}{2} - \varphi\right)} - \left[\left(L_{tc} + L_{ramp} + L_{sb}\right)\frac{\cos\varphi}{\sin\varphi} - w_{sb}\right]\cos\varphi \tag{2.30}$$

Using Equation (2.30) in the phase formula yields the expression for the last point to be considered in this derivation:

Point 8 Phase Shift for $\varphi \in \left(0, \frac{\pi}{2}\right]$:

$$\frac{\dfrac{L_{tc} + L_{ramp} + L_{sb}}{\cos\left(\frac{\pi}{2} - \varphi\right)} - \left[\left(L_{tc} + L_{ramp} + L_{sb}\right)\dfrac{\cos\varphi}{\sin\varphi} - w_{sb}\right]\cos\varphi}{\lambda} 2\pi$$

Phase Shift for $\varphi = 0$: $\dfrac{w_{sb}}{\lambda} 2\pi$

The phase shifts for Case 2 have now been completely determined for all of the points considered in Figure 2.4. These phase shifts are used in the SimMechanics computer program to represent the incoming wavefronts.

2.3 L'Hôpital's Rule and Summary of Phase Shifts for Wavefront Model

A summary of the phase shifts for all of the cases that were just explored are provided in this section in order to facilitate quick referencing. The phase shift expressions for points 3, 4, 6, and 8 in Case 2 all have the extra condition for when φ = 0 as previously discussed. This condition was said to be pulled directly from the corresponding formula in Case 3. However, it is interesting to note that for Case 2, the terms that do not blow up in the expressions defined for $\varphi \in \left(0, \frac{\pi}{2}\right]$ are exactly those terms that are retained when φ = 0. This is not a coincidence, but rather a consequence of L'Hôpital's rule that was alluded to.

In Stewart [6], L'Hôpital's rule is defined for two differentiable functions f and g, where g'(x) ≠ 0 (except at a) such that the following conditions hold:

$$\lim_{x \to a} f(x) = 0 \quad and \quad \lim_{x \to a} g(x) = 0$$

or that $$\lim_{x \to a} f(x) = \pm\infty \quad and \quad \lim_{x \to a} g(x) = \pm\infty$$

Then the limit formed when dividing the two functions can be found from:

$$\lim_{x \to a} \frac{f(x)}{g(x)} = \lim_{x \to a} \frac{f'(x)}{g'(x)}$$

For simplicity, the calculation of the limit as φ approaches zero will only be done for the phase shift of point 3. However, all of the work here easily extends to the phase formulas that correspond to the other points. Consider first the length portion of the phase shift formula given for point 3 (provided by Equation (2.18)). Simply taking the limit as φ tends to zero yields the expression:

$$\lim_{\varphi\to 0}\left\{\frac{L_{tc}}{\cos\left(\frac{\pi}{2}-\varphi\right)}-\left[L_{tc}\frac{\cos\varphi}{\sin\varphi}-\left(\frac{w_{sb}}{2}-\frac{w_{tc}}{2}\right)\right]\cos\varphi\right\} \tag{2.31}$$

The following terms in the preceding formula blow up in the limit taken above:

$$\lim_{\varphi\to 0}\frac{L_{tc}}{\cos\left(\frac{\pi}{2}-\varphi\right)}=\frac{L_{tc}}{\sin\varphi}=\infty \quad \text{and} \quad \lim_{\varphi\to 0}L_{tc}\frac{\cos^2\varphi}{\sin\varphi}=\infty$$

Therefore, the problem in Equation (2.31) has ∞ - ∞ along with the subtraction of a term containing the widths w_{sb} and w_{tc} and a cosine. Unfortunately, L'Hôptial's rule cannot yet be applied directly to solve this limit problem. This is because we do not have the standard indeterminate form of type 0/0 or ∞/∞. A little bit of algebra in order to get rid of the terms containing the widths must be used to reach this form. First expand the expression in Equation (2.31) out and separate the terms with the widths as done below:

$$\lim_{\varphi\to 0}\left\{\frac{L_{tc}}{\sin\varphi}-L_{tc}\frac{\cos^2\varphi}{\sin\varphi}+\left(\frac{w_{sb}}{2}-\frac{w_{tc}}{2}\right)\cos\varphi\right\}$$

$$=\lim_{\varphi\to 0}\left\{\frac{L_{tc}}{\sin\varphi}-L_{tc}\frac{\cos^2\varphi}{\sin\varphi}\right\}+\lim_{\varphi\to 0}\left(\frac{w_{sb}}{2}-\frac{w_{tc}}{2}\right)\cos\varphi$$

$$=\lim_{\varphi\to 0}\left\{\frac{L_{tc}}{\sin\varphi}-L_{tc}\frac{\cos^2\varphi}{\sin\varphi}\right\}+\left(\frac{w_{sb}}{2}-\frac{w_{tc}}{2}\right) \tag{2.32}$$

Now the problem has reduced to finding the limit of the following expression:

$$\lim_{\varphi\to 0}\left\{\frac{L_{tc}}{\sin\varphi}-L_{tc}\frac{\cos^2\varphi}{\sin\varphi}\right\} \tag{2.33}$$

Combining the two terms in Equation (2.33) then yields the following simple fraction and gets rid of the ∞ - ∞ issue:

$$\lim_{\varphi \to 0} \frac{L_{tc} - L_{tc} \cos^2 \varphi}{\sin \varphi} \tag{2.34}$$

Defining $f(x) = L_{tc} - L_{tc} \cos^2 \varphi$ and $g(x) = \sin \varphi$ in Equation (2.34), it is apparent that the conditions for L'Hôptial's rule are now satisfied for the 0/0 indeterminate form:

$$\lim_{\varphi \to 0} f(x) = L_{tc} - L_{tc} \cos^2 \varphi = 0 \quad and \quad \lim_{\varphi \to 0} g(x) = \sin \varphi = 0$$

We now know from L'Hôptial's rule that the following equalities of the limits hold:

$$\lim_{x \to a} \frac{f(x)}{g(x)} = \lim_{\varphi \to 0} \frac{L_{tc} - L_{tc} \cos^2 \varphi}{\sin \varphi} = \lim_{x \to a} \frac{f'(x)}{g'(x)} = \lim_{\varphi \to 0} \frac{2L_{tc} \cos \varphi \sin \varphi}{\cos \varphi} = \frac{0}{1} = 0$$

Therefore, it can be concluded that the limit of Equation (2.33) is equal to zero:

$$\lim_{\varphi \to 0} \left\{ \frac{L_{tc}}{\sin \varphi} - L_{tc} \frac{\cos^2 \varphi}{\sin \varphi} \right\} = 0$$

The limit given by Equation (2.32) is then equal to:

$$= \lim_{\varphi \to 0} \left\{ \frac{L_{tc}}{\sin \varphi} - L_{tc} \frac{\cos^2 \varphi}{\sin \varphi} \right\} + \left(\frac{w_{sb}}{2} - \frac{w_{tc}}{2} \right) = \left(\frac{w_{sb}}{2} - \frac{w_{tc}}{2} \right)$$

This means that in the phase formula for point 3, by taking the limit as φ approaches zero we finally arrive at:

$$\lim_{\varphi \to 0} \frac{\dfrac{L_{tc}}{\cos\left(\dfrac{\pi}{2} - \varphi\right)} - \left[L_{tc} \dfrac{\cos \varphi}{\sin \varphi} - \left(\dfrac{w_{sb}}{2} - \dfrac{w_{tc}}{2} \right) \right] \cos \varphi}{\lambda} 2\pi = \frac{\dfrac{w_{sb}}{2} - \dfrac{w_{tc}}{2}}{\lambda} 2\pi$$

This is precisely the conditional statement that is provided for point 3 when φ = 0. Therefore, L'Hôptial's rule validates the choice that was previously made to simply use the expressions from Case 3. It can now be said with complete confidence that as φ = 90 degrees (θ = 0°), the formulas for Case 2 reduce to those in Case 1, and when φ = 0 degrees (θ = 90°), the expressions for Case 2 simplify to those given for Case 3. All of the phase shifts that simulate the approach of a wavefront at any angle between θ = 0° and θ = 90° are provided below:

Summary of Phase Shifts for Case 1 (Bow-to-Stern Configuration)

Points 1 and 2	Phase: 0
Points 3 and 4	Phase: $\frac{L_{tc}}{\lambda} 2\pi$
Points 5 and 6	Phase: $\frac{L_{tc} + L_{ramp}}{\lambda} 2\pi$
Points 7 and 8	Phase: $\frac{L_{tc} + L_{ramp} + L_{sb}}{\lambda} 2\pi$

Summary of Phase Shifts for Case 3 (Bow-to-Stern Configuration)

Points 5 and 7	Phase: 0
Points 6 and 8	Phase: $\frac{w_{sb}}{\lambda} 2\pi$
Points 1 and 3	Phase: $\frac{\frac{w_{sb}}{2} - \frac{w_{tc}}{2}}{\lambda} 2\pi$
Points 2 and 4	Phase: $\frac{\left(\frac{w_{sb}}{2} - \frac{w_{tc}}{2}\right) + w_{tc}}{\lambda} 2\pi$

Summary of Phase Shifts for Case 2 (Bow-to-Stern Configuration)

Point 1 Phase: $\dfrac{\left(\dfrac{w_{sb}}{2}-\dfrac{w_{tc}}{2}\right)\sin\left(\dfrac{\pi}{2}-\varphi\right)}{\lambda}2\pi$

Point 2 Phase: $\dfrac{\left(w_{tc}+\dfrac{w_{sb}}{2}-\dfrac{w_{tc}}{2}\right)\sin\left(\dfrac{\pi}{2}-\varphi\right)}{\lambda}2\pi$

Point 3 Phase for $\varphi\in\left(0,\dfrac{\pi}{2}\right]$: $\dfrac{\dfrac{L_{tc}}{\cos\left(\dfrac{\pi}{2}-\varphi\right)}-\left[L_{tc}\dfrac{\cos\varphi}{\sin\varphi}-\left(\dfrac{w_{sb}}{2}-\dfrac{w_{tc}}{2}\right)\right]\cos\varphi}{\lambda}2\pi$

Phase for $\varphi=0$: $\dfrac{\dfrac{w_{sb}}{2}-\dfrac{w_{tc}}{2}}{\lambda}2\pi$

Point 4 Phase for $\varphi\in\left(0,\dfrac{\pi}{2}\right]$: $\dfrac{\dfrac{L_{tc}}{\cos\left(\dfrac{\pi}{2}-\varphi\right)}-\left[L_{tc}\dfrac{\cos\varphi}{\sin\varphi}-\left(w_{tc}+\dfrac{w_{sb}}{2}-\dfrac{w_{tc}}{2}\right)\right]\cos\varphi}{\lambda}2\pi$

Phase for $\varphi=0$: $\dfrac{w_{tc}+\dfrac{w_{sb}}{2}-\dfrac{w_{tc}}{2}}{\lambda}2\pi$

Point 5 Phase: $\dfrac{\left(L_{tc}+L_{ramp}\right)\sin\varphi}{\lambda}2\pi$

Point 6 Phase for $\varphi\in\left(0,\dfrac{\pi}{2}\right]$: $\dfrac{\dfrac{L_{tc}+L_{ramp}}{\cos\left(\dfrac{\pi}{2}-\varphi\right)}-\left[\left(L_{tc}+L_{ramp}\right)\dfrac{\cos\varphi}{\sin\varphi}-w_{sb}\right]\cos\varphi}{\lambda}2\pi$

Phase for $\varphi=0$: $\dfrac{w_{sb}}{\lambda}2\pi$

Point 7 Phase: $\dfrac{\left(L_{tc}+L_{ramp}+L_{sb}\right)\sin\varphi}{\lambda}2\pi$

Point 8 Phase for $\varphi\in\left(0,\dfrac{\pi}{2}\right]$: $\dfrac{\dfrac{L_{tc}+L_{ramp}+L_{sb}}{\cos\left(\dfrac{\pi}{2}-\varphi\right)}-\left[\left(L_{tc}+L_{ramp}+L_{sb}\right)\dfrac{\cos\varphi}{\sin\varphi}-w_{sb}\right]\cos\varphi}{\lambda}2\pi$

Phase for $\varphi=0$: $\dfrac{w_{sb}}{\lambda}2\pi$

2.4 Alternative Ship and Ramp Configuration

The two ships connected by a ramp can also be expressed in a starboard-to-port configuration. Such an arrangement is illustrated in Figure 2.9 where the ramp is connected to the port side of the T-Craft and the starboard side of the Sea Base (the front of the ship is assumed to be in the positive y quadrant). All other aspects of the problem such as the method of wave forcing, local coordinate systems, etc. remain identical. Figure 2.9 shows that the geometry (on the x-y plane with z = 0) of this alternative way of representing the system is identical to the bow-to-stern configuration except that the lengths and widths of the ships are switched. Therefore, an in-depth derivation of the phase shifts is unnecessary. Instead, the phase shifts are determined by using the expressions in the previous section while noting that everywhere L_{tc} and L_{sb} are found, they are to be replaced with w_{tc} and w_{sb} respectively (and the same holds conversely).

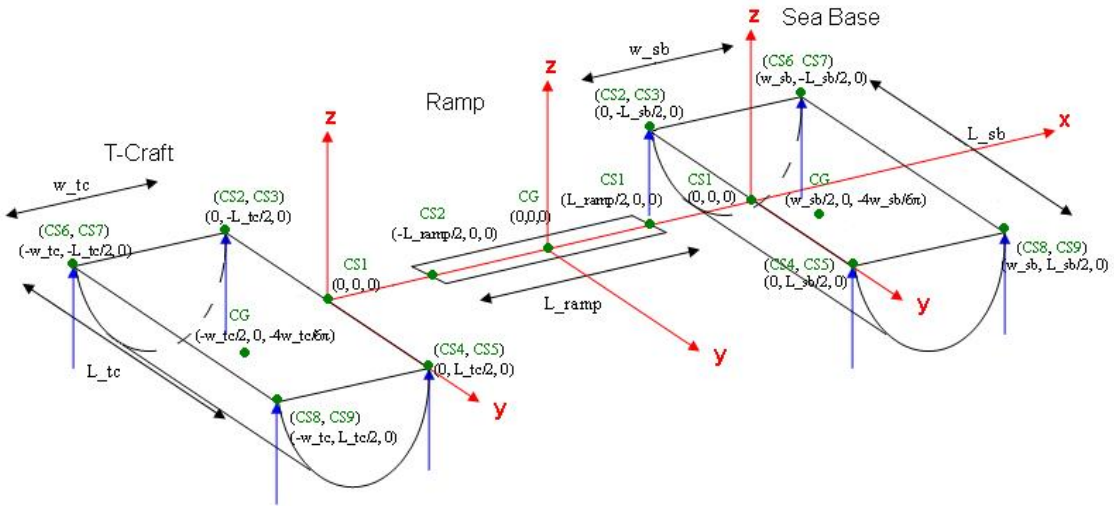

Figure 2.9: SimMechanics representation of the Sea Base connected to the T-Craft by a ramp in a starboard-to-port configuration

The different scenarios of wavefront orientations that may be encountered in the starboard-to-port situation are depicted below in Figure 2.10. This illustration is basically identical to Figure 1.4. The only distinction in the two figures is that the ships are now “taller” whereas before they were “wider”, but there is no fundamental difference in the geometry beyond that.

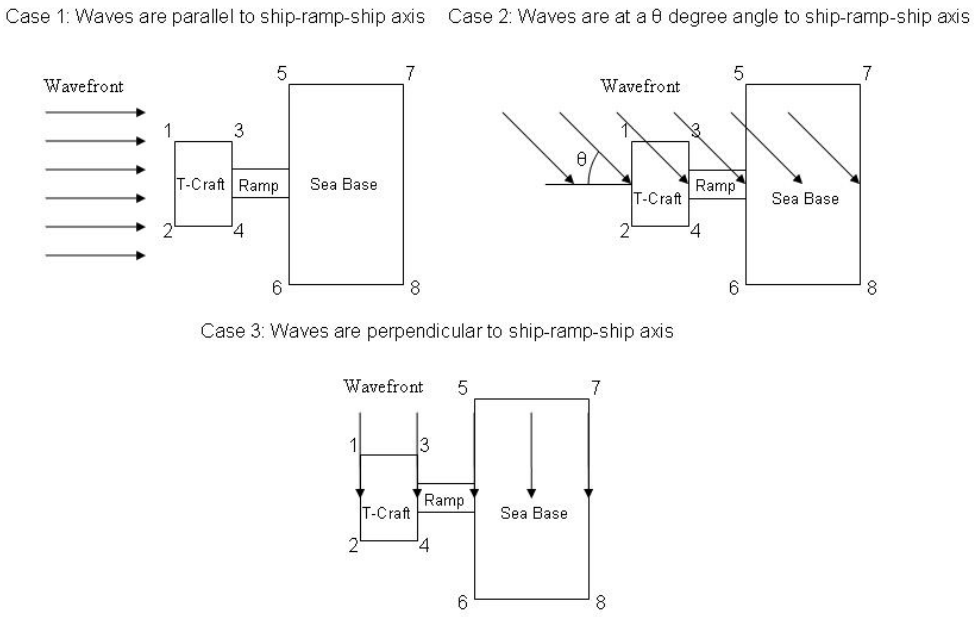

Figure 2.10: Different cases of wavefront orientations in the simulation for the starboard-to-port configuration

In this report, only the bow-to-stern configuration is examined as it takes full advantage of the actuation capabilities that the T-Craft has in creating a variable ramp length. Using the T-Craft surge velocity to extend the ramp will ultimately be employed as a method of minimizing the angles formed between the ships and ramp. Unfortunately, such a beneficial effect is not provided in the starboard-to-port configuration (it is difficult to manually move a ship in the sway direction). Because of this, and the reality that the geometries are identical when considering phase shifts, means that this arrangement will not be studied.

CHAPTER 3: SHIP MODELING AND ASSUMPTIONS

3.1 Uncoupled Ship Equations of Motion

Due to the complexity that is inherent in this interconnected dynamic system, a complete description of the equations of motion is not provided in this report. Instead, the system is modeled as a second order spring-mass-damper similar to that given by Equation (1.2). From this equation we know that there is a damper with a coefficient b and a spring with a constant equal to $\rho g A_W$. However, it should be recognized that this formulation was developed for uncoupled heave motions and does not account for the pitch and roll motions that are also affected by hydrostatic restoring forces. Although no rigorous mathematical model is provided, it is still necessary to extend Equation (1.2) to the pitch and roll motions. This in turn will influence the choices of damping coefficients and spring constants along the pitch and roll degrees of freedom that are used in the computer simulations.

Denoting the roll state variable (angle) by α, the pitch state variable (angle) by β, and the heave state variable by x, the uncoupled equations of motion taken from Biran [2] can be used to extend the spring-mass-damper analogue to include heave, pitch, and roll. It should be noted that the remaining degrees of freedom in surge, yaw, and sway are not opposed by hydrostatic restoring forces, and thus the respective spring constants and damping coefficients are set to zero. As such, the equations governing the motion in those

directions are not considered here. The uncoupled roll equation of motion is given by:

$$\ddot{\alpha} + 2b\dot{\alpha} + \omega_{nr}^2 \alpha = \omega_{nr}^2 \frac{2\pi\zeta_0}{\lambda} \sin(\omega t) \tag{3.1}$$

where ω_{nr} is the ship natural angular frequency of roll, ω is the ocean wave exciting frequency, ζ_0 is the wave amplitude, b is the damping coefficient of roll, and λ is the wavelength. Notice that Equation (3.1) is almost of the spring-mass-damper form given by Equation (1.1) except that no mass term appears in front of the acceleration $\ddot{\alpha}$. The ship natural angular frequency of roll is commonly expressed as:

$$\omega_{nr} = \sqrt{\frac{gGM_R}{i_{mr}^2}} \tag{3.2}$$

where GM_R is defined as the metacentric height in roll and i_{mr} is the mass radius of gyration for roll. The meaning of the metacentric height will be discussed later. Substitution of Equation (3.2) into Equation (3.1) yields a slightly more transparent version of the equation of motion in roll:

$$\ddot{\alpha} + 2b\dot{\alpha} + \frac{gGM_R}{i_{mr}^2} \alpha = \frac{gGM_R}{i_{mr}^2} \frac{2\pi\zeta_0}{\lambda} \sin(\omega t) \tag{3.3}$$

The mass radius of gyration about the axis of inclination for roll motions is proportional to the width (in naval terminology referred to as breadth) of the ship and is given for our half-cylinder ship geometry as:

$$i_{mr} = \frac{w}{2\sqrt{3}} \tag{3.4}$$

This quantity can also be used to relate the mass moment of inertia, J to the mass displacement, Δ by the following expression.

$$J = i_m^2 \Delta \tag{3.5}$$

The mass displacement is formally defined as the mass of the water displaced by a floating body. By Archimedes' principle the mass of the water displaced is equal to the mass of the ship, therefore, $\Delta = m_{ship}$. The mass moment of inertia, J is typically thought of as the rotational analogue of mass. Substitution of Equation (3.5) into Equation (3.3) results in:

$$J\ddot{\alpha} + 2Jb\dot{\alpha} + g\Delta GM_R \alpha = g\Delta GM_R \frac{2\pi\zeta_0}{\lambda}\sin(\omega t) \tag{3.6}$$

This equation is now of the spring-mass-damper form given by Equation (1.1). Likewise, the following equation describes uncoupled and undamped pitch:

$$\ddot{\beta} + \frac{gGM_P}{i_{mp}^2}\beta = \frac{gGM_P}{i_{mp}^2}\gamma\sin(\omega t) \tag{3.7}$$

where γ is the maximum pitch amplitude and i_{mp} is the mass radius of gyration for pitch. It is known that i_{mp} is proportional to the length of the ship:

$$i_{mp} = \frac{L}{2\sqrt{3}} \tag{3.8}$$

Substitution of Equation (3.5) in order to introduce a mass term in front of the acceleration yields:

$$J\ddot{\beta} + g\Delta GM_P\beta = g\Delta GM_P\gamma\sin(\omega t) \tag{3.9}$$

Once again, the heave equation of motion is represented below:

$$(m + A_{33})\ddot{x} + b\dot{x} + \rho g A_W x = \rho g A_W \xi_0 \cos(\omega t) \tag{3.10}$$

Equations (3.6), (3.9), and (3.10) represent the uncoupled ship equations of motion for roll, pitch, and heave. These equations were developed for a single ship, and thus cannot be used to accurately describe the motion of the interconnected ship-ramp-ship system. However, at each CS point (refer to Figure 1.1 for the locations of the CS points) on the ships there is a connected spring and damper in parallel. As discussed in Chapter 1, these springs and dampers emulate the roles of gravity and buoyancy. Therefore, Equations (3.6), (3.9), and (3.10) may at the very least be used to form an estimate of the spring constants and damping coefficients in the computer simulations. Upon comparison with the standard spring-mass-damper system provided by Equation (1.1), it is obvious that the spring constants for roll, pitch, and heave are given as:

$$k_{roll} = g\Delta GM_R \qquad k_{pitch} = g\Delta GM_P \qquad k_{heave} = \rho g A_W \tag{3.11}$$

The damping coefficients are not explicitly given in Biran [2]; however, from Equation (3.8) we know that no damping is used on the pitch motions. With regard to the heave and roll motions it is only known that the damping coefficient is a function of the frequency of oscillation. Thus, the damping coefficients will be chosen in an ad hoc manner such that the resulting motions make physical sense. In order to implement the choices of spring constants given above, A_w, GM_R, and GM_P must be solved for. Although these quantities change as a ship is in motion, they will be assumed invariant such that k remains constant.

The waterplane area, A_w is defined as a horizontal slice of the ship hull at the water level. Consider a cross section of the ship hull geometry partly submerged in water as depicted in Figure 3.1.

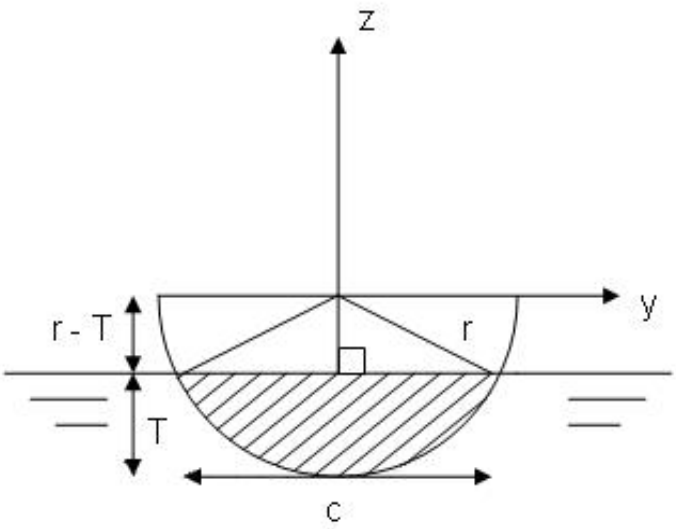

Figure 3.1: Cross section of the ship hull in hydrostatic equilibrium where the shaded region is submerged under water

It is clear that the width of the ship (distance along the y axis) at the waterline is equal to the variable denoted by c. The waterplane area would be this width multiplied by the length of the ship (distance along the x axis). Unfortunately, c is a quantity that is not readily available, and instead must be expressed in terms of other variables. In particular, the draught, T is defined as the vertical distance between the waterline and the bottom of the hull and can be easily measured provided the ship has a "draught scale" on the side of the hull. As a result of this definition, the distance from the waterline to the surface of the ship is given by r – T. Now consider the triangle on the right with a base of c/2, height of r – T, and a hypotenuse of r. The Pythagorean Theorem then yields:

$$\left(\frac{c}{2}\right)^2 + (r-T)^2 = r^2$$

After a little bit of algebra, c can be represented in terms of r and T as follows:

$$c = 2\sqrt{r^2 - (r-T)^2} = 2\sqrt{2Tr - T^2} \tag{3.12}$$

The waterplane area is then expressed in terms of known variables as:

$$A_W = cL = 2L\sqrt{2Tr - T^2} \tag{3.13}$$

It can also be reasoned that the quantity r – T is perhaps easier to measure. In this case the waterplane area is equal to:

$$A_W = 2L\sqrt{r^2 - (r - T)^2} \tag{3.14}$$

The metacentric height, GM is a familiar term in the study of ship hydrostatics and is best understood by observation of Figure 3.2.

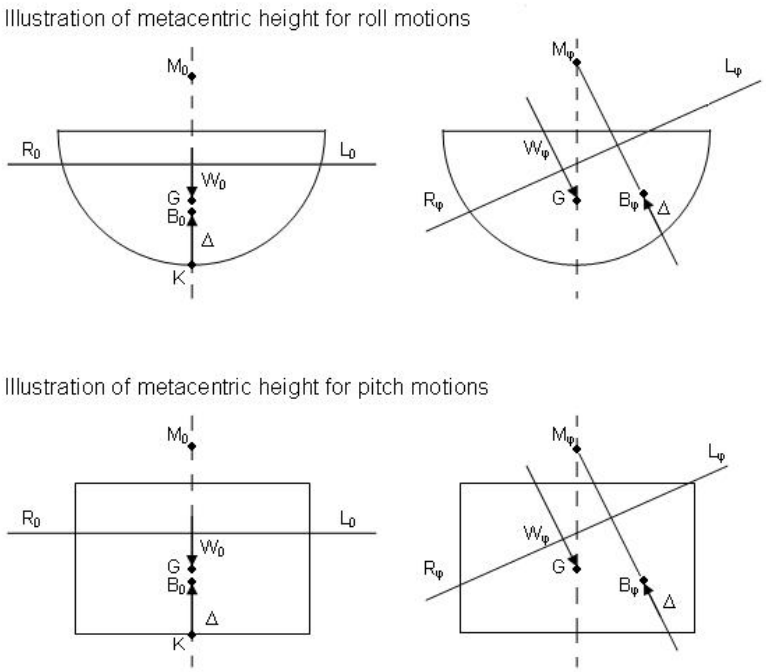

Figure 3.2: Metacentric heights for both the roll, GM_R and pitch, GM_P geometry. This drawing is based on the discussion of Figure 2.9 in [2]

In the drawings above, the ship is in an initial, upright position denoted by the subscripts 0, and is then perturbed to an angle denoted by the subscripts φ. G is the center of gravity through which the weight force, W of the ship acts through. B_0 is the initial center of buoyancy through which the buoyancy force, Δ acts

through. M_0 is the original metacenter which lies along the line of action of the buoyancy force. R_0L_0 is the initial waterline and is always perpendicular to the line of action of the buoyancy force. When the ship rolls at an angle φ, the waterline is now $R_\varphi L_\varphi$, the center of buoyancy moves to a new position B_φ, and the line of action of the buoyancy force moves as well. The metacenter, M_φ is defined as the intersection of the new buoyancy force line of action and that of the old buoyancy force line of action. The metacentric height is expressed as:

$$\vec{GM} = \vec{KB} + \vec{BM} - \vec{KG} \tag{3.15}$$

where KB is the z coordinate of the center of buoyancy, BM is the metacentric radius, and KG is the z coordinate of the center of gravity. In order to solve for GM, these quantities must first be determined.

KG is the easiest vector to determine as the center of gravity for common shapes is usually available. For simplicity, it will be assumed that the mass of both ships is uniformly distributed, meaning that the center of gravity (center of mass) is identical to the geometric centroid. For the roll motions, the center of gravity corresponds to the location of the point G on the top drawings of Figure 3.2. The centroid of a semicircle measured from the flat side is given as:

$$CG = \frac{4r}{3\pi}$$

By defining the keel of the hull at point K as having the value z = 0, and measuring positive z upwards, the distance KG for the semicircle is then:

$$\vec{KG}_{roll} = r - \frac{4r}{3\pi} \tag{3.16}$$

Finding the center of gravity for the pitch motions is even simpler as the geometry along this plane is now that of a rectangle as shown on the bottom drawings of Figure 3.2. The length of the vector KG is given as:

$$\vec{KG}_{pitch} = \frac{r}{2} \tag{3.17}$$

KB can be determined by finding the location of the center of buoyancy, which is identical to the centroid of the submerged part of the hull in Figure 3.3.

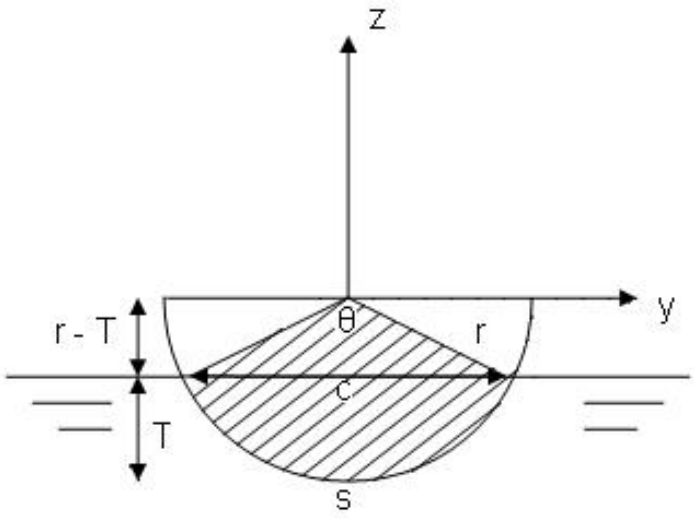

Figure 3.3: Cross section of the ship hull in hydrostatic equilibrium

Several intermediate quantities must first be determined before the coordinates of the center of buoyancy can be found. First consider the area of the two right triangles from Figure 3.1, which when combined form an isosceles triangle. Using Equation (3.12), the area of this triangle is given as:

$$A_{triangle} = \frac{1}{2}c(r-T) = (r-T)\sqrt{r^2-(r-T)^2} \tag{3.18}$$

Now consider the shaded area in Figure 3.3 which includes the isosceles triangle and the region below the waterline. This area of this sector is given as:

$$A_{sector} = \frac{1}{2} r^2 \theta \tag{3.19}$$

The angle θ can be expressed in terms of the radius and draught as:

$$\theta = 2\cos^{-1}\left(\frac{r-T}{r}\right) \tag{3.20}$$

Therefore, by inserting Equation (3.20) into Equation (3.19) we arrive at:

$$A_{sector} = r^2 \cos^{-1}\left(\frac{r-T}{r}\right) \tag{3.21}$$

From Figure 3.3 it is clear that the area of the submerged hull is the area of the sector defined in Equation (3.21) minus that of the triangle in Equation (3.18).

$$A_{subhull} = r^2 \cos^{-1}\left(\frac{r-T}{r}\right) - (r-T)\sqrt{r^2 - (r-T)^2} \tag{3.22}$$

The weighted mean of z measured from the flat surface of the submerged hull can be found from integration and is given as (where Equation (3.20) is used for the angle θ):

$$\langle z \rangle = \frac{2}{3} r^3 \sin^3\left(\frac{1}{2}\theta\right) = \frac{2}{3} r^3 \sin^3\left(\cos^{-1}\left(\frac{r-T}{r}\right)\right) \tag{3.23}$$

The geometric centroid of the submerged hull is then given as the distance from point K to point B (the center of buoyancy). This vector is found from the division of Equation (3.23) with Equation (3.22) while making sure to measure from z = 0:

$$\vec{KB}_{roll} = r - \bar{z} = r - \frac{\langle z \rangle}{A_{subhull}} = r - \frac{\frac{2}{3} r^3 \sin^3\left(\cos^{-1}\left(\frac{r-T}{r}\right)\right)}{r^2 \cos^{-1}\left(\frac{r-T}{r}\right) - (r-T)\sqrt{r^2 - (r-T)^2}} \tag{3.24}$$

The value of KB for the pitch motions is far easier to determine due to the simpler geometry. Once again assuming that K is located at z = 0, then the distance from the bottom of the hull to the center of buoyancy is given by:

$$\vec{KB}_{pitch} = \frac{1}{2}T \tag{3.25}$$

All that is left in the computation of GM is to find BM, the metacentric radius. In Biran [2], the metacentric radius is defined as:

$$\vec{BM} = \frac{I}{\nabla} \tag{3.26}$$

where I is the moment of inertia of the waterplane about the axis of inclination, and ∇ is the volume of the immersed part of the ship. The volume is the area of the submerged hull given by Equation (3.22) multiplied by the length of the ship:

$$\nabla = L\left[r^2 \cos^{-1}\left(\frac{r-T}{r} \right) - (r-T)\sqrt{r^2 - (r-T)^2} \right] \tag{3.27}$$

Since the top faces of the ships are rectangles, the moment of inertia of the waterplane about the axis of inclination is the same as finding the area moment of inertia of a rectangle. For roll, the axis of inclination is parallel to the length, and thus the area moment of inertia is given as:

$$I_{roll} = \frac{Lw^3}{12} \tag{3.28}$$

On the other hand, for pitch, the axis of inclination is perpendicular to the length. Therefore, the area moment of inertia is now expressed as:

$$I_{pitch} = \frac{wL^3}{12} \tag{3.29}$$

By substituting Equations (3.27) through (3.29) into Equation (3.26), we arrive at the final expressions for the metacentric radius:

$$\vec{BM}_{roll} = \frac{I_{roll}}{\nabla} = \frac{\frac{Lw^3}{12}}{L\left[r^2 \cos^{-1}\left(\frac{r-T}{r}\right) - (r-T)\sqrt{r^2-(r-T)^2}\right]} \tag{3.30}$$

$$\vec{BM}_{pitch} = \frac{I_{pitch}}{\nabla} = \frac{\frac{wL^3}{12}}{L\left[r^2 \cos^{-1}\left(\frac{r-T}{r}\right) - (r-T)\sqrt{r^2-(r-T)^2}\right]} \tag{3.31}$$

Now that the vectors KB, BM, and KG have all been determined for both the pitch and the roll cases, the metacentric heights GM_R and GM_P are given as:

$$\vec{GM}_R = \vec{KB}_{roll} + \vec{BM}_{roll} - \vec{KG}_{roll}$$

$$\vec{GM}_R = r - \frac{\frac{2}{3}r^3 \sin^3\left(\cos^{-1}\left(\frac{r-T}{r}\right)\right)}{r^2 \cos^{-1}\left(\frac{r-T}{r}\right) - (r-T)\sqrt{r^2-(r-T)^2}} + \ldots$$

$$\ldots + \frac{\frac{Lw^3}{12}}{L\left[r^2 \cos^{-1}\left(\frac{r-T}{r}\right) - (r-T)\sqrt{r^2-(r-T)^2}\right]} - \left(r - \frac{4r}{3\pi}\right) \tag{3.32}$$

$$\vec{GM}_P = \vec{KB}_{pitch} + \vec{BM}_{pitch} - \vec{KG}_{pitch}$$

$$\vec{GM}_P = \frac{1}{2}T + \frac{\frac{wL^3}{12}}{L\left[r^2 \cos^{-1}\left(\frac{r-T}{r}\right) - (r-T)\sqrt{r^2-(r-T)^2}\right]} - \frac{r}{2} \tag{3.33}$$

Finally, all of the unknown quantities listed in Equation (3.11) for the spring constants are now determined in terms of the known variables: Length L, width w, radius r, mass ∆, gravity g, density of water ρ, and draught T. The spring constants used to represent the hydrostatic restoring moments and forces that oppose motion through F = -kx are given as:

Heave spring constants:

$$k_{heave} = \rho g A_W$$

$$= \rho g \, 2L\sqrt{r^2 - (r-T)^2}$$

Roll spring constants:

$$k_{roll} = g\Delta GM_R =$$

$$g\Delta\left[r - \frac{\frac{2}{3}r^3 \sin^3\left(\cos^{-1}\left(\frac{r-T}{r}\right)\right)}{r^2\cos^{-1}\left(\frac{r-T}{r}\right) - (r-T)\sqrt{r^2-(r-T)^2}} + \frac{\frac{Lw^3}{12}}{L\left[r^2\cos^{-1}\left(\frac{r-T}{r}\right) - (r-T)\sqrt{r^2-(r-T)^2}\right]} - \left(r - \frac{4r}{3\pi}\right)\right]$$

Pitch spring constants:

$$k_{pitch} = g\Delta GM_P = g\Delta\left[\frac{1}{2}T + \frac{\frac{wL^3}{12}}{L\left[r^2\cos^{-1}\left(\frac{r-T}{r}\right) - (r-T)\sqrt{r^2-(r-T)^2}\right]} - \frac{r}{2}\right]$$

3.2 Modification of Spring Constants and Damping Coefficients

Recall the uncoupled equations of motion for heave, pitch, and roll that were used in the previous section to choose the spring constants:

Roll: $J\ddot{\alpha} + 2Jb\dot{\alpha} + g\Delta GM_R\alpha = g\Delta GM_R \frac{2\pi\zeta_0}{\lambda}\sin(\omega t)$

Pitch: $J\ddot{\beta} + g\Delta GM_P\beta = g\Delta GM_P\gamma\sin(\omega t)$

Heave: $(m + A_{33})\ddot{x} + b\dot{x} + \rho g A_W x = \rho g A_W \xi_0 \cos(\omega t)$

It was noted that these equations resemble the typical second order spring-mass-damper system but with different values of mass, damping, and spring constants. In order to better compare these equations with Equation (1.1), neglect the added mass term, A_{33} in heave and express $2\pi\zeta_0/\lambda$ in the roll and γ in the pitch as amplitudes: ξ_0. Also, now consider damping in the pitch motions as this damping will be used in the simulations to attenuate some of the high frequency behavior that would otherwise be present:

Roll: $J\ddot{\alpha} + 2Jb\dot{\alpha} + g\Delta GM_R\alpha = g\Delta GM_R\xi_0\sin(\omega t)$

Pitch: $J\ddot{\beta} + 2Jb\dot{\beta} + g\Delta GM_P\beta = g\Delta GM_P\xi_0\sin(\omega t)$

Heave: $m\ddot{x} + b\dot{x} + \rho g A_W x = \rho g A_W \xi_0 \cos(\omega t)$

Except for the masses that multiply the accelerations, the terms on the left hand side (damping and spring constants) can be implemented independently for each individual degree of freedom. This is due to the fact that separate spring-mass-damper systems can be inserted for roll, pitch, and heave. The fact that the

masses cannot be changed for the different equations is inconsequential since the same mass (translational and then rotational) is multiplying all of the accelerations. It should be noted that significant damping will be used in the roll and pitch equations since the damping coefficients are multiplied by the mass moment of inertia. Substitution of Equations (3.4), (3.5), and (3.8) expresses the terms that multiply the velocity components by the translation mass:

Roll: $$J\ddot{\alpha} + 2\Delta\left(\frac{w}{2\sqrt{3}}\right)^2 b\dot{\alpha} + g\Delta GM_R\alpha = g\Delta GM_R\xi_0 \sin(\omega t)$$

Pitch: $$J\ddot{\beta} + 2\Delta\left(\frac{L}{2\sqrt{3}}\right)^2 b\dot{\beta} + g\Delta GM_P\beta = g\Delta GM_P\xi_0 \sin(\omega t)$$

Now assuming that the actual damping coefficients, b are all very small compared to the spring constants and have values around ~ 0.01, the damping will still be very large in the rotational components due to the multiplication of the extra mass and length terms.

On the right hand side of the rotational equations dealing with roll and pitch are sinusoidal moments with amplitudes of $g\Delta GM\xi_0$. Since a moment is defined as a force acting over a distance, and the distance here is the metacentric height GM, the force component of the amplitude is just $g\Delta\xi_0$. On the right hand side of the translational equation for heave is another force with an amplitude of $\rho g A_w \xi_0$. Thus, the force components of the moments in the rotational equations and the force in the heave equation are not equivalent because generally $g\Delta\xi_0 \neq \rho g A_w \xi_0$ (often by many orders of magnitude). This introduces a significant problem in implementing the spring-mass-damper

concept into the computer program, as the program only allows for one force (i.e. either having a magnitude of $g\Delta\xi_0$ or $\rho g A_w \xi_0$). Since the wavefront is introduced as a series of sine wave actuators along the z axis, the term $\rho g A_w \xi_0$ from the heave force is used as the magnitude for all of the forces. Unfortunately, the equations cannot be correctly implemented into the program as the pitch and roll moments with $\rho g A_w \xi_0$ as the force component magnitude will turn out to be much less than they should be with $g\Delta\xi_0$ (generally $g\Delta\xi_0 > \rho g A_w \xi_0$). In order to cope with this shortcoming, the pitch and roll spring constants will be modified by the multiplication of a term $\eta < 1$ which will decrease the spring constants accordingly to cope with the smaller force component of the moments. This constant is defined as the ratio of the components that make the force in the heave equation and the forces of the moments in the pitch and roll equations different:

$$\eta = \frac{\rho A_W}{\Delta} \tag{3.34}$$

If this procedure is not used, with the force component of the moments having a magnitude of $\rho g A_w \xi_0$ and the spring constants still having magnitudes of $g\Delta GM\xi_0$, then even for a considerable sea state there will be virtually no roll or pitch motions at all - quite unrealistic. Lastly, it is worth nothing that the terms that comprise the damping in the equations can also be multiplied by this constant. However, this is not necessary as the damping terms have a tunable parameter b that can offset any change that multiplication by η would introduce.

3.3 Possibilities of Joints for the Ships and Ramp

Now that the wavefront and ships have been mathematically represented for the simulations, it is worth discussing the importance of the choice of joints that link the Sea Base and T-Craft to the ramp. The six degrees of freedom possible for the joints are listed depicted below, where the arrows indicate the motions that may occur between the ships and ramp. The naval terminology for these degrees of freedom (i.e. sway, pitch, surge, etc) is also used to describe the motions of the ships themselves throughout this report.

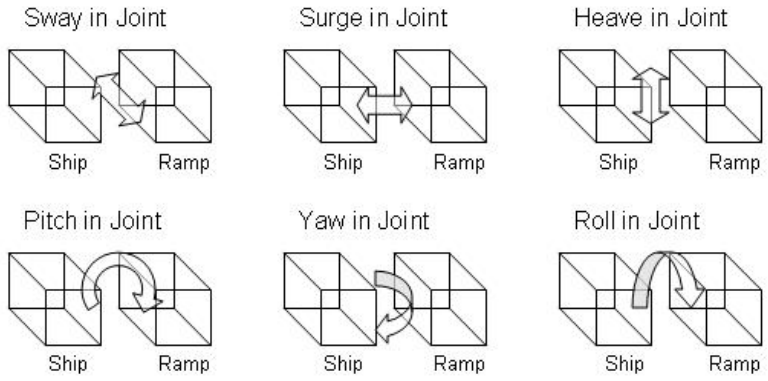

Figure 3.4: Motions that may occur in the joints linking the ships to the ramp

Due to the extremely complex motions that may be created from the external wave forcing (which can come from any direction) of this interconnected system, all six of the above motions can be experienced between the ships and ramp. However, it would not be realistic to design such a joint that permits all six motions, and it is more likely that some of the motions would not be allowed (constrained), while others would be penalized, possibly by a stiff spring. It should be noted that although not present in the SimMechanics framework, motions that are not allowed, or are penalized, will result in stresses within the

ramp. Because it is unreasonable to study all of the different combinations of these degrees of freedom in a joint (and on top of that varying the spring constants in the joints), only the most physically realistic combinations are of interest here. In particular, it is assumed that the translational motions (sway, surge, and heave) are constrained as those would result in a very complex joint. Pitch is the most obvious motion to allow, as it is the type of rotation that results from using a simple hinge. Therefore, the simulations will use a revolute joint that allows for only pitch, and constrains all other motions. In addition, a revolute joint that enables pitch and roll motions will also be studied. The differences between using a torsional spring on the roll motions in this joint and not using a spring at all will be explored. Lastly, a gimbal type joint which allows for pitch, and has torsional springs on both the roll and yaw motions will be used in the simulations.

As an aside, it was mentioned in the introduction that up to 24 state equations would be necessary in order to completely describe the interconnected system of two ships and a ramp. When unconnected, the three rigid bodies would result in a system of 18 degrees of freedom (6 for each body), and thus 36 states. The presence of the constraints imposed by the joints then accordingly decreases the number of degrees of freedom depending on how many motions are suppressed. As such, there are 24 states with the pitch-roll-yaw joint, 20 states with the pitch-roll joint, and 16 states with the pitch-only joint. These numbers are easily calculated by realizing that the total system can be described by 6 DOF (12 states) and the additional DOF contributed by each motion allowed between the ships and ramp (two DOF for each motion as two joints are used).

3.4 Discussion of Assumptions

The most critical limitation of the simulation results in the next chapter is that they become less accurate for large rotations (in the x-y plane) of the ship-ramp-ship system. This is due to the fact that the phase formulas of Chapter 2 must be defined relative to a ship's local coordinate system rather than a global coordinate system. As a result, when the ships rotate away from the starting position, the wavefront also rotates in order to maintain the same angle of incidence on the ships. This is physically unrealistic as the wavefront should really be modeled as a vector field that remains in the same direction for all time. Fortunately, this limitation does not invalidate the simulations in this report, as fairly small time scales (100 seconds) are used, thus preventing large angles of rotation. Also, the optimization results of Chapters 5 and 6 that examine the effects of wave orientation on the pitch and roll angles between the ships and ramp are not impacted by this shortcoming. This is because a new simulation is performed for each individual wave orientation. While not considerably detracting from the results in this paper, a real-time method of updating the phase formulas to cope with a changing ship heading direction (equally, the wave incidence angle) will be necessary to apply extremum seeking. Research efforts have in fact yielded a program that relies on a feedback loop that measures the amount of rotation and then updates the phase formulas accordingly.

In Chapter 1 it was recognized that the waves approaching the ships act purely as surface disturbances along the x-y plane. This was obvious from Figure

1.1, where the wave force vectors all reach the same surface. To arrive at a more realistic model of the waves, one could instead consider a polyhedral shape for the ship hull (although the semicircle would still be possible in SimMechanics). At each extreme point of the polyhedron, a force vector from the waves could be used. This would introduce a “depth” to the wave, removing the assumption of it being a surface disturbance. Then, incorporating some knowledge of ocean waves, the relative strength vs. depth of the wave forces could be used to arrive at a more realistic model (at the expense of a far more complicated program).

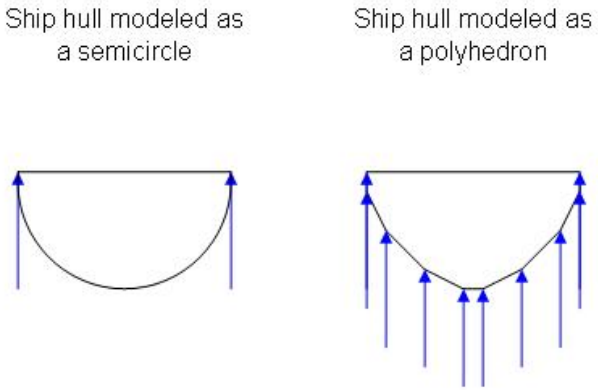

Figure 3.5: Cross section of ship hulls. Blue vectors indicate wave forcing vectors

Another assumption made in the simulations was that the waves act only along the z axis. It is reasonable to think that when the ships are out at sea, there would be considerable movement and even drift in the sway and surge directions (directions perpendicular to the z axis) due to wave-induced forces. However, the simulation results in Chapter 4 will show that even though the waves act along the z axis, there will still be movement in the sway and surge directions. This seems to indicate that the assumption of the waves acting only along the z axis is a decent one. Alternatively, one could still implement forces along the x-y plane to simulate both ships in motion, or to create a more viscous fluid.

CHAPTER 4: SIMULATION RESULTS

4.1 Opening Comments

The following pages document simulation results using various different combinations of joints between the ships and ramp while examining three cases of wave incidence angles. The scenario when the waves are aligned parallel to the ship-ramp-ship axis with $\theta = 0°$ is referred to as Case 1. On the other hand, Case 3 will refer to the waves approaching perpendicular to the ships with an angle of $\theta = 90°$. In Chapter 2, Case 2 referred to the general situation with the waves at an arbitrary $\theta°$ angle to the ship-ramp-ship axis. It was shown that this case includes Case 1 and Case 3 (after application of L'Hôptial's rule). However, here Case 2 will refer to the intermediate situation when $\theta = 45°$. All of the simulations examine the behavior of the ships given a constant ramp length and assume the bow-to-stern configuration in Figure 1.1. Sections 4.2-4.4 explore the situation when the joints between the ships and ramp allow only for pitch, and constrain all other motions. Using this joint, Case 1 is explored in Section 4.2, Case 3 in Section 4.3, and Case 2 in Section 4.4. Section 4.5 examines the joint that allows both pitch and roll between the ships and ramp for Case 3. Section 4.6 documents the results from using a spring on the roll motions but for the same wave orientation as in Section 4.5. Likewise, Sections 4.7-4.8 explore the joint that allows for pitch and roll with and without springs on roll motions for Case 2. Sections 4.9-4.10 consider a gimbal type joint that permits pitch, roll, and

yaw motions, but has springs inserted for the roll and yaw degrees of freedom. A table summarizing the various findings is included in Section 4.11.

The particular m-file that is used for the following simulations is included in the appendix. However, for easy reference some of the numerical values that were chosen are provided below:

Mass of Sea Base: 45,359,237 kg or 50,000 tons

Length of Sea Base: 200 meters

Radius of Sea Base: 15 meters

Draught of Sea Base: ½ of radius

Mass of T-Craft: 2,721,554.22 kg or 3,000 tons

Length of T-Craft: 40 meters

Radius of T-Craft: 8 meters

Draught of T-Craft: ¼ of radius

Length of Ramp: 25 meters

Wave Amplitude (trough to crest): 2 meters (mid to high sea state 4)

Spring Constant between Joints: 500,000 N/m (50,000 N/m for yaw joint)

Time between Wave Crests: 8 seconds

Distance between Wave Crests: 38.1 meters

The geometry and moments of inertia of the craft and ramp are given by the pictures and equations in Figures 1.2 and 1.3. The forces of buoyancy and gravity are emulated using springs and dampers in parallel on the heave, pitch, and roll degrees of freedom. The particular spring constants and damping coefficients used in the simulations are taken from the results of Chapter 3.

4.2 Case 1: Waves are Parallel to Ship-Ramp-Ship Axis (Pitch in Joint)

The simulation is first performed using the phase values from the first case in order to simulate the waves aligned with the ship-ramp-ship axis. Only pitch is allowed in the joint between the ships and ramp, and there is no spring in the joint. This is the only time this wave orientation will be studied, as the future joints will not change ship motions when the waves are parallel. Figure 4.1 shows the heave motions that result and the relative pitch between the ramp and ships. It is interesting to note that there is very little pitch of the ships themselves. This can be attributed to two important factors. First, the restoring forces for pitch motions are proportional to the longitudinal metacentric height along the x-z plane which has a cubed length term. This causes the metacentric height to be significant, and thus results in a large spring constant to oppose the pitch motions. Secondly, the length of the T-Craft (and the length of the Sea Base) is nearly divisible by the ocean wavelength, thus causing the ship to heave up and down together without much tilt or pitch (see Figure 2.2). Further implications regarding the length of the ships compared to the wavelength will be discussed in Chapter 5.

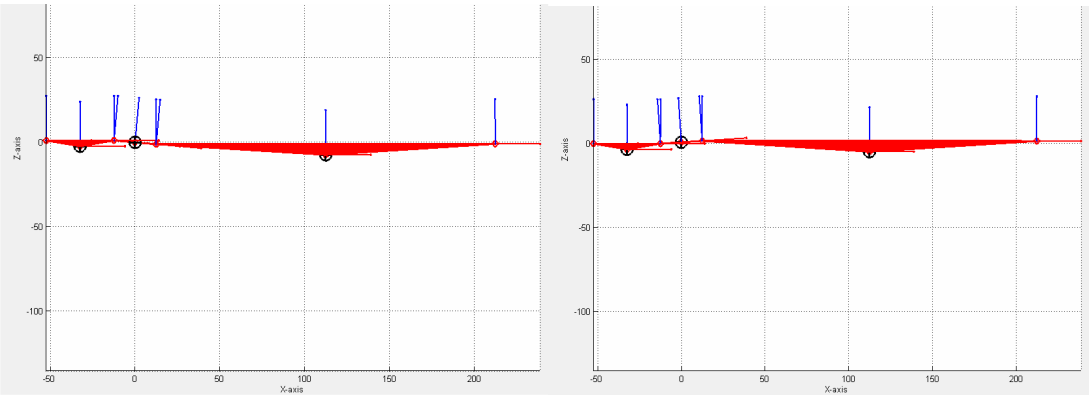

Figure 4.1: View of the ship-ramp-ship configuration along the x-z plane

Since the waves are approaching parallel to the ships, there are no roll, yaw, or sway motions present as indicated in the second picture of Figure 4.2.

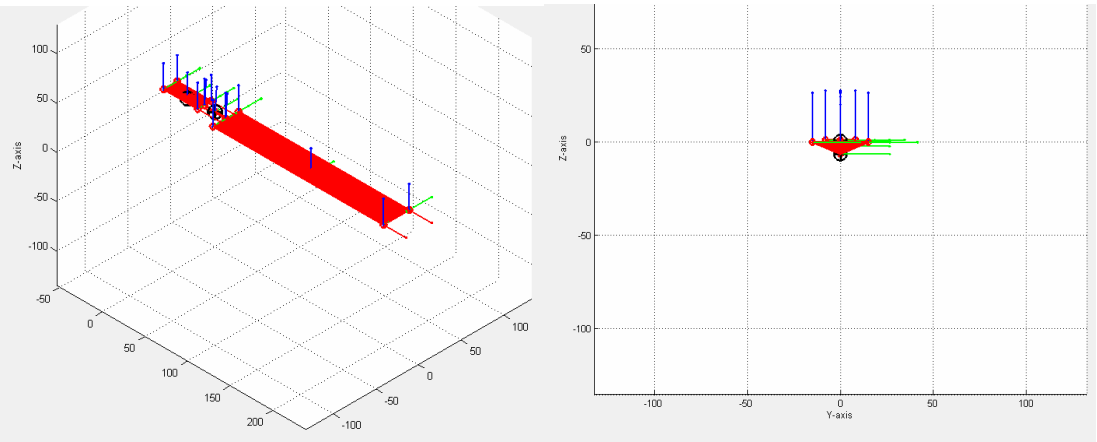

Figure 4.2: Left: 3-Dimensional view. Right: View along the y-z plane

In order to better quantify the motions observed in the simulations, the displacements along particular directions as functions of simulation time will be provided in this chapter. Graph 4.1 compares the heaving motions of the two ships along with the exciting ocean wave (input signal), where it is apparent that for this wave orientation the two ships have comparable heave magnitudes.

Graph 4.1: Left: Heave motion of Sea Base. Right: Heave motion of T-Craft

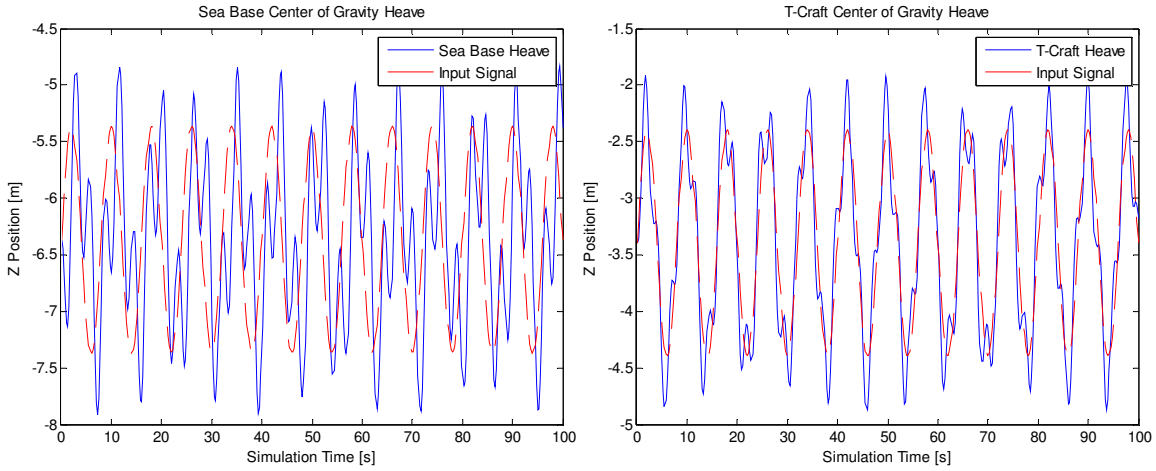

Both ships have complex heave motions which are combinations of many sinusoids. The dominant component of these sinusoids has the same frequency

of the exciting ocean wave but with a phase shift and a difference of amplitude that is a result of the dynamics of the system. In addition, there are some lower frequency components shown by the periodic motions that occur every 30 seconds as well as higher frequency components (especially in the Sea Base heave plot). The left plot in Graph 4.2 shows that surge (a degree of freedom that is not opposed by hydrostatic forces) develops for the T-Craft. A comparable amount of surge is also experienced for the Sea Base. On the right in Graph 4.2 is a plot of the pitch angle between the Sea Base and ramp which varies between ±5.5° with a maximum magnitude of 5.37°. This angle is dependent on quantities such as wave orientation, ship length, and ramp length. The input signal is superimposed to show that the dominant component of the pitch angle has the same frequency of the ocean waves but with a considerable phase shift. As with the heaves, this phase shift is a result of the dynamics of the system. It should be noted that the amplitude of the input signal is meaningless here as it is measured in meters while the pitch angle is measured in degrees.

Graph 4.2: Left: T-Craft surge. Right: Pitch angle between Sea Base and Ramp

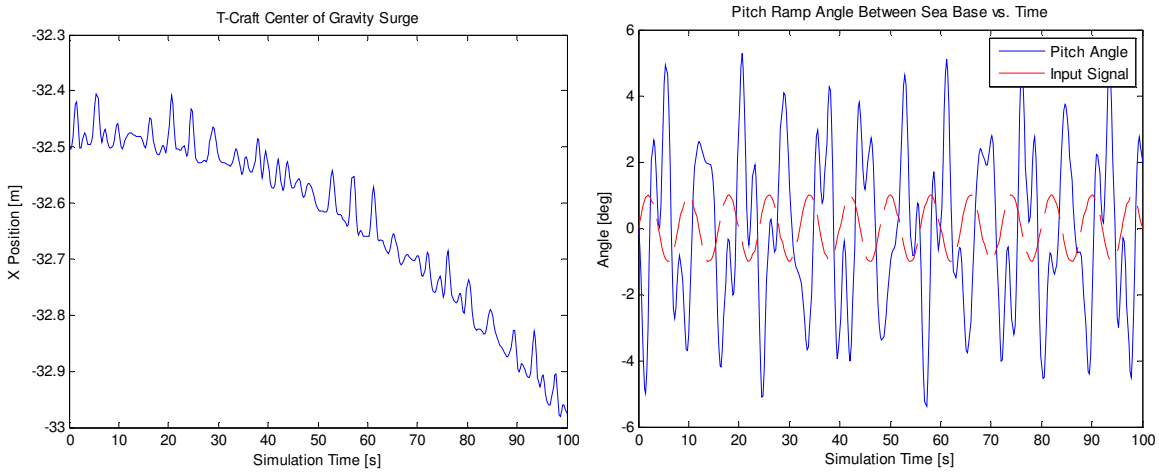

4.3 Case 3: Waves are 90° to Ship-Ramp-Ship Axis (Pitch in Joint)

Performing the simulation with the waves perpendicular to the ship-ramp-ship axis shows that now roll motions, although small, occur as would be expected. Since only pitch is allowed between the ramp and ships, the two ships roll together as one rigid body. While in Case 1 only surge was detected, here the ships undergo sway motions despite the fact that the forces act in the z direction. In fact, as the ships undergo sway, they also experience yaw as shown by the slightly non-horizontal alignment depicted in Figure 4.3 (the system experiences yaw as one rigid body since the joints only allow for pitch). In addition, the simulations show that surge is negligible (the little surge that does occur is induced by yaw), and that the ships heave up and down without pitch.

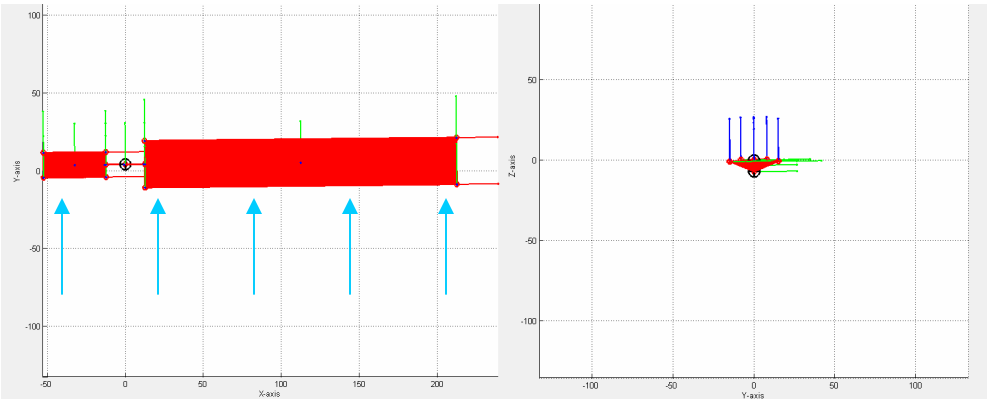

Figure 4.3: Left: View along the x-y plane. Right: View along the y-z plane. Waves approach in direction indicated by cyan arrows

The heave motions are provided in Graph 4.3, where it is noted that these motions are measured with respect to the center of gravity. With the waves approaching from this orientation, the heave motions are reduced drastically for the T-Craft: down from a magnitude of 2.8 meters in the previous section to only

0.8 meters. The Sea Base is less affected by the change in orientation, as the heave only decreases by 0.1 meters. Once again, the dominant component of the heave motions has the same frequency of the excitation waves (input signal).

Graph 4.3: Left: Heave motion of Sea Base. Right: Heave motion of T-Craft

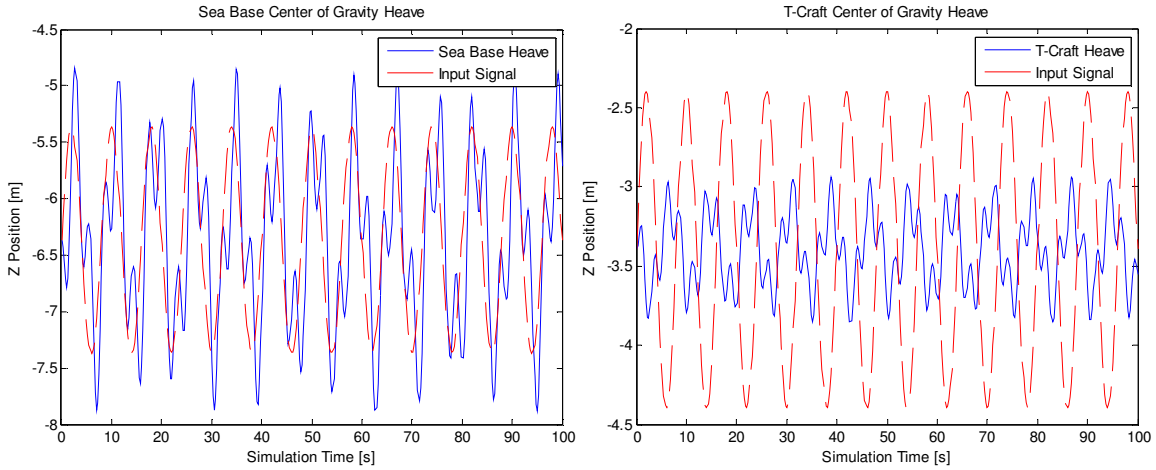

The ships now experience sway instead of surge as evident by Graph 4.4 which shows the sway of the T-Craft. The net sway of the Sea Base is comparable, but slightly larger. The sway is due to the waves approaching in the perpendicular direction but also to the yaw. In addition, Graph 4.4 shows that the pitch angles have been reduced and now vary between ±4° with a maximum value of 4.42°.

Graph 4.4: Left: T-Craft sway. Right: Pitch angle between Sea Base and Ramp

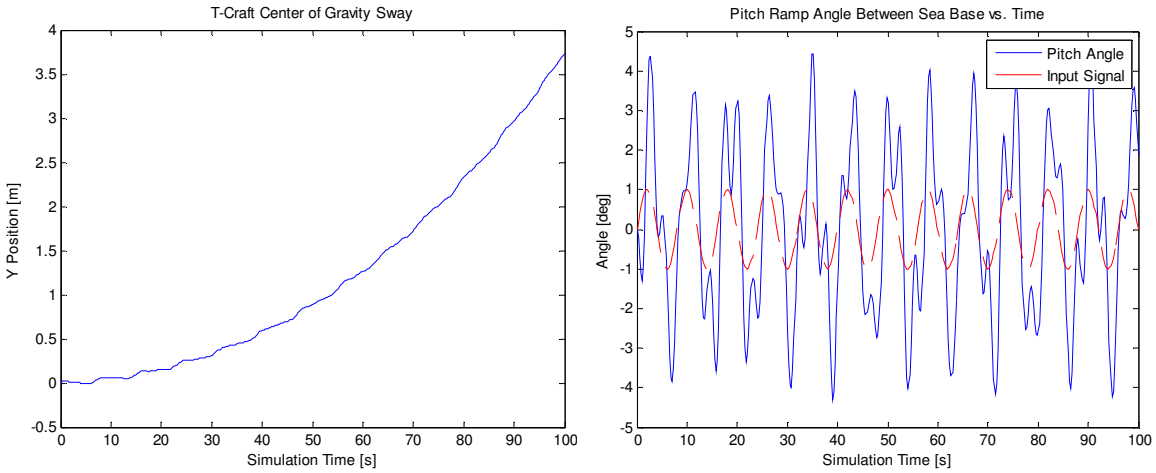

4.4 Case 2: Waves are 45° to Ship-Ramp-Ship Axis (Pitch in Joint)

Simulation results with the waves coming in at a 45° angle to the ship-ramp-ship axis show that more motions are observed than in the previous cases. Due to the waves approaching at this intermediate angle, the system begins rotating clockwise. The reason for the rotation is largely due to the fact that the T-Craft is of much smaller mass, size, and inertia that the Sea Base, and is thus more readily affected by the waves. The greater sway and surge displacements for the T-Craft than those for the Sea Base are evidence of this fact. This disparity in surge and sway magnitudes in turn causes the system to rotate.

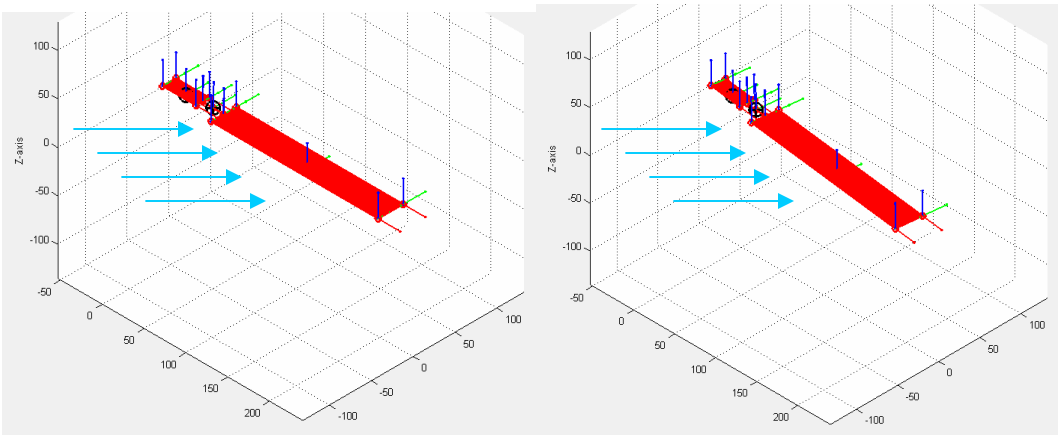

Figure 4.4: 3-Dimensional view showing the clockwise rotation of the system. Waves approach in direction indicated by cyan arrows

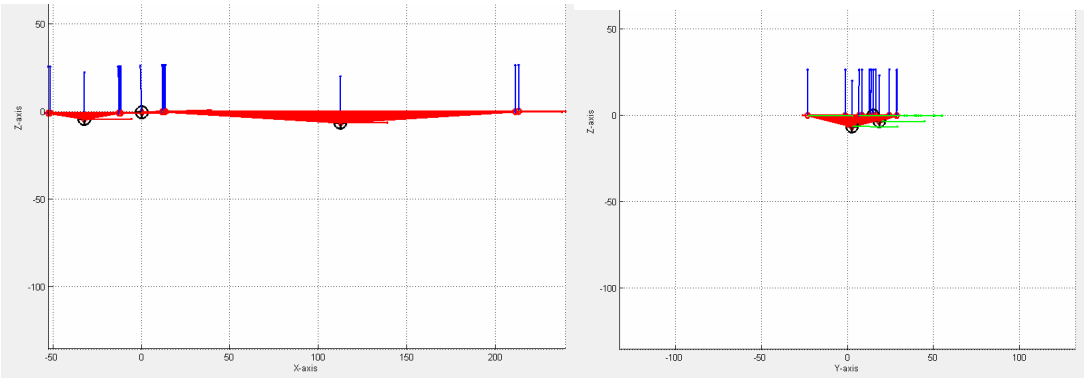

Figure 4.5: Left: x-z plane showing pitch. Right: y-z plane showing yaw and roll
(It is easier to see pitch and roll during a running simulation)

In addition to the net rotation, it is apparent that all of the rotational degrees of freedom: pitch, roll, and yaw are active upon the entire system as illustrated in Figure 4.5 above (although the pitch and roll motions are small and quite hard to detect). The surge and sway motions that were discussed as they pertained to the rotation of the system are included below for the T-Craft. While the T-Craft has a net surge of about 1 meter and a net sway of 20 meters, the surge and sway values for the Sea Base are only -0.02 and 2.9 meters respectively.

Graph 4.5: Left: Surge motion of T-Craft. Right: Sway motion of T-Craft

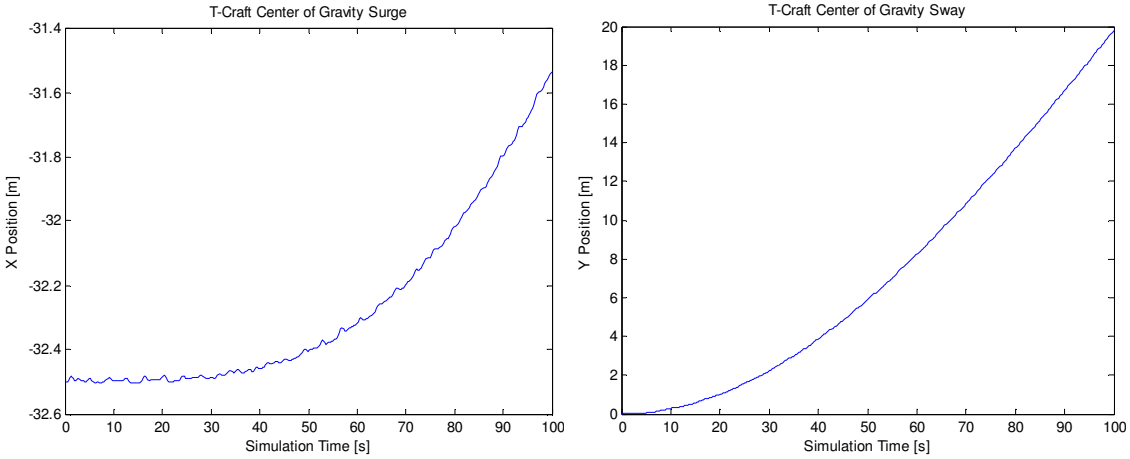

Included in Graph 4.6 on the following page are the heave motions of the Sea Base and T-Craft. The T-Craft has a larger heave of 1.7 meters, whereas the Sea Base has a heave of only about 0.4 meters. The T-Craft heave is larger than in the previous case (perpendicular waves) but smaller than the first case (parallel waves). On the other hand, for the Sea Base this is clearly the case with the smallest heave values. It seems that it would be reasonable to think that with the waves oriented further from the ship-ramp-ship axis, the heaves should be reduced (i.e. smallest in Case 3). However, the ratio between the length of the

ships and the wavelength of the ocean wave must also be taken into consideration. Recall that when the length of the ship is divisible (or nearly) by the wavelength, the ship will heave up and down without tilt. This type of relationship affects the heave since pitch motions are known to induce heave.

Graph 4.6: Left: Heave motion of Sea Base. Right: Heave motion of T-Craft

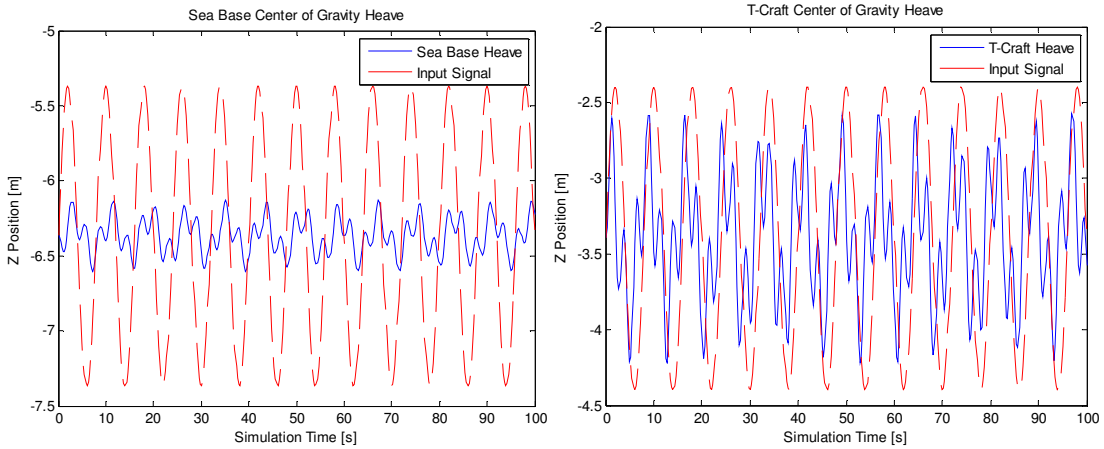

The same observation can be made about the pitch angle evolution shown below in Graph 4.7. The pitch angles between the Sea Base and ramp now only vary between ±2° with a maximum of 2.22°. Hence, we get the surprising result (a consequence of the ship length to wavelength ratio) that a perpendicular wave does not always attenuate the pitch angles the most.

Graph 4.7: Pitch angle between Sea Base and Ramp

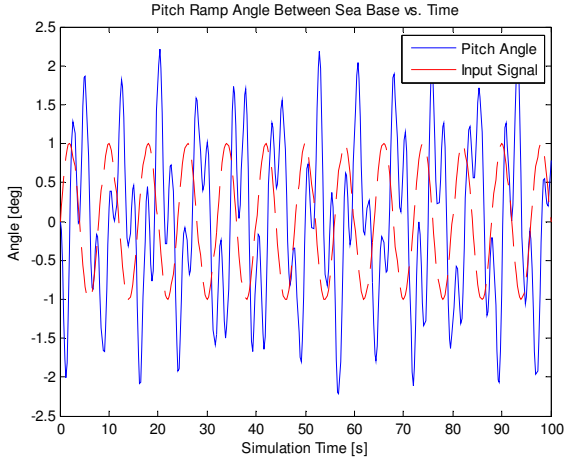

4.5 Case 3: Waves are 90° to Ship-Ramp-Ship Axis (Pitch and Roll)

The simulation is performed with the waves perpendicular to the ship-ramp-ship axis, but now allowing for pitch and roll in the joints (without springs to hinder these motions). The visualizations in Figure 4.6 (which use a larger wave to highlight the motions) below show that roll is now experienced in the joint. Before the ships rolled together; however, now they are allowed to roll at different rates due to an extra degree of freedom being added to the joint. As was the case when using the pitch-only joint for this wave orientation, there is still a slight amount of yaw experienced by the total system (but not between the ships and ramp). This causes a small amount of rotation as depicted in Figure 4.7.

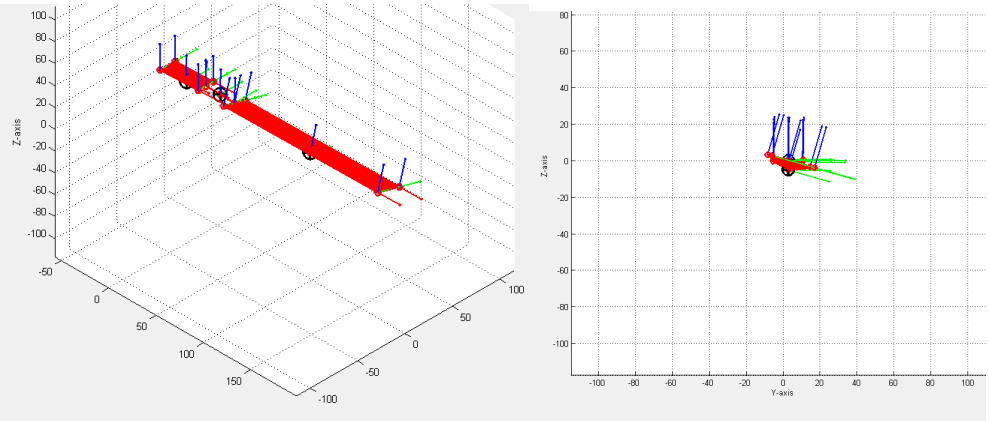

Figure 4.6: Left: 3-D view. Right: View along the y-z plane (all motions are exaggerated)

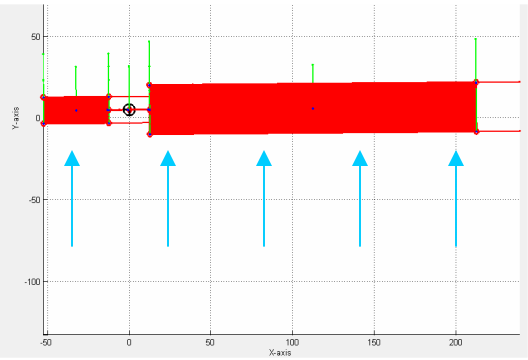

Figure 4.7: View along the x-y plane.

It is immediately obvious that the rotation shown in Figure 4.7 is considerably less than the 45° case. This is due to the fact that the difference between the sway motions of the two ships is not as great. As an aside, it should be noted that rotation can still occur if the sway magnitudes of the two ships are equal but opposite in sign. The surge and sway of the T-Craft are depicted in Graph 4.8, where it is noted that the surge is comparable to the previous 90° case. Because of the extremely small values and periodic nature of the surge, it is likely that this motion is induced by the combination of roll and yaw (the roll can affect the surge motions due to the rotation of the system from the presence of yaw). The T-Craft sway is increased by about 1 meter from the 90° case with the other joint. The Sea Base still has a slightly larger sway (now ~6 meters) than the T-Craft and exhibits negligible surge. This difference in sway values of the two ships is what contributes to the yaw motions that were previously observed. The reason for this discrepancy is due to the size and mass differences of the two ships. Also, the fact that the sway values of the ships have changed compared to the previous joint can be attributed to the ships now being able to roll at different rates.

Graph 4.8: Left: Surge motion of T-Craft. Right: Sway motion of T-Craft

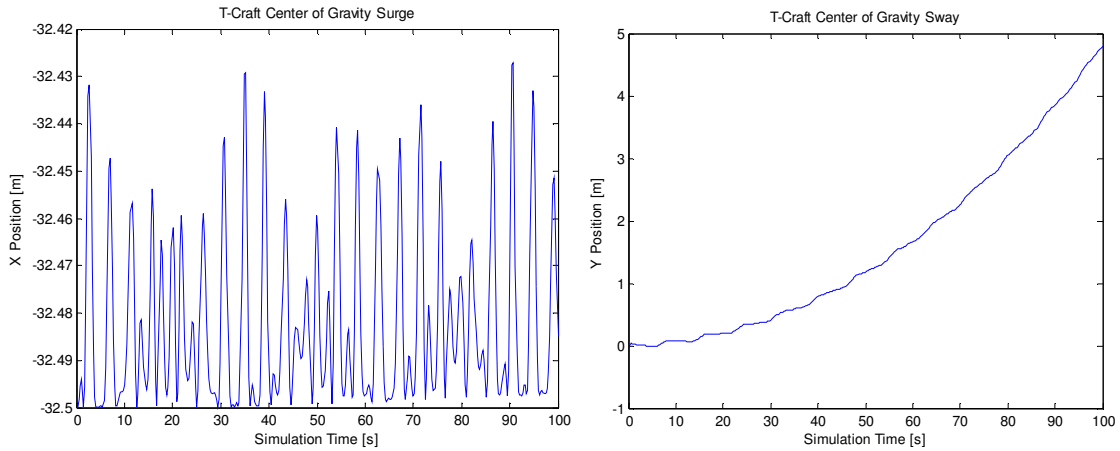

The heave motions of both ships are shown below in Graph 4.9. Upon comparison with Graph 4.3, it obvious that these heaves are extremely similar to the heave motions with this same wave orientation but using the pitch-only joint.

Graph 4.9: Left: Heave motion of Sea Base. Right: Heave motion of T-Craft

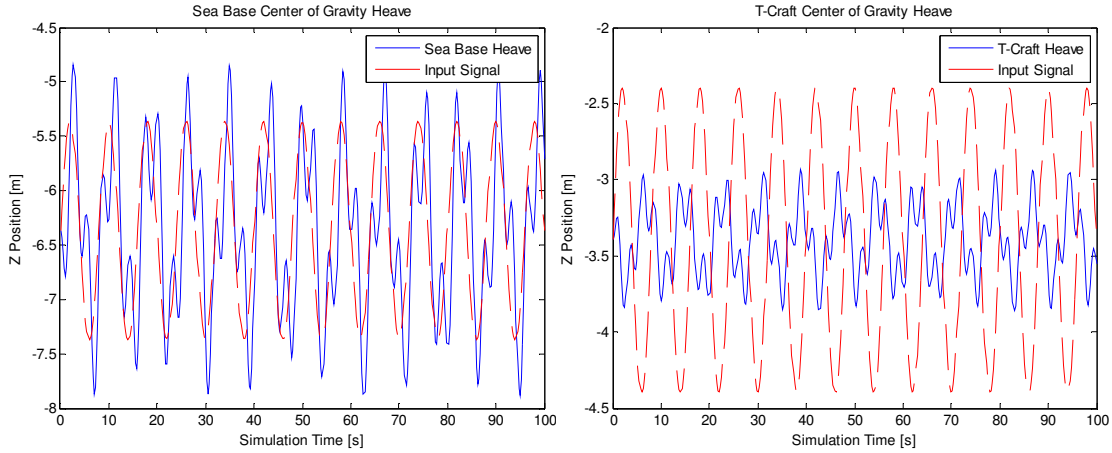

The joint now allows for both pitch and roll motions to occur between the ships and the ramp, as evident by Graph 4.10 below. The pitch angles are basically the same as before, varying between ±4° with a maximum value of 4.43° (increased by 0.01°). The roll angles are quite small, ranging between ±0.6° with a maximum value of 0.70°. The roll motions are almost completely a single sinusoid with the same frequency of the ocean wave but with a phase shift.

Graph 4.10: Left: Ramp pitch angle. Right: Ramp roll angle

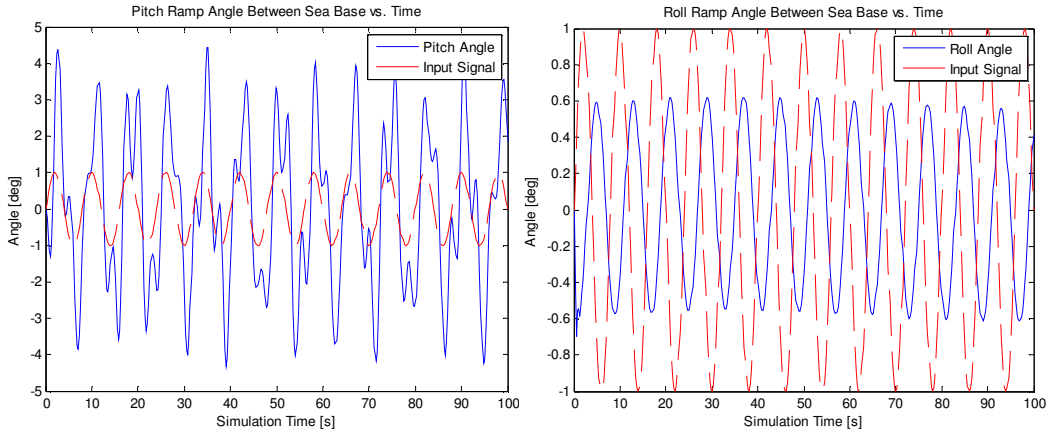

4.6 Case 3: Waves are 90° (Pitch and Roll with Springs on Roll Motions)

A similar scenario to that in Section 4.5 is explored here, with the waves approaching perpendicular to the ship-ramp-ship axis, but now with a torsional spring inserted for the roll motions. For simplicity, the spring constant is given the value of 500,000 (which is considerably less than the spring constants used for gravity and buoyancy). The purpose of this spring is to attenuate the roll motions that were observed in Graph 4.10. However, the roll motions between the ships and the ramps are not at all constrained, as can be observed in Graph 4.11.

Graph 4.11: Left: Ramp pitch angle. Right: Ramp roll angle

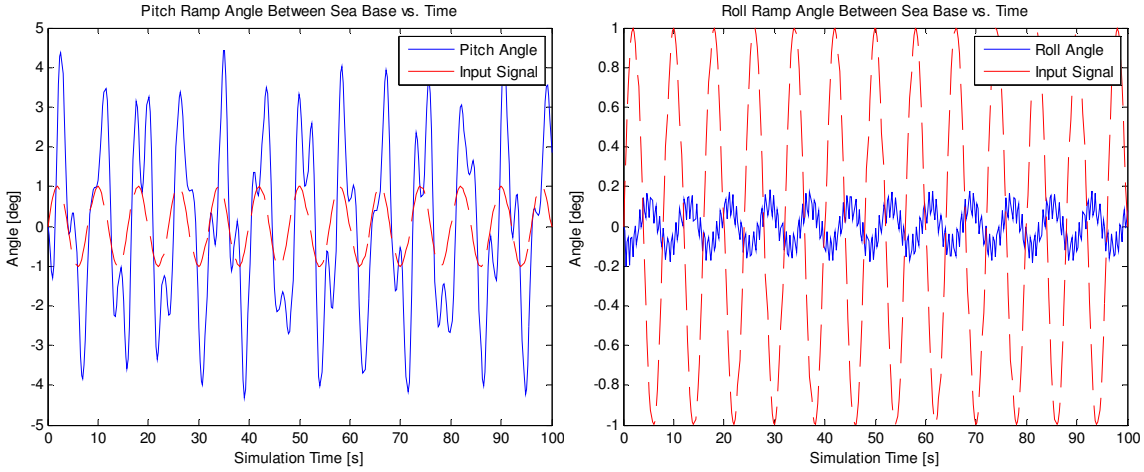

While the tendency for the ships to want to roll at different rates has not been eliminated from this choice of spring constant, the ship-ramp roll angles have clearly been reduced. The presence of the spring has also introduced an additional high frequency component to the time evolution of the roll. Here, the roll angles vary between ±0.2° with a maximum value of 0.20°, which is down from 0.70° when no spring was used. Interestingly, the pitch motions are almost

identical, with a maximum value of 4.43°. In fact, the heave, surge, and sway motions are all nearly the same as without the spring. Therefore, it can be concluded that introducing a spring to decrease the roll motions has little effect on the other motions of the ships. The little differences that do exist are most likely due to components of the motions that are induced from the roll of the ships. Since the total roll of the system and the relative roll between the ships and ramp are always very small for these simulations, the induced effects of roll on other motions are minimal. Graph 4.12 shows the heave plots of the two ships, whereas the sway of the Sea Base and T-Craft are plotted in Graph 4.13.

Graph 4.12: Left: Heave motion of Sea Base. Right: Heave motion of T-Craft

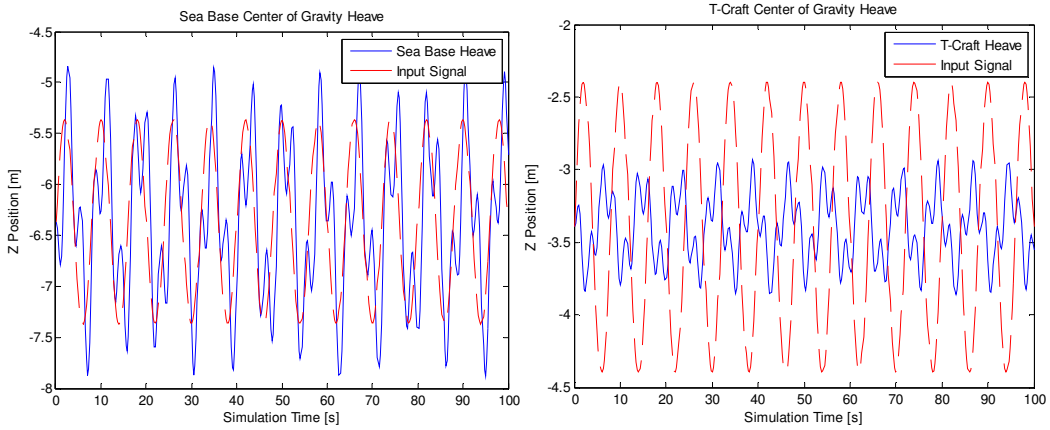

Graph 4.13: Left: Sway motion of Sea Base. Right: Sway motion of T-Craft

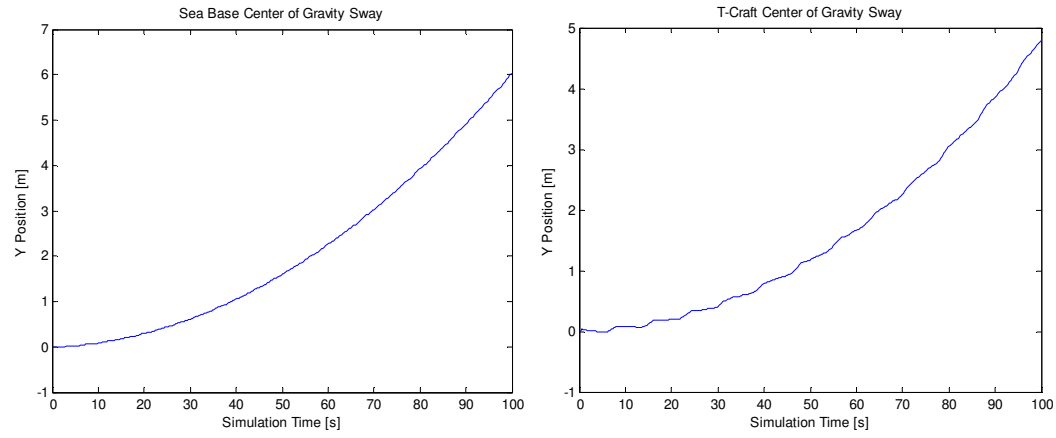

4.7 Case 2: Waves are 45° to Ship-Ramp-Ship Axis (Pitch and Roll)

Now we revert back to using the pitch and roll joint without any springs, and instead introduce the 45° wave orientation into the simulation. Similar to when the pitch-only joint was utilized for this case, there is a significant amount of clockwise rotation experienced by the system. This fact is depicted in Figure 4.8.

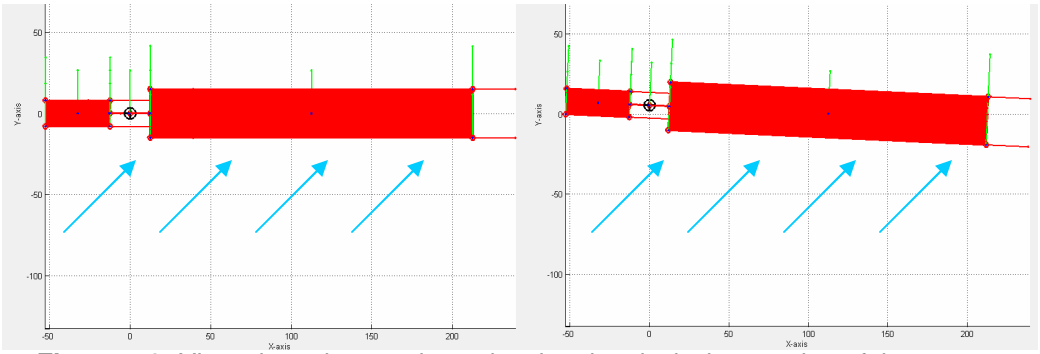

Figure 4.8: View along the x-y plane showing the clockwise rotation of the system

Also, as before when the waves were at a 45° angle using the pitch-only joint, all six ship motions are easily observed. The most significant difference is that the two ships are now allowed to roll at different rates due to the addition of a joint that allows for both pitch and roll. This fact is obvious from Figure 4.9, where the motions are exaggerated by using a larger wave to highlight this important fact.

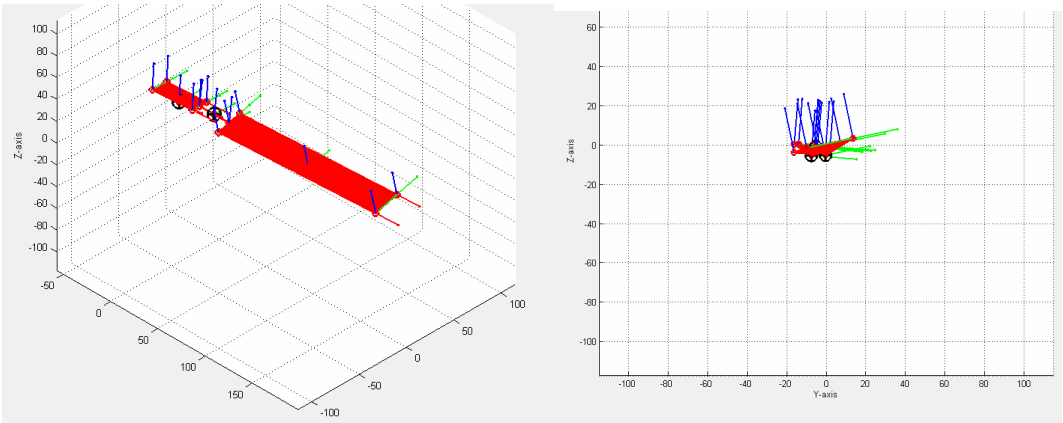

Figure 4.9: Left: 3-D view. Right: View along the y-z plane (all motions are exaggerated)

It was discovered in the 90° case that when transitioning from using a pitch-only joint to a joint that also allows for roll, the sway of the two craft were affected. Whereas with that orientation the addition of the roll degree of freedom in the joint only altered the net sway displacements by about 1 meter each, the joint now has a greater influence. As evident from Graph 4.14, the net sway of the T-Craft is only 7 meters, down from 20 meters when using the other joint (for the same 45° wave orientation). The Sea Base is also significantly affected, as the sway has decreased from 2.9 meters with the pitch-only joint to only 0.32 meters. However, now the magnitudes of surge are affected as well. The T-Craft surge has decreased by 0.83 meters while the Sea Base surge has switched directions.

Graph 4.14: Left: Sway motion of Sea Base. Right: Sway motion of T-Craft

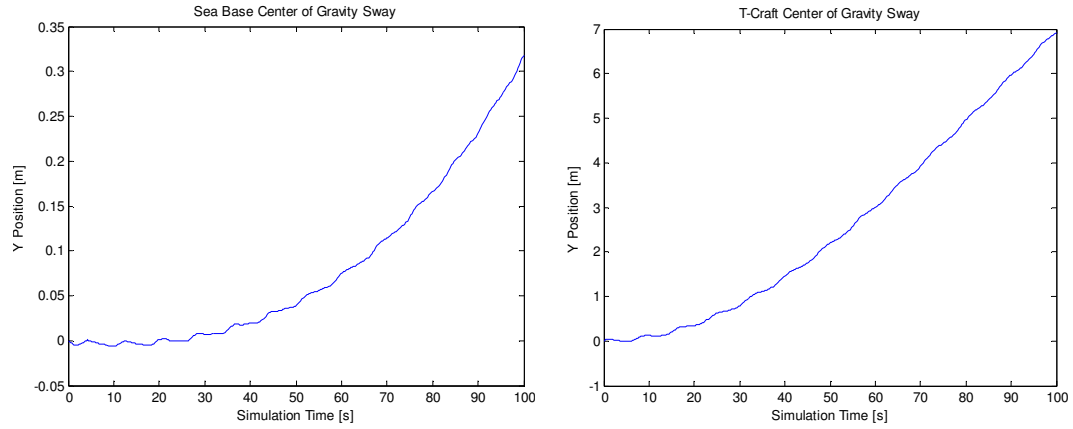

Graph 4.15: Left: Surge motion of Sea Base. Right: Surge motion of T-Craft

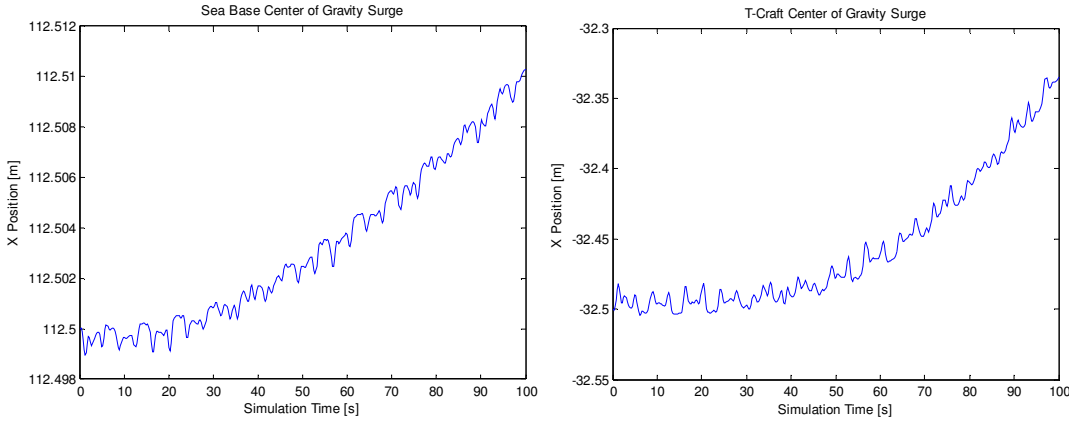

The reasons for the changes in the surge and sway motions when implementing this new joint can be attributed to the fact that the ships are now allowed to roll at different rates. This same observation was made for the 90° case, except then the surges were less affected as they were extremely small to begin with. It was also found in the 90° case that the heaves of the two ships were not considerably altered by the pitch-roll joint. Graph 4.16 shows that the same can be said here:

Graph 4.16: Left: Heave motion of Sea Base. Right: Heave motion of T-Craft

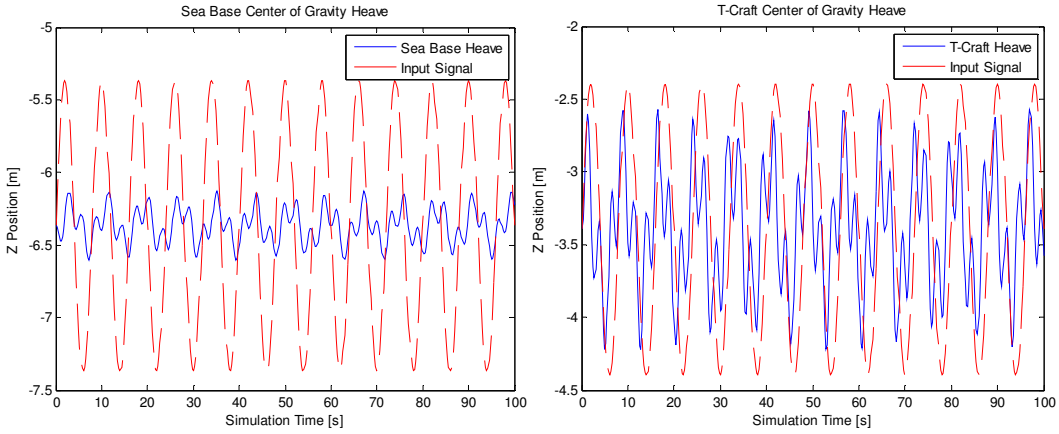

Graph 4.17 includes the plots of the pitch and roll angles between the Sea Base and ramp. The maximum pitch is now 2.20° instead of 2.22° when using the pitch-only joint, whereas the new roll angle has a maximum value of 0.60°.

Graph 4.17: Left: Ramp pitch angle. Right: Ramp roll angle

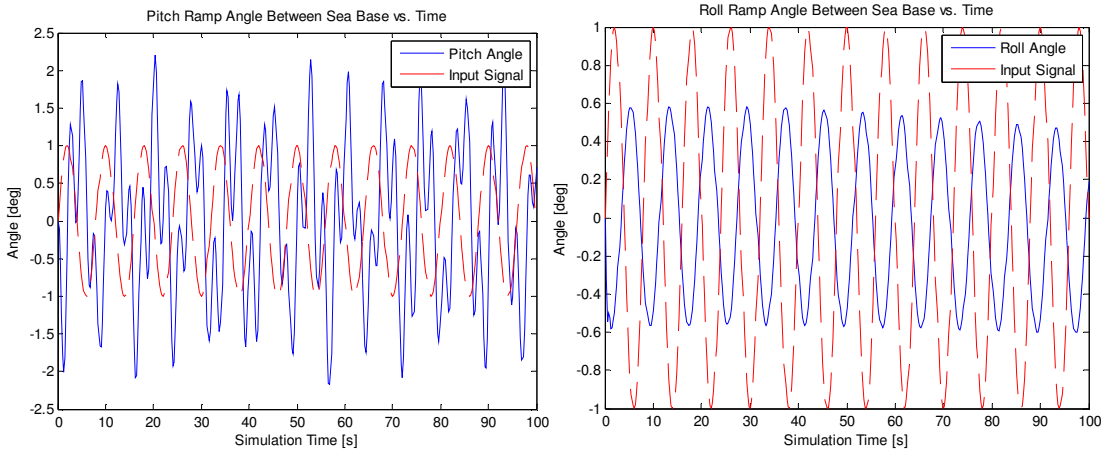

4.8 Case 2: Waves are 45° (Pitch and Roll with Springs on Roll Motions)

A similar scenario to that in Section 4.7 is explored here, with the waves approaching at a 45° angle to the ship-ramp-ship axis, but now a torsional spring is inserted for the roll motions. As in Section 4.6 when the spring was used for the 90° case, the purpose of this spring is to attenuate the roll motions between the ships and the ramp. Graph 4.18 shows that the Sea Base-ramp roll angles now only vary between ±0.25° with a maximum of 0.31°. Without the spring, this maximum angle was 0.60°. It is important to note that the decrease from using the spring with this orientation is 0.29°, whereas the decrease from using the spring in the 90° case is 0.5°. Therefore, it seems that the springs are more efficient at decreasing the roll angles for the perpendicular orientation. Furthermore, as a consequence of this, the roll angle is smaller for the 90° case when using a spring, but without a spring the roll angle is smaller in the 45° case. Graph 4.18 also shows that the ship-ramp pitch angle has remained unchanged.

Graph 4.18: Left: Ramp pitch angle. Right: Ramp roll angle

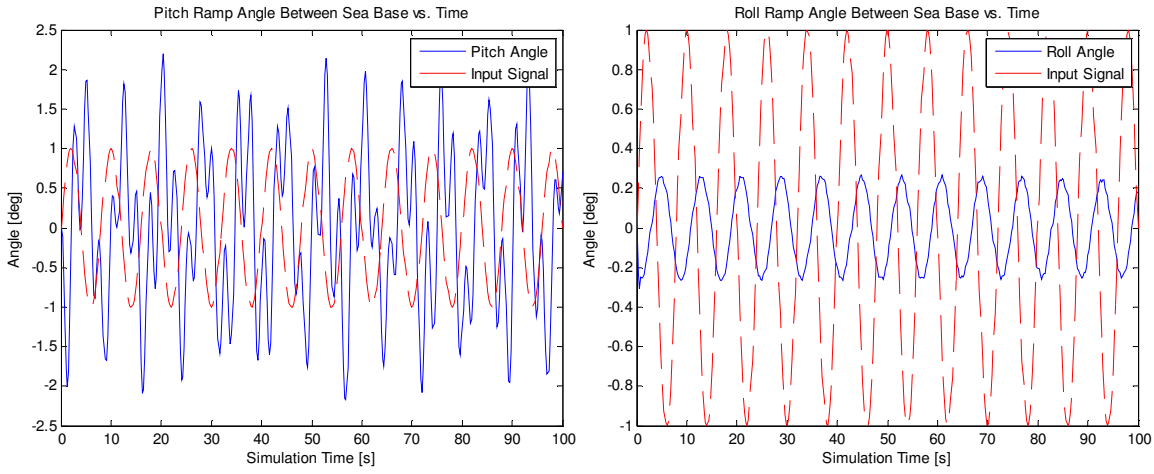

In Section 4.6 it was noted that the addition of the torsional spring on roll motions has very little influence on other motions. The same is true here, as both the sway plots in Graph 4.19, and the heave plots in Graph 4.20 are very similar to those when no spring is used. In Section 4.6 it was also postulated that the changes that do occur when using the spring are mostly due to the influence the roll has on certain aspects of the other motions. Since the roll magnitudes of the ships themselves as well as the roll between the joints are both very small for this wave orientation, the effects of the roll on other motions must also be very small.

Graph 4.19: Left: Sway motion of Sea Base. Right: Sway motion of T-Craft

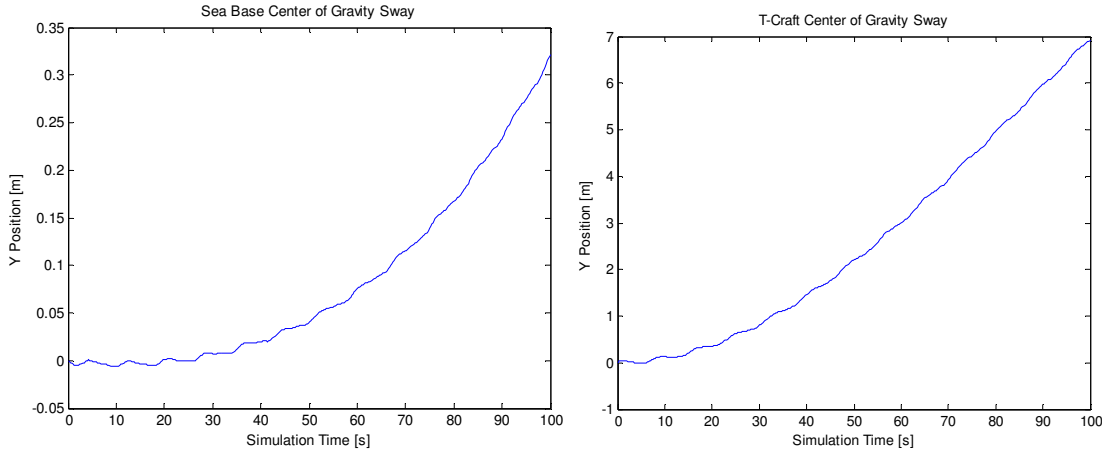

Graph 4.20: Left: Heave motion of Sea Base. Right: Heave motion of T-Craft

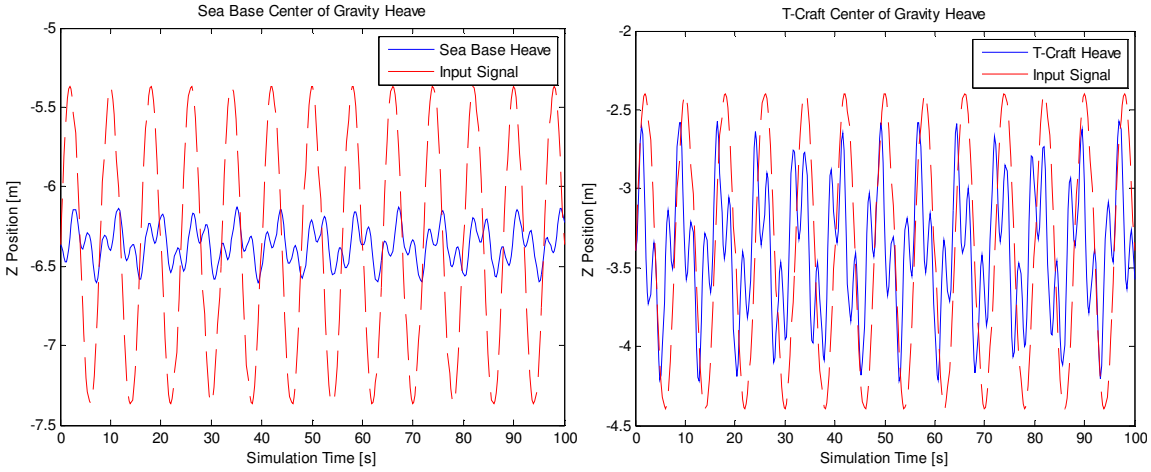

4.9 Case 3: Waves are 90° (Pitch, Roll, and Yaw with Springs on Roll and Yaw Motions)

The last joint that will be investigated is a gimbal joint that allows for all of the rotational degrees of freedom to occur between the ships and the ramp. Torsional springs are used for the roll and yaw motions, although the spring constant will be decreased to only 50,000 in order to better examine the effect of this additional degree of freedom. Figure 4.10 shows the system at two different times, where it is apparent that there is now a yaw angle between the ships and ramp. Before, when no yaw was allowed in the joint, there was a slight rotation of the entire system for this wave orientation. In Figure 4.10, the system still appears to rotate, although now the ships are allowed to rotate at different rates due to yaw in the joint. It is also interesting to note that the rotation of the system is a combination of the usual counterclockwise rotation (observed for all of the 90° angle scenarios) and the effects of the new yaw motions from this joint.

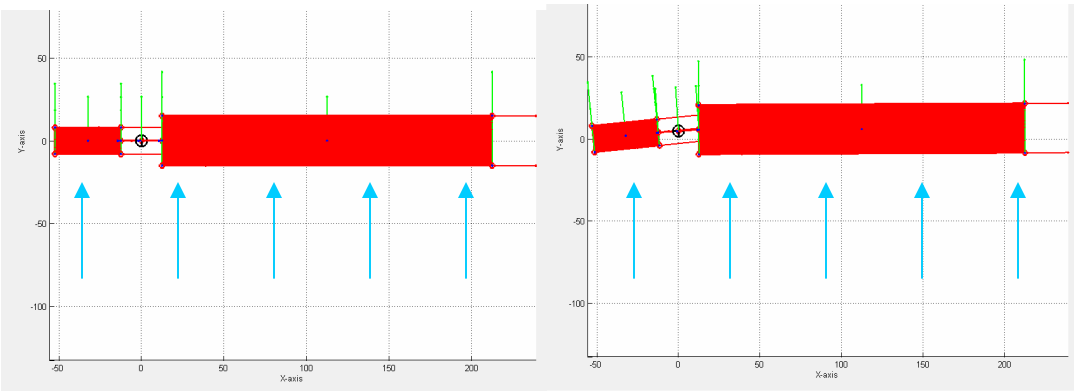

Figure 4.10: View along the x-y plane showing the yaw between the ships and ramp

As would be expected, the surge and the sway are slightly different when using this new joint. Graph 4.21 shows the net sway displacements experienced by

both the Sea Base and T-Craft. The Sea Base sway has increased by about 0.2 meters when using this joint as opposed to the joint with pitch and roll. The T-Craft sway is affected even more, as it is only 2 meters instead of the 4.9 meters before. It is obvious from Figure 4.10 that a great deal of this sway is due to the yaw rotation rather than a translational displacement. Furthermore, it can be concluded that the T-Craft sway is now only 2 meters because the entire system wants to move in the positive y direction (as before with any of the other joints), but the yaw causes the T-Craft center of gravity to move in the negative y direction, thus resulting in a canceling effect. This same basic idea can be attributed to the slight increase in the Sea Base sway. The yaw angle of the Sea Base and ramp has an opposite sign from that of the T-Craft and ramp, meaning that the yaw here causes the Sea Base center of gravity to move in the positive y direction - the same direction of the translational movement.

Graph 4.21: Left: Sway motion of Sea Base. Right: Sway motion of T-Craft

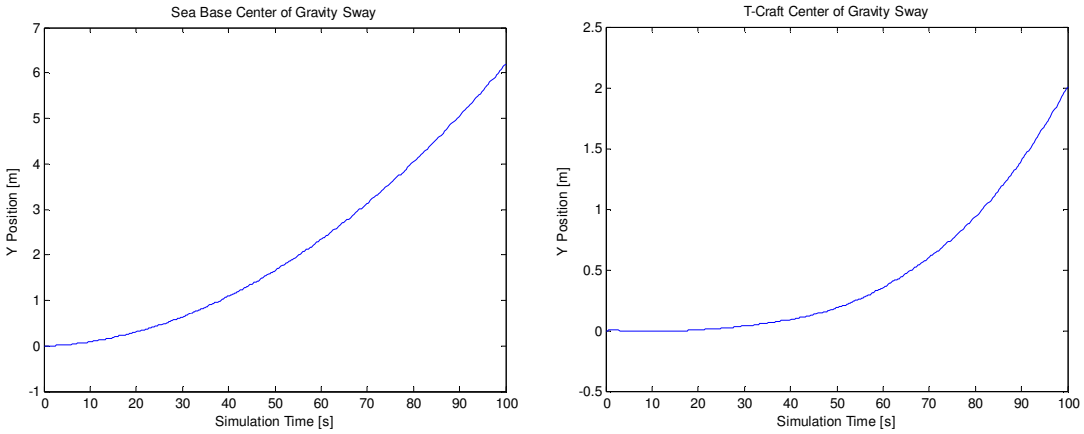

Graph 4.22 shows that the surge values have also changed when compared to those from the pitch-roll joint. However, the surge magnitudes are still quite small, and are mostly a result of motions induced from pitch, roll, and yaw.

Graph 4.22: Left: Surge motion of Sea Base. Right: Surge motion of T-Craft

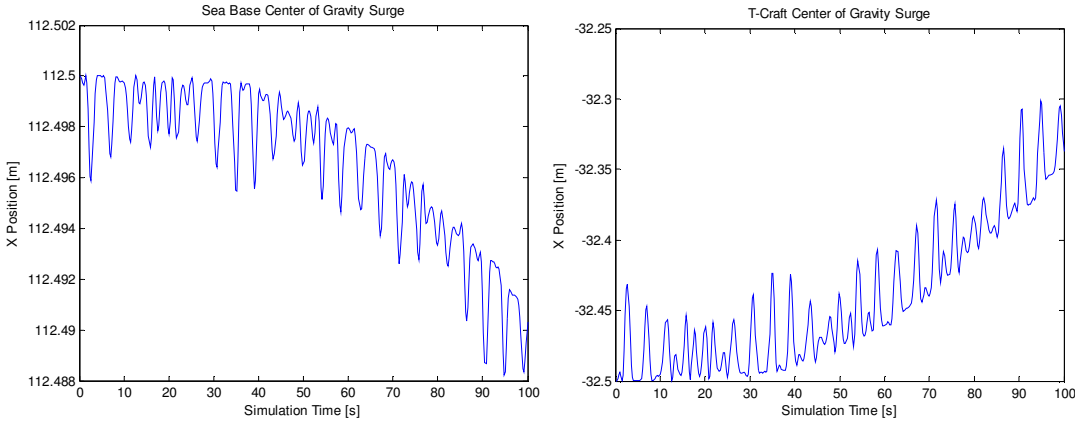

Unlike the surge and sway, the heave motions shown in Graph 4.23 are relatively unaffected. In fact, the Sea Base and T-Craft heaves are nearly identical to the case when the pitch-roll joint was used. One possible reason for this is that yaw is a degree of freedom that acts perpendicular to the heave motions, and thus fails to have any considerable effect. Instead, the addition of yaw has a larger effect on motions along its plane of action, namely surge and sway.

Graph 4.23: Left: Heave motion of Sea Base. Right: Heave motion of T-Craft

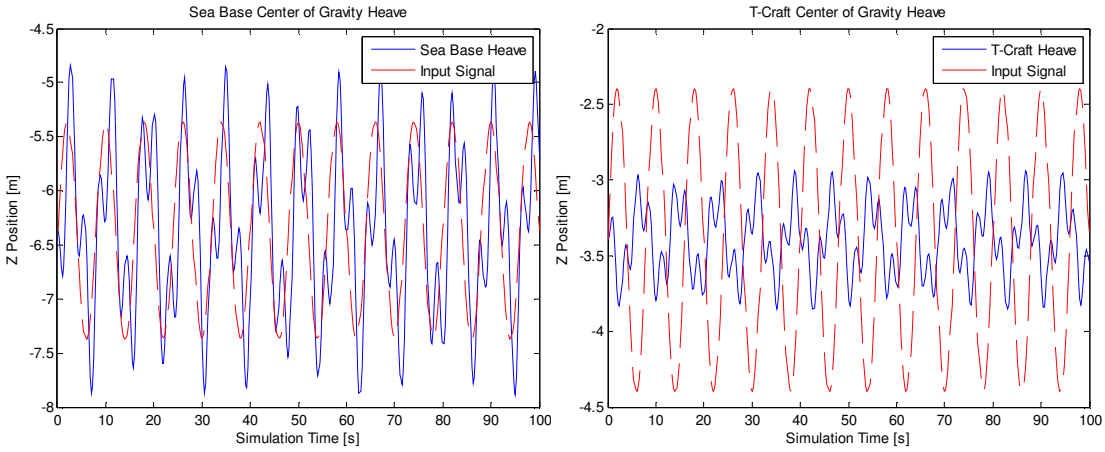

Along with the heave motions, the ship-ramp pitch angles are not greatly influenced by the addition of yaw. Graph 4.24 contains a plot of the Sea Base-ramp pitch angle that shows the maximum value to be 4.43°. This is nearly the same value that was found when using the joint that allowed for pitch and roll.

The roll motions are different now, varying between ±0.25° with a maximum angle of 0.33°. This value is up from the 0.20° when using the pitch-roll joint with springs. The reason for the different roll motions is not due to yaw but to the smaller spring constant that was used in this joint. When considering the pitch-roll joint, the spring constant was 500,000. However, here we are using a spring constant of 50,000, which naturally results in a larger range of roll values. The yaw angles of both the Sea Base with the ramp and the T-Craft with the ramp are provided below in Graph 4.25. It is apparent that the angles have different signs, a fact that was just discussed as it pertained to the changes in sway motions.

Graph 4.24: Left: Ramp pitch angle. Right: Ramp roll angle

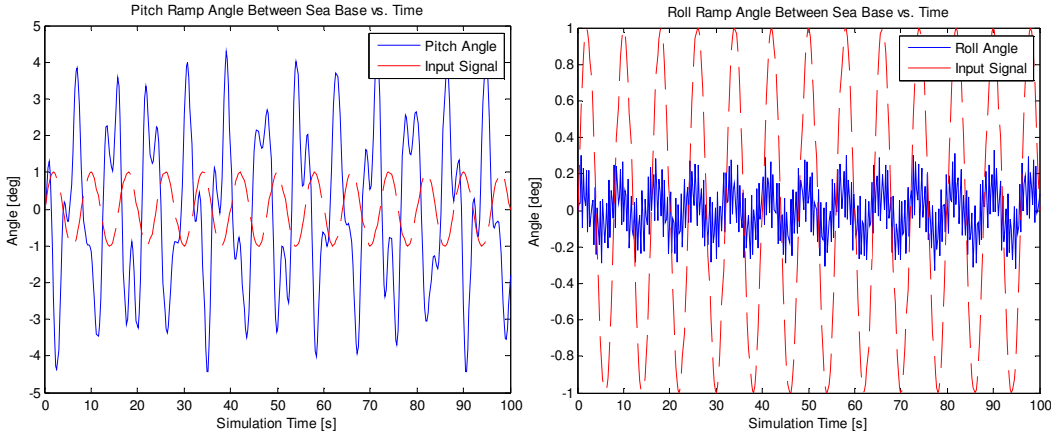

Graph 4.25: Left: Sea Base and ramp yaw angle. Right: T-Craft and ramp yaw angle

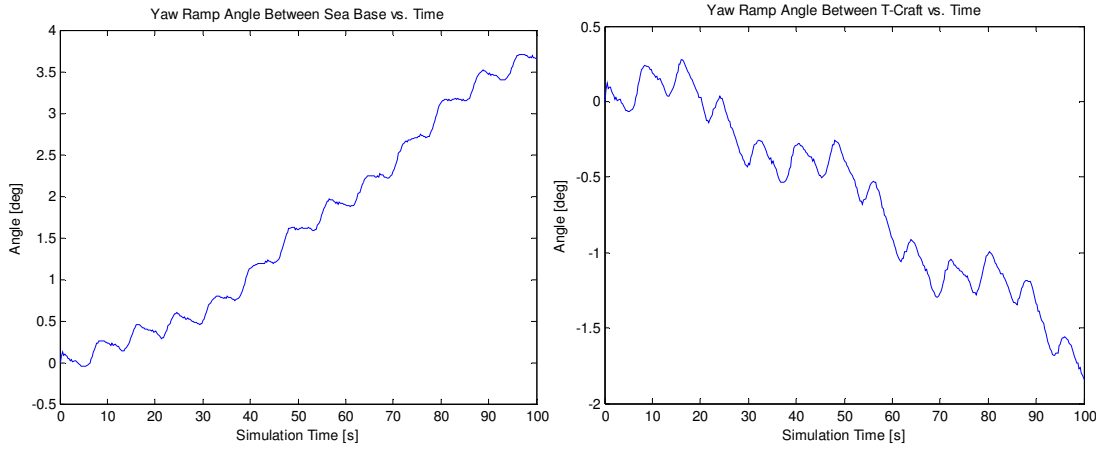

4.10 Case 2: Waves are 45° (Pitch, Roll, and Yaw with Springs on Roll and Yaw Motions)

Once again, the joint with all of the rotational degrees of freedom is allowed, but this time the waves are oriented at a 45° angle to the ship-ramp-ship axis. As was the case with the previous scenarios studied for this wave orientation, the system experiences considerable clockwise rotation shown in Figure 4.11. The yaw motions that are now allowed between the joints that connect the ships with the ramp can also be easily observed. The amount of rotation that is experienced by the system is affected by these yaw motions. This is because the yaw motions affect the surge and sway of the ships, which then in turn influence how much the system will appear to rotate.

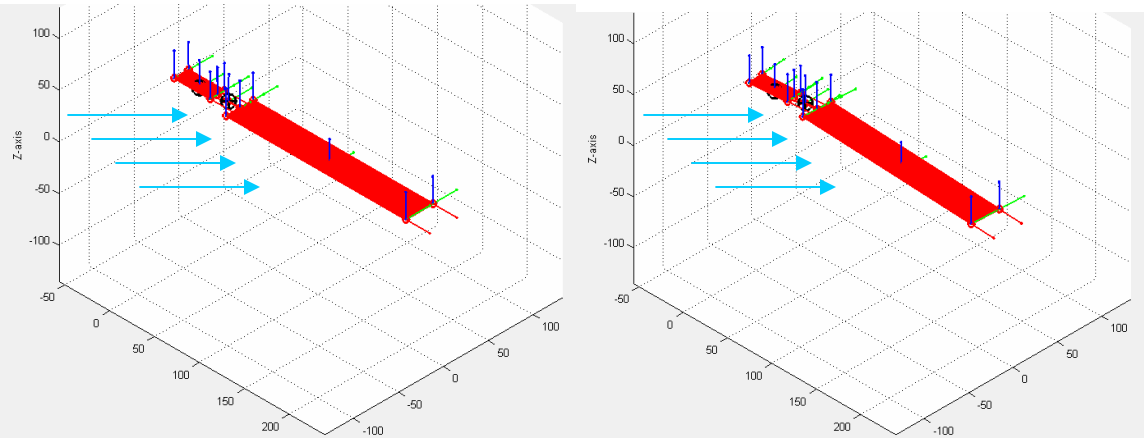

Figure 4.11: 3-Dimensional view showing the yaw between the ships and ramp

In order to better quantify the impact the yaw motions have on the system, Graph 4.26 is provided below which shows the angles between both the Sea Base and ramp and the T-Craft and ramp. In the previous section (waves at a 90° orientation) the yaw angle between the Sea Base and ramp was positive, and

thus resulted in an increase in the total sway experienced by that ship. The exact opposite case was present for the T-Craft, instead causing a decrease of the sway. The same can be said here, in that the yaw angle between the Sea Base and ramp, which reaches up to 5.2°, results in an increase of sway from 0.32 meters (when using the pitch-roll joint) to now 0.55 meters. Likewise, the negative yaw ramp angle for the T-Craft decreases the sway from 7 meters with the pitch-roll joint to only 3.1 meters. To help illustrate these facts, the evolution of the sway with time for both ships is included below in Graph 4.27.

Graph 4.26: Left: Sea Base and ramp yaw angle. Right: T-Craft and ramp yaw angle

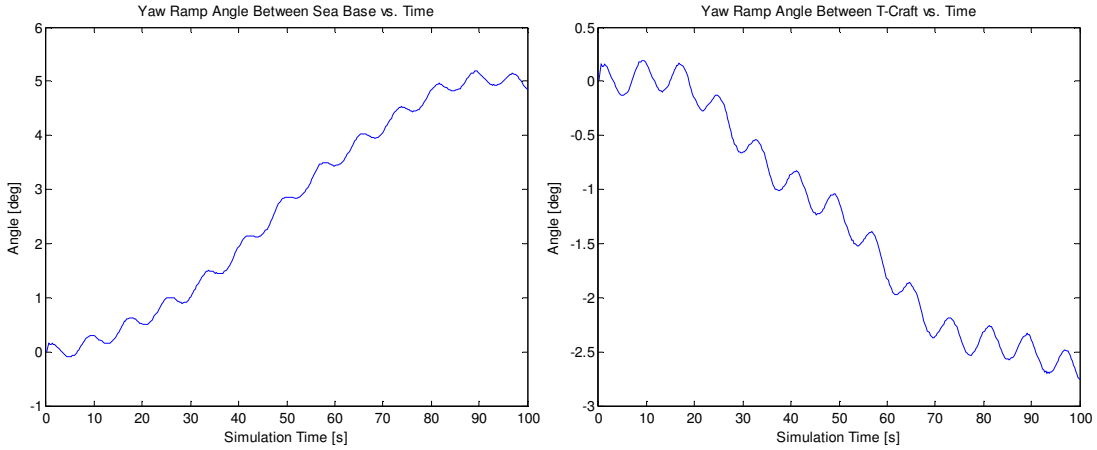

Graph 4.27: Left: Sway motion of Sea Base. Right: Sway motion of T-Craft

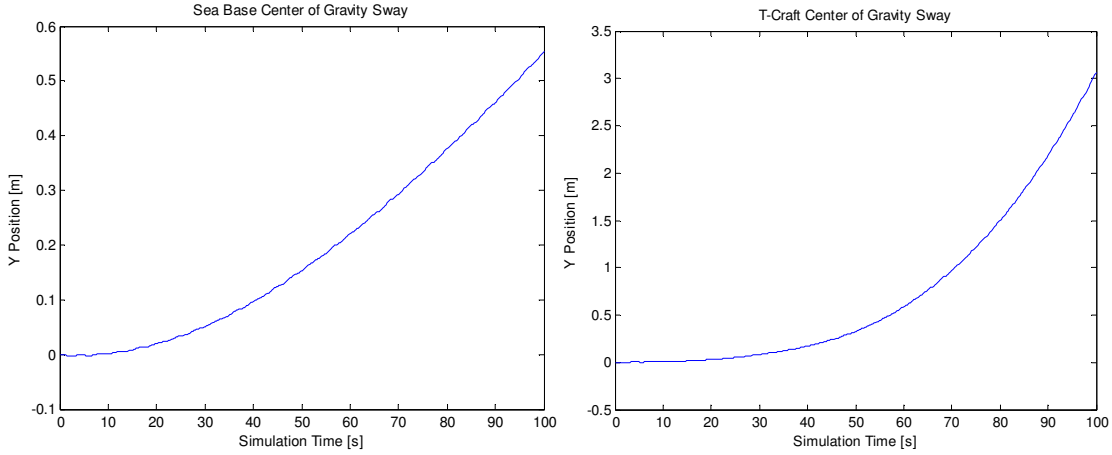

The surge of the ships is also affected by the introduction of yaw in the joint; however, these motions are of less importance due to their already small magnitudes. Nevertheless, Graph 4.28 is included below to show the surge values of both ships, where it is apparent that once again the higher frequency periodic type motions are present. This behavior is due to motions induced from pitch, roll, and yaw. When compared to the previous pitch-roll joint, the surge of the Sea Base has decreased by 0.001 meters whereas the surge of the T-Craft has increased by 0.06 meters. A decrease in Sea Base surge and increase in T-Craft surge was also observed in the previous section using the 90° wave orientation. However, it should be clarified that the absolute value of the Sea Base surge increased in that case due to the surge having a negative sign.

Graph 4.28: Left: Surge motion of Sea Base. Right: Surge motion of T-Craft

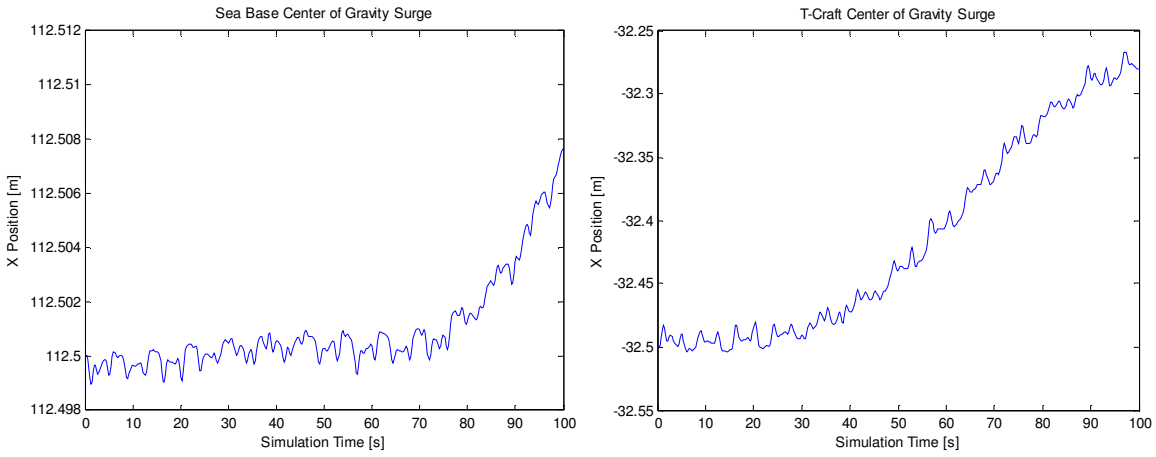

In the previous section, it was reasoned that the new degree of freedom in the joint should have little influence on the heave motions. Graph 4.29 on the next page shows that the heave motions of the two craft are extremely similar to the motions when using the previous joint. This seems to further validate the conclusion that heave is not significantly affected by yaw in the joints.

Graph 4.29: Left: Heave motion of Sea Base. Right: Heave motion of T-Craft

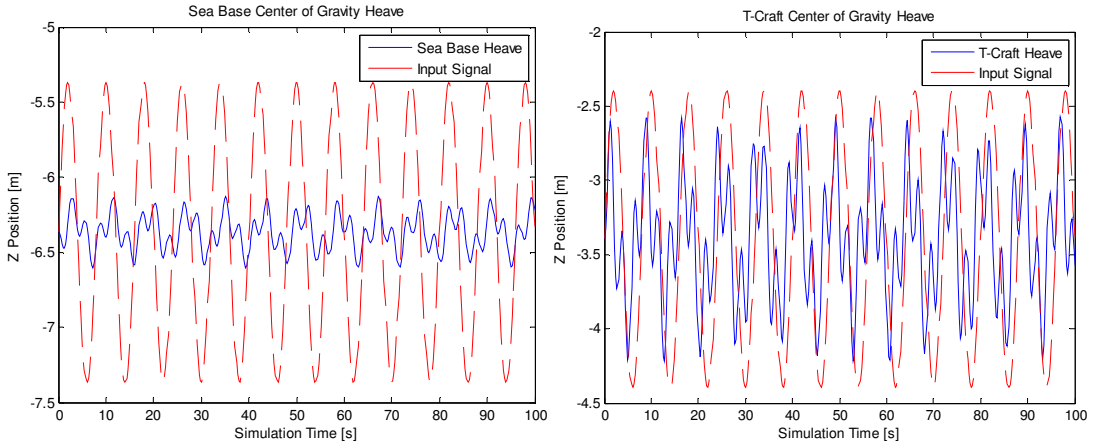

Graph 4.30 includes the pitch and roll angles between the Sea Base and ramp over the simulation time. Unsurprisingly, the pitch angle is relatively unchanged, with a maximum angle of 2.20°. However, the roll angles now vary between ±4° with a maximum value of 0.45°. This is up from 0.31° when using the previous pitch-roll joint. As was touched upon in the previous section, the reason for the different roll angles here is because of the new spring constants in the joint. The spring constant used on the roll motions is 50,000 instead of 500,000, a fact that can be attributed to the increase of roll experienced.

Graph 4.30: Left: Ramp pitch angle. Right: Ramp roll angle

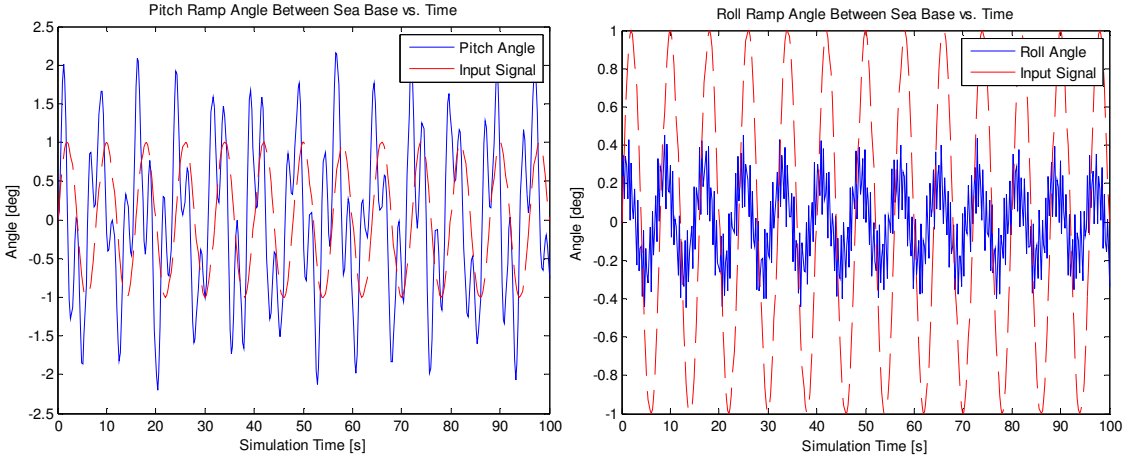

4.11 Summary of Results

Provided in the table below are the maximum values of the pitch, roll, and yaw angles between the Sea Base and ramp during the various scenarios that were just analyzed. These values are only valid within the 100 second simulations that were studied and may increase slightly for longer simulations.

Table 4.1: Maximum angles between the Sea Base and ramp for various scenarios

	Max Pitch Angle Between Sea Base and Ramp (deg °)	**Max Roll Angle Between Sea Base and Ramp (deg °)**	**Max Yaw Angle Between Sea Base and Ramp (deg °)**
Joint: Pitch (no spring)			
Case 1 (parallel)	5.3703	0	0
Case 2 (45°)	2.2202	0	0
Case 3 (perpendicular)	4.4244	0	0
Joint: Pitch, Roll (no spring)			
Case 2 (45°)	2.2024	0.6009	0
Case 3 (perpendicular)	4.4284	0.6990	0
Joint: Pitch, Roll (large spring on Roll)			
Case 2 (45°)	2.2024	0.3055	0
Case 3 (perpendicular)	4.4286	0.2012	0
Joint: Pitch, Roll, Yaw (small springs on Roll and Yaw)			
Case 2 (45°)	2.2006	0.4548	5.1846
Case 3 (perpendicular)	4.4326	0.3330	3.7076

The translational motions of the ships are listed in the next table. The trough to crest values of the T-Craft and Sea Base heaves are provided, as well as the net surge and sway displacements for each ship. It should be understood that

whereas the rotational values provided in the previous table were measured between the Sea Base and ramp, the translational values here are measured between the ships and a global coordinate system.

Table 4.2: Translational quantities of the ships for various scenarios

	T-Craft Heave (m)	Sea Base Heave (m)	Net T-Craft Surge (m)	Net Sea Base Surge (m)	Net T-Craft Sway (m)	Net Sea Base Sway (m)
Joint: Pitch (no spring)						
Case 1 (parallel)	2.8	3.0	-0.5	-0.5	0	0
Case 2 (45°)	1.7	0.4	1.0	-0.022	20	2.9
Case 3 (perpendicular)	0.8	2.9	0.07	-0.006	3.8	5.3
Joint: Pitch, Roll (no spring)						
Case 2 (45°)	1.7	0.4	0.17	0.01	7	0.32
Case 3 (perpendicular)	0.8	2.9	0.07	-0.006	4.8	6.0
Joint: Pitch, Roll (large spring on Roll)						
Case 2 (45°)	1.7	0.4	0.16	0.01	7	0.32
Case 3 (perpendicular)	0.8	2.9	0.07	-0.006	4.9	6.0
Joint: Pitch, Roll, Yaw (small springs on Roll and Yaw)						
Case 2 (45°)	1.7	0.4	0.22	0.009	3.1	0.55
Case 3 (perpendicular)	0.8	3.0	0.2	-0.012	2.0	6.2

CHAPTER 5: CONSEQUENCES OF RAMP LENGTH AND WAVE ORIENTATION

5.1 Motivation for Studying a Variable Ramp Length

The simulations performed in the previous chapter assumed a constant ramp length of 25 meters. With this constant length, various relationships were observed using the different joints and wave orientations. Of particular interest were the angles (pitch, roll, and yaw) that form between the ramp and ships, as they are quantities that are undesirable for cargo transfer and need to eventually be minimized. Chapter 4 briefly touched upon some consequences that the wave orientation has on these angles, such that aligning the waves parallel to the ship-ramp-ship axis generally results in the largest pitch angle. However, these findings do not provide us with enough information for a method of minimizing the angles. As a result, the scope of wave orientations must be increased beyond the three cases studied in the previous chapter. In addition, a variable ramp length should also be taken into consideration as it also affects the angles of interest. Even neglecting the dynamics of the system, it is clear from geometry that a longer ramp length will generally decrease the pitch angle. This is illustrated in Figure 5.1 which shows that the length of the arc is given by $s = L\theta$.

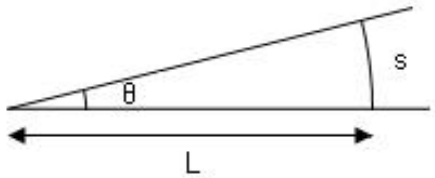

Figure 5.1: Geometry showing that with constant arc length s, increasing L decreases θ

Now consider L to represent the length of the ramp whereas s represents the heave of one of the ships. Although the heave acts along a straight line and not a curve, for small angles the arc in Figure 5.1 can be approximated by a straight line. Realizing that the heave of the ship is for the most part independent of the ramp length (it depends on the wave conditions), and thus fixing s to be a constant, it is apparent that for longer ramp lengths the angle θ decreases accordingly. Therefore, from a purely geometric standpoint, a longer ramp length will decrease the pitch angles. Unfortunately, this increase in length fails to decrease the roll and yaw angles as they act along different planes. The next few pages will present various graphs to show that the roll angle is constant over a wide range of ramp lengths. This is because the roll is dependent on ramp width (since roll acts along the transverse direction), a quantity that will not be varied.

Before considering a continuous range of wave orientations, some important relationships can first be observed by examining the ship-ramp angles for a fixed ship heading and a large number of ramp lengths as in Graph 5.1.

Graph 5.1: Sea Base-ramp angles vs. ramp length for pitch-only joint

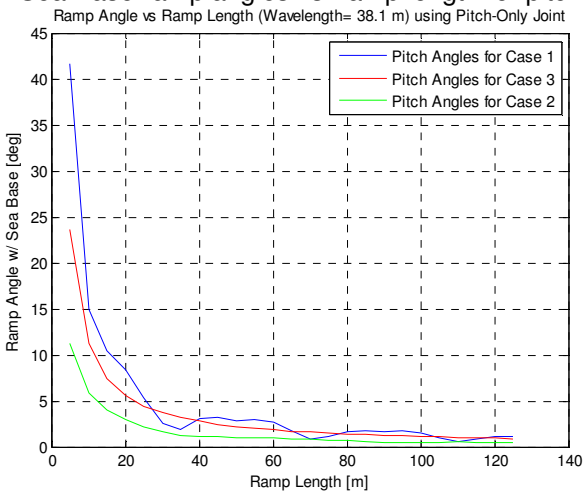

Graph 5.1 shows the maximum pitch angle between the Sea Base and ramp for increasing ramp lengths. The three basic cases of wave orientations represent each line, and the pitch-only joint is used. From this graph, it is evident that the pitch angles do indeed generally decrease for longer ramp lengths. However, it is also apparent that for the parallel case (blue line) there are certain regions in which there are temporary increases in the angles with ramp length. This is because the geometric approach previously described does not account for everything. In particular, recall that the ratio between the length of a ship and the wavelength of the ocean wave also characterizes the heave and pitch motions of that ship. If the length of a ship is nearly divisible by the wavelength then the ship will tend to heave up and down without much tilting. This tilting then in turn obviously has an effect on the pitch angle between the ship and ramp. From Graph 5.1 it can be concluded that with ramp lengths of about 45, 83, and 120 meters there are peaks of local maxima in which the pitch angle has actually increased. These ramp lengths are all about 1/6 greater than being perfectly divisible by the ocean wave wavelength of 38.1 meters. In addition, since the waves approach from the T-Craft side, and because that ship has a length of 40 meters, the T-Craft will move up and down without much tilting. Apparently, it is then the case that the largest angles between the Sea Base and ramp are formed for this particular situation. It is obvious from the graph that the largest pitch angles are generally experienced when the waves are parallel to the ship-ramp-ship axis (blue curve), and the smallest angles occur when the waves are at an intermediate angle (green curve).

It was already discussed that the roll angle between the ships and ramp should be relatively constant over a wide range of ramp lengths. Graph 5.2 depicts both the pitch and roll angles vs. ramp lengths for the pitch-roll joint. Once again, the three wave orientations from Chapter 4 are provided, and separate curves designate each angle (roll or pitch) and case that is considered. It is clear from the graph that this new joint has little effect on the pitch angles- a conclusion that was also reached in the previous chapter. In fact, for Case 1 the pitch angle is identical to that when using the pitch-only joint. This is a consequence of the absence of roll motions for the parallel wave orientation. The magenta and cyan lines show that the roll angles are indeed fairly constant over the range of ramp lengths. The yellow line represents the roll angles for Case 1, which is always zero as there is never any roll in this situation (the fact that there is no roll for parallel waves, but there is pitch for perpendicular waves is due to alignment of the ramp and symmetry about the x axis instead of the y axis).

Graph 5.2: Sea Base-ramp angles vs. ramp length for pitch-roll joint

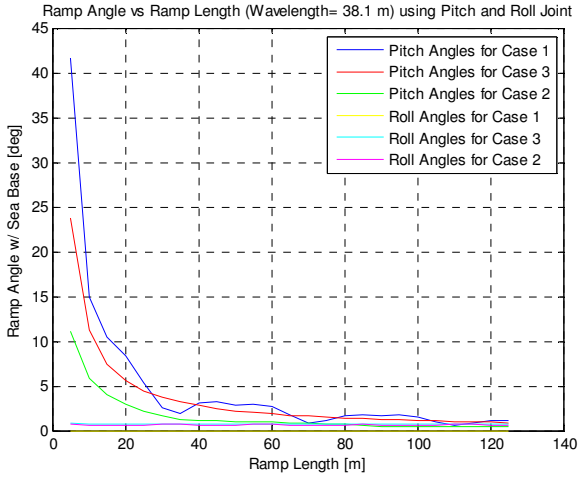

It was found in Chapter 4 that adding a torsional spring to decrease the roll motions between the ships and ramp has little impact on other motions and

quantities, such as the pitch angles. Graph 5.3 shows the pitch and roll angle correlation with ramp length when using the pitch-roll joint with a spring inserted for the roll motions. Although the roll angles have been generally diminished, the pitch angles remain unaffected by this change.

Graph 5.3: Sea Base-ramp angles vs. ramp length for pitch-roll joint with a spring for roll

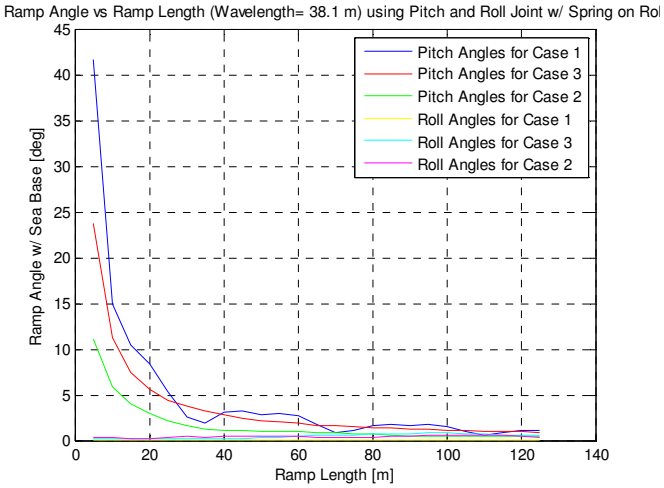

The last joint that was explored allowed for all of the rotational degrees of freedom to occur between the ships and ramp: pitch, roll, and yaw. These angles as functions of ramp length are provided below in Graph 5.4 where it is apparent that the yaw angles are also relatively independent of ramp length.

Graph 5.4: Angles vs. ramp length for pitch-roll-yaw joint with springs for roll and yaw

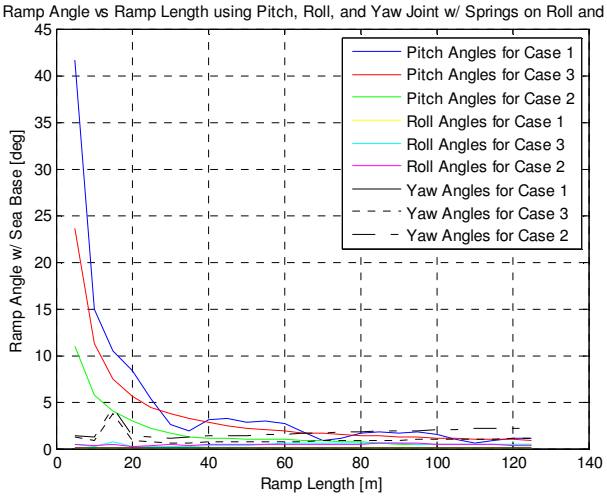

The one shortcoming of the previous graphs is that they use a scalar quantity (maximum angle generated during a simulation) to describe what is essentially a vector. The pitch, roll, and yaw angles are functions of time, and in the case of the pitch and roll, are fairly periodic in time (the yaw is not periodic, and its time history is more complicated to describe). It is beneficial to instead express the angles as functions of both simulation time and ramp length, thus creating a three-dimensional surface plot. These plots must assume a constant wave orientation, and the only scenarios considered here are when the waves are approaching parallel to the ship-ramp-ship axis with the pitch-only joint. The angles between the ramp and T-Craft (left pitch angles) and the ramp and Sea Base (right pitch angles) are both provided in Graphs 5.5 and 5.6.

Graph 5.5: Pitch angle vs. ramp length and time (waves approaching T-Craft first)

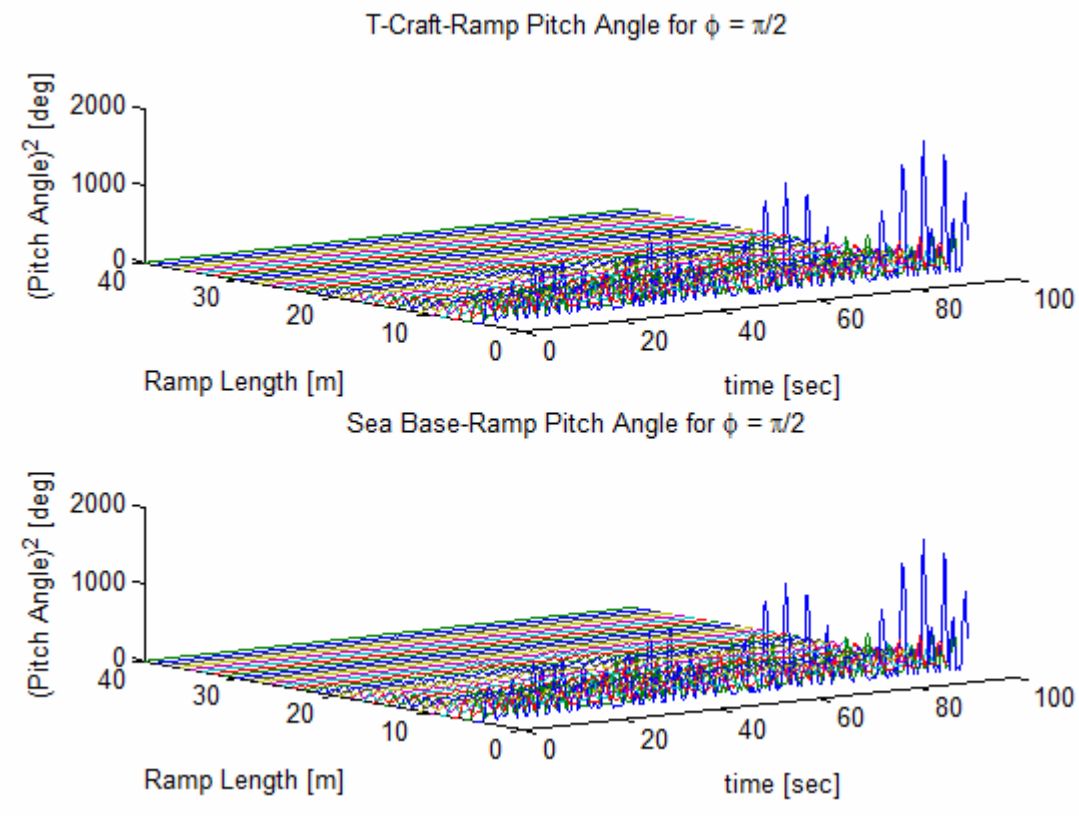

The angles have been squared to better highlight the decreasing nature with respect to ramp length and to prevent negative values. This can also explain why the pitch angle evolution vs. time does not look like the pitch angle plots in Chapter 4. As would be expected, with greater ramp lengths the mean amplitude of the pitch angle oscillations does decrease. It should be acknowledged that here we are only using ramp lengths up to 40 meters, and for greater lengths the slight pitch angle increases observed in Graph 5.1 do exist. Lastly, it should be noted that the pitch angles are slightly different when the waves approach the Sea Base side first due to the differences in size and mass of the two ships. These results are provided below, where φ = -π/2 is the angle for the waves parallel to the ship-ramp-ship axis but approaching the Sea Base side first.

Graph 5.6: Pitch angle vs. ramp length and time (waves approaching Sea Base first)

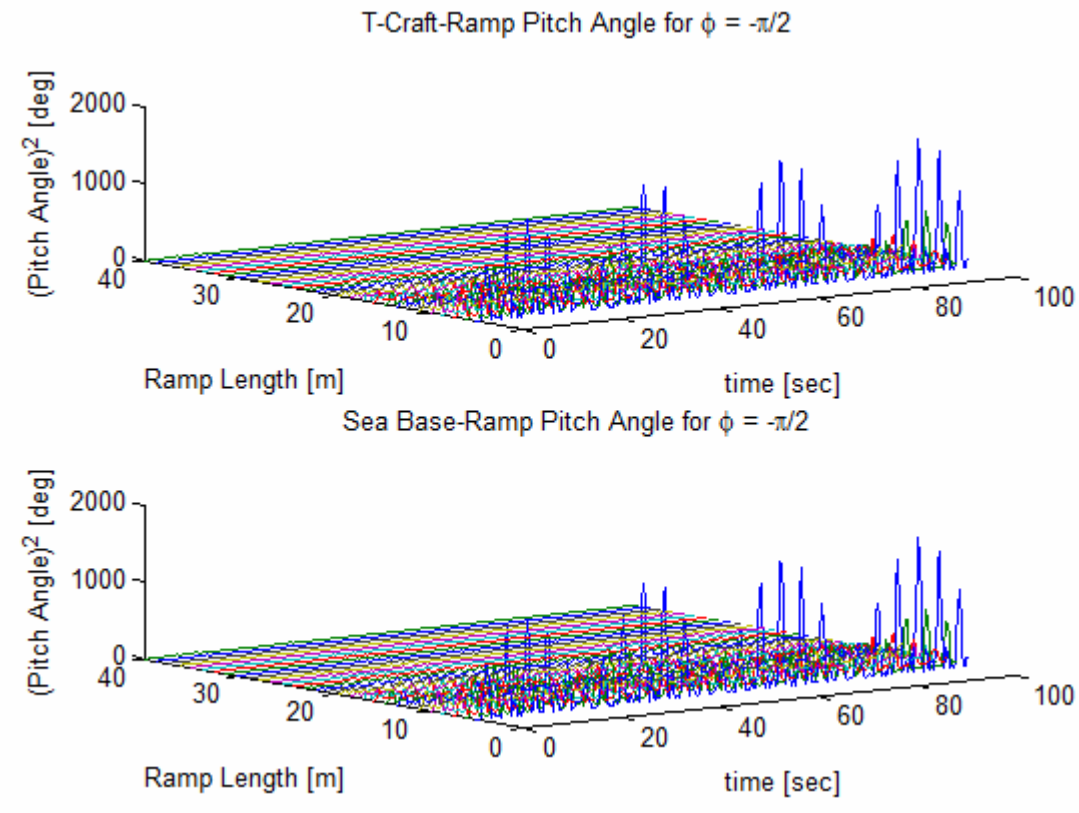

5.2 Dependence of Angles on Wave Orientation and Ramp Length

Now that some basic relationships have been established between the ship-ramp angles and ramp lengths, the dependence on the wave orientation can also be included for φ = 90° (Case 1), to φ = 0° (Case 3), up to φ = -90° (similar to Case 1 but approaching the Sea Base side). Variable ramp lengths will still be considered, and the surface plots will be generated with the angles as functions of wave direction and ramp length. Since the ship-ramp-ship system is symmetric along the widths, it is only necessary to consider wavefront angles from 90° to -90°. Figures 5.2 and 5.3 below illustrate the range of these wave orientations. The situation when φ varies from 0° to -90° is slightly different than when it varies from 90° to 0°, so new phase formulas must be derived. The derivations of these formulas are omitted in this report as they follow the same basic trigonometric ideas used in Chapter 2. A complete list of the phase formulas for angles between φ = 90° and φ = -90° is provided in the appendix.

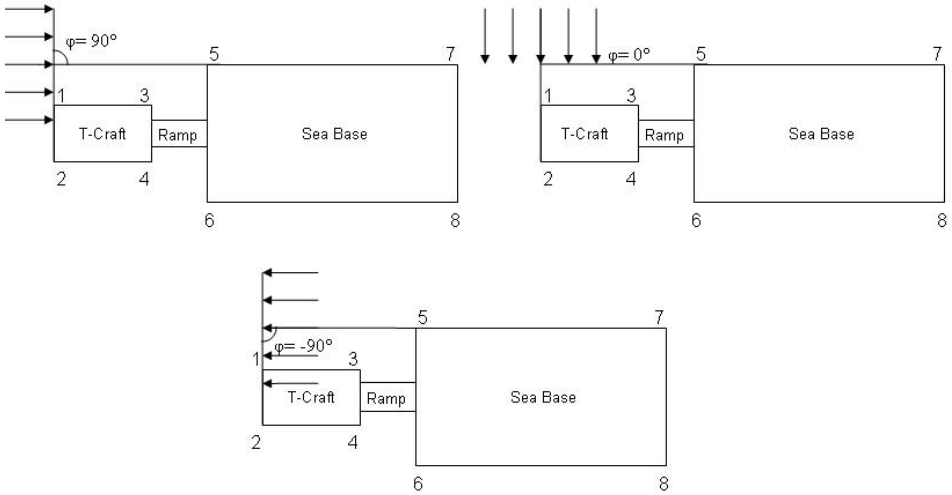

Figure 5.2: Illustration of the angle φ varying from 90° to -90°

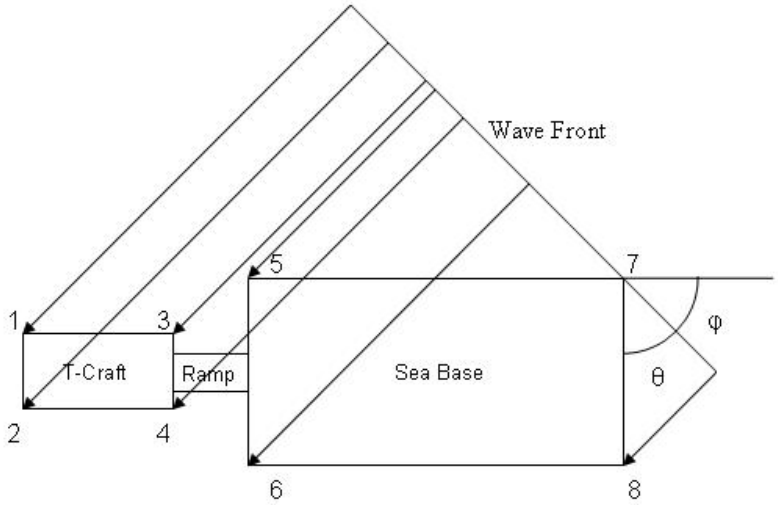

Figure 5.3: Wavefront approaching the ship-ramp-ship axis at an arbitrary angle from the Sea Base side first

In the following sections, the maximum ship-ramp pitch and roll angles will be provided as functions of wave orientations from φ = -90° to 90° and ramp lengths from 5 to 40 meters. This will result in surface plots where the ramp length will form one axis, φ another axis, and the ship-ramp angle the vertical axis. It should be acknowledged that the ramp angles here are back to being defined as the maximum angle encountered during the simulation time. Furthermore, for simplicity, only the angles subtended by the ramp and Sea Base will be considered. Instead of examining all of the possibilities, the pitch-only and pitch-roll joints will be the only joints studied. The pitch-roll joint with a spring on roll motions and the pitch-roll-yaw joint will be omitted as they generally have the same behavior as the pitch-roll joint. Recall that when using a spring, the only quantity that changed was the roll angle, which would decrease according to the size of the spring constant. Furthermore, the introduction of yaw, while having an impact on the sway and surge of the ships, does not appreciably change the pitch or roll angles. The plots all use a 30×30 grid, meaning 900 data points.

5.2.1 Analysis of Pitch-Only Joint

The maximum pitch angle as a function of ramp length and wave orientation for the pitch-only joint is provided in Graph 5.7. It is apparent that the pitch angle decreases nearly monotonically with respect to the ramp length. However, the rate of decrease is contingent on the wave orientation. For example, at φ = 27.93° the pitch angle only decreases from 2.40° to 0.28° whereas when φ = -83.70° the angle decreases from 37.2° to 3.45°. The greatest decreases are seen when the waves are aligned parallel to the ship-ramp-ship axis. Although it is difficult to detect, there are minor increases in pitch angles around the ramp length of 40 meters. As previously mentioned, this increase can be attributed to the ratio of the ship/ramp lengths vs. the ocean wave wavelength.

Graph 5.7: Maximum pitch angle vs. ramp length and wave orientation

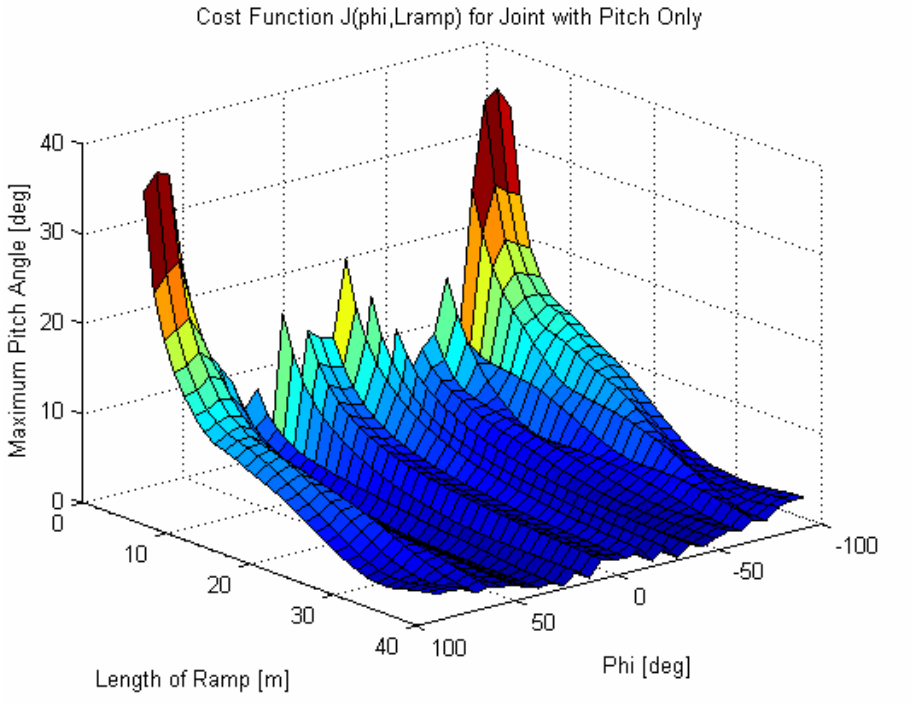

The relationship between the pitch angle and wave orientation is more complex as there are many local peaks and valleys. However, on average the largest pitch angles form when the waves are parallel (φ = 90°) and the smallest angles are found when φ = ± 28° (which means 62° removed from the parallel cases). This is consistent with the result found in Chapter 4 that the pitch angles are not minimized when the waves approach perpendicular to the ship-ramp-ship axis (φ = 0°). It is also worth mentioning that while the largest angles are found for the parallel orientations, this is also when the decrease with respect to increasing ramp lengths is the greatest. Likewise, although the smallest angles are found when φ = ± 28°, the rate of decrease is smaller compared to the other wave directions. Graph 5.8 portrays the relationship of the maximum pitch angle and wave orientation from a two-dimensional perspective.

Graph 5.8: Maximum pitch angle vs. wave orientation

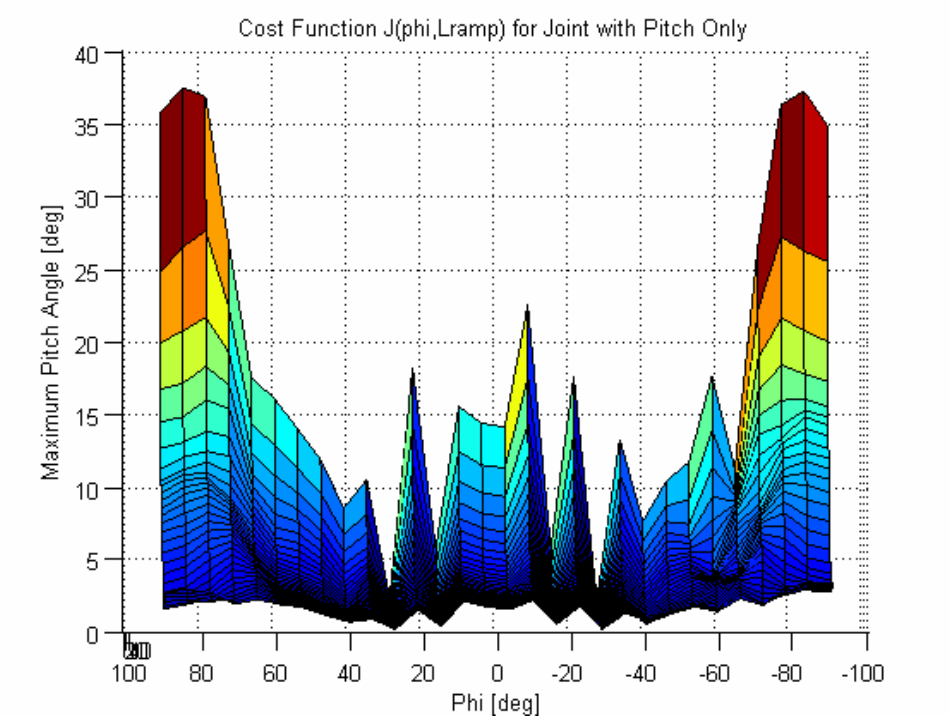

5.2.2 Analysis of Pitch-Roll Joint

The additional degree of freedom in roll that is allowed by the pitch-roll joint is important in that it is also an undesirable quantity that needs to be minimized. As such, it is now necessary to show both the maximum pitch and roll angles as functions of ramp length and wave orientation. First consider Graph 5.9 which contains information on the maximum pitch angle for this new joint.

Graph 5.9: Maximum pitch angle vs. ramp length and wave orientation

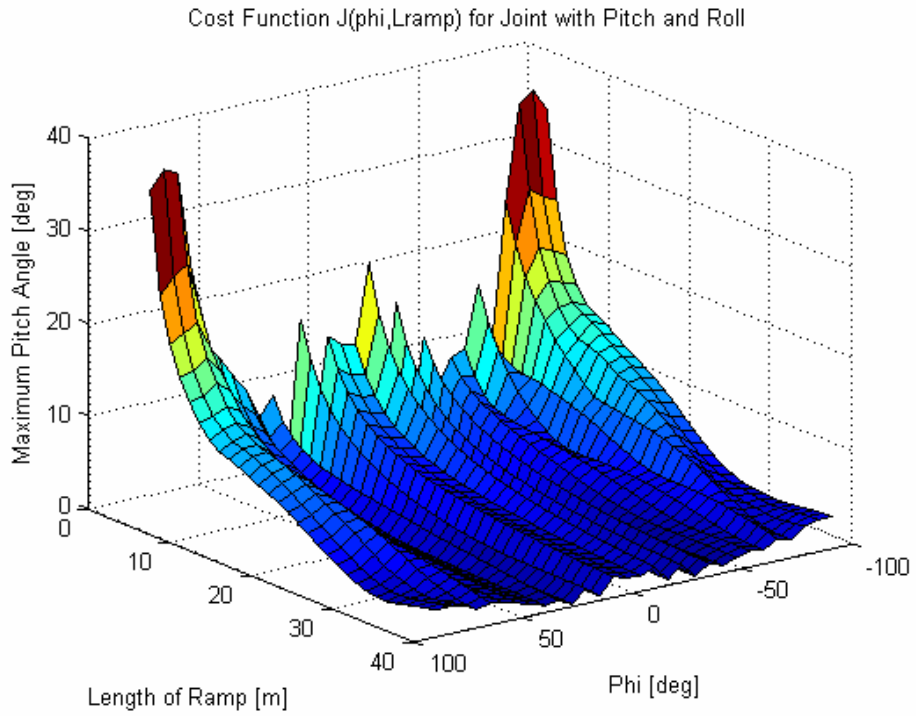

This plot is almost exactly the same as Graph 5.7 which represented the pitch-only joint in the previous section. In fact, for φ = 90° and -90° the plots should be identical as no roll ever occurs for these scenarios (even though the joint allows for roll). At other locations, the differences that do occur are usually on the order of 0.01°, and as a result cannot be visibly distinguished in the surface plots.

The dependence of the maximum roll angles on the ramp length and wave incidence angle is provided in Graph 5.10. It is immediately obvious that except for some anomalous results for the smaller ramp lengths, the roll angle is basically independent of the ramp length. The uncharacteristic peaks that are observed for the smaller ramp lengths occur at L = 6.21 meters and φ = -77.59° as well as L = 5 meters and φ = 71.38°. It can only be guessed as to why these peaks occur, but perhaps all the conditions: ramp length, wave orientation, ship length, and ocean wave wavelength somehow create a unique situation that is very favorable to a large roll angle.

Graph 5.10: Maximum roll angle vs. ramp length and wave orientation

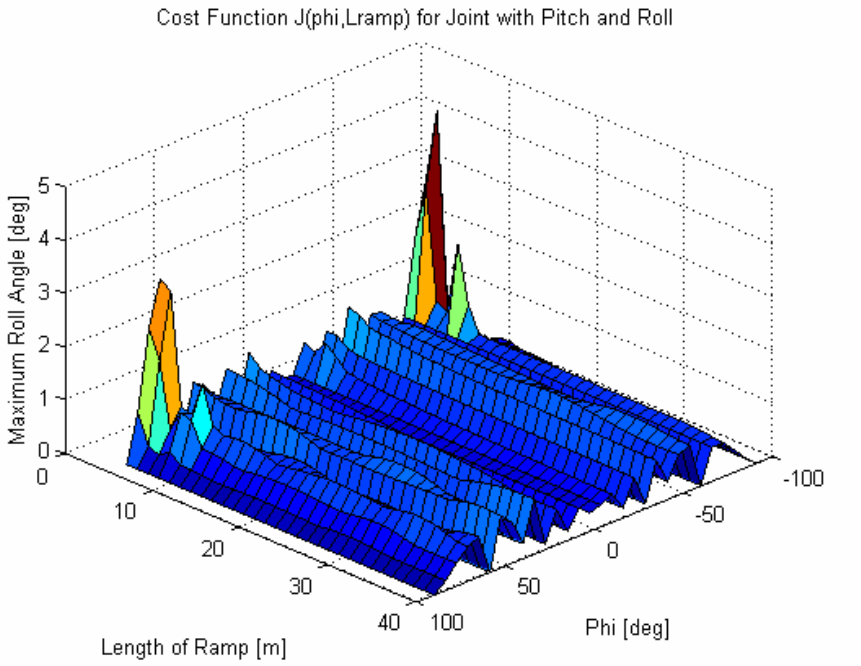

Graph 5.11 on the next page shows a “zoomed” in visualization of Graph 5.10 for ramp lengths greater than 10 meters. It is apparent from this surface plot that the roll angles do indeed drop off to zero when the waves are parallel to the ship-ramp-ship axis (φ = 90°). It is also clear that the roll angles are largely

independent of ramp length. More surprising is the overall lack of a strong dependence on wave orientation as well. Although the plot is very active along the φ axis, with many local peaks and valleys, it lacks the almost convex behavior that the pitch angles demonstrated in Graph 5.8 for wave orientations from φ = [90°, 0°] and φ = [0°, -90°]. This will make the roll angle a very difficult quantity to deal with when considering optimization. Nevertheless, a few conclusions can still be made. First, the parallel orientation clearly minimizes the roll angle whereas values of φ around ±70° with ramp lengths less than 10 meters maximize the angle. Also, wave orientations around 34° result in the largest roll angles when considering all ramp lengths. The value of φ = 28° that minimized the pitch angle is a very good wave orientation here as it lies in a valley. Lastly, although the roll angle is basically constant over ramp length, either a ramp longer than 10 meters should be used, or the ships should stay away from the φ = ±70° regions in order to avoid the peaks that are present.

Graph 5.11: Considering only ramp lengths greater than 10 meters

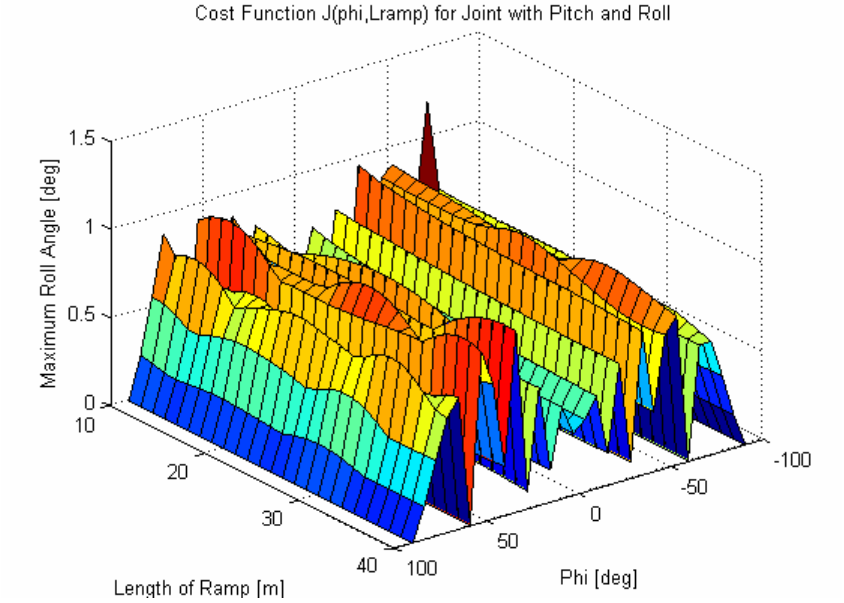

It is constructive to include a single surface plot which incorporates both the pitch and roll angles. Therefore, a composite cost function which is a linear combination of the roll and pitch angles can be used:

$$J(\varphi, L_{ramp}) = \alpha P_{\max}(\varphi, L_{ramp}) + \beta R_{\max}(\varphi, L_{ramp}) \quad (5.1)$$

where P_{max} and R_{max} are the maximum pitch and roll angles respectively, and α and β are weighting constants. These constants determine which angle should be emphasized more in the composite cost function. A greater emphasis on a certain angle means that this angle is considered to be more important and potentially more dangerous for cargo transfer. For example, minimization of a cost function with the ship-ramp pitch angle weighted more means that the optimal ramp length and ship orientation will be more dependent on the pitch angle than the roll angle. In Graph 5.12, equal weighting is given to both angles.

Graph 5.12: Composite cost function vs. ramp length and wave orientation

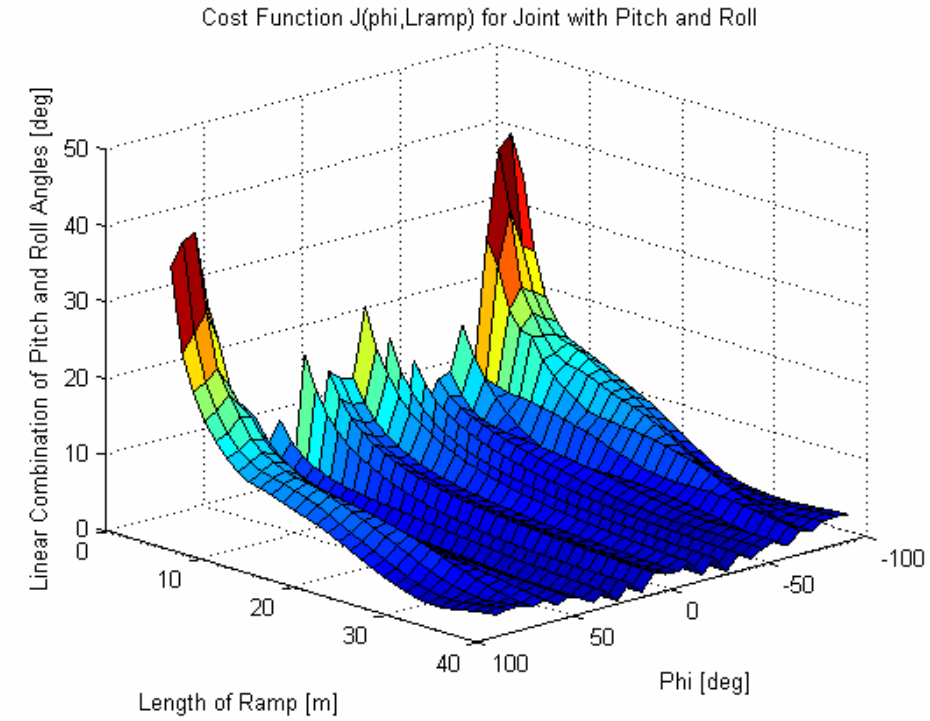

Since the roll angles are small compared to the pitch angles for the simulation parameters used in this report, the composite cost in the graph above more readily resembles the pitch angle surface plot. However, instead setting $\alpha = 1$ and $\beta = 10$ in Equation (5.1) increases the emphasis on the roll angles and generates the plot shown in Graph 5.13. One interesting outcome of this is that for longer ramp lengths, the composite cost function fails to decay anymore. This is because in those regions the roll angles are now larger than the pitch angles (the pitch angles continue to decrease with ramp length yet the roll angles remain constant). Since the roll angles are independent of ramp length, the composite cost function reaches a constant state and fails to decrease anymore.

Graph 5.13: Composite cost function vs. ramp length and wave orientation with additional weighting on roll

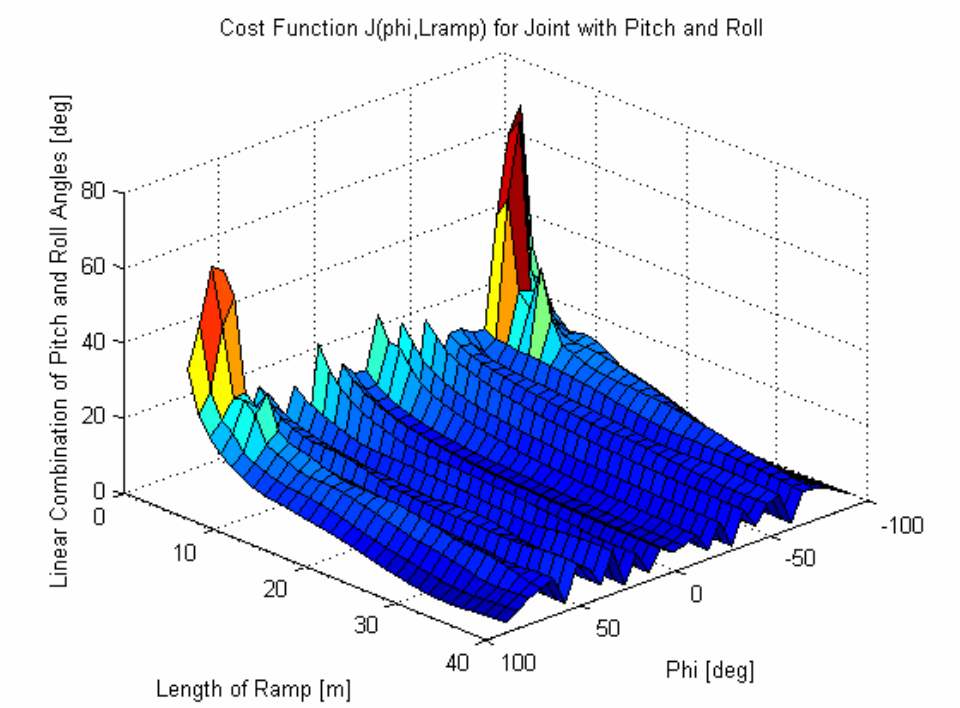

CHAPTER 6: OPTIMIZATION RESULTS

6.1 Optimization of Ramp Length

By now it is clear that generally (with the exception of a few local maxima) the pitch angles between the ships and ramp decrease with the length of the ramp. This information alone would lead one to believe that choosing an infinitely long ramp may be the best method of minimizing the angles. However, except for small lengths, increasing the ramp length has little effect on the roll and yaw angles, and thus seems to result in a wasted effort. Combining this observation with the fact that an extensive ramp would introduce a prohibitive weight leads to the conclusion that a very long ramp is actually not desirable.

Given that an infinitely long ramp is not a reasonable option for minimizing the ship-ramp angles, the following discussion can instead be used to motivate a method of finding an optimal length. It was previously found that the pitch angle vs. ramp length plot does not decrease monotonically for the parallel wave orientation. This can be observed in Graph 5.1, where the regions around 35, 70, and 110 meters form areas of local minima. These regions are locally convex, and the minima represent the smallest pitch angles in a certain neighborhood. Unfortunately, the fact that there exist many local minima raises the question as to which one to choose. However, of the three primary cases, these areas of local convexity exist only for the scenario when the waves are parallel to the ship-ramp-ship axis. For the other wave orientations the pitch angle and ramp

length relationship is indeed represented by a monotonic decrease. Instead, it would be advantageous to force the pitch angle plots to be globally convex for all wave orientations. This can be accomplished by utilizing a penalty function (which may be linear, exponential, etc) that increases monotonically with longer ramp lengths and is added to the curve that represents pitch angle vs. ramp length. Such an increasing function can be defended as it takes into account both the prohibitive weight and wasted effort with respect to the yaw and roll angles when using longer ramps. By adding the penalty function to the pitch angle curve, the resulting curve is nearly globally convex, and contains a clear minimum value. The ramp length that corresponds to this minimum value is then deemed the optimal ramp length for minimizing the pitch angles. It should be noted that it is unnecessary to add this penalty to the roll or yaw plots as they are fairly constant with ramp length, and would not become convex. Instead, the penalty is only added to the pitch angle plots as in Graph 6.1 (for clarity and simplicity only the parallel wave case with the pitch-only joint is presented below).

Graph 6.1: Optimal value of ramp length for minimizing the pitch angle with a linear penalty

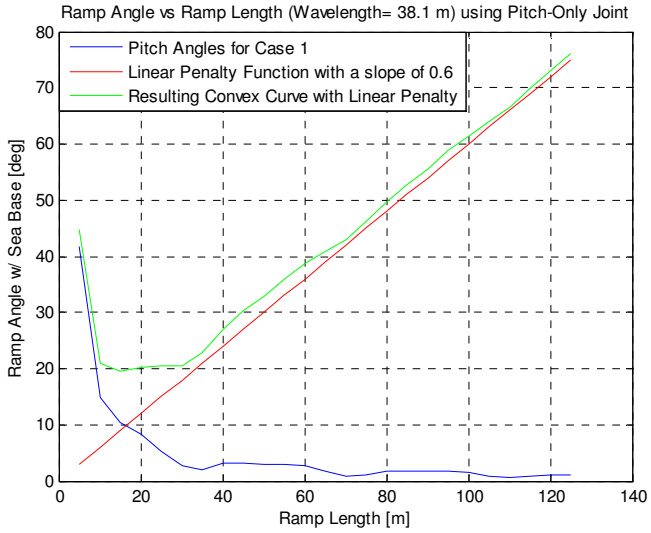

When considering the linear penalty function provided in Graph 6.1, it is apparent that the optimal ramp length for the parallel wave orientation is about 15 meters. By simply increasing the penalty function's slope, this optimal ramp length can be pushed back. A penalty with a greater slope is a function that further emphasizes the need for a shorter ramp. The quadratic curve in Graph 6.2 places less of an importance on achieving smaller lengths, but penalizes the longer lengths even more due to the continuously increasing slope. As a result, the optimal value is now 30 meters as opposed to 15 meters. It is important to note that the convex curves are simply tools used to determine the optimal ramp length in the pitch angle plots. Although they can find the best ramp length, the corresponding minimum angle is always larger than the actual minimum angle due to the addition of a positive function. Also, the penalty functions are user-defined and can be used to arrive at any desired "optimal value". As such, these functions should be chosen carefully by considering the physical constraints of increased ramp lengths and then approximating these "trade-offs" with a curve.

Graph 6.2: Optimal value of ramp length for minimizing the pitch angle with a quadratic penalty

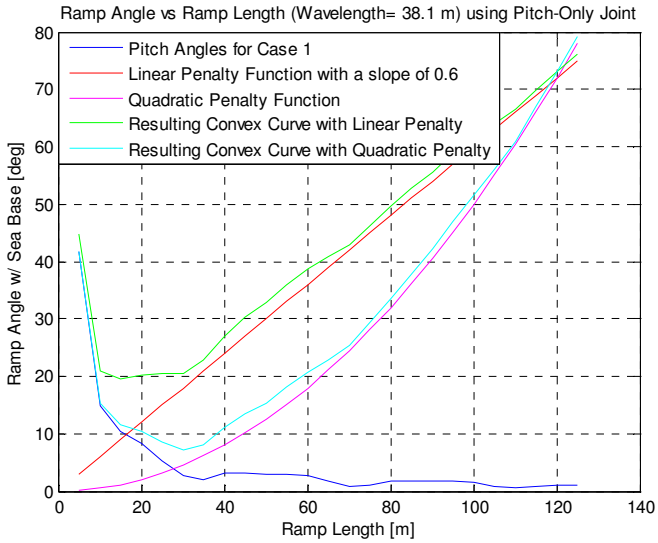

6.2 Optimization of Ramp Length and Ship Heading

The results of the previous section were provided for the scenario when the waves are aligned parallel to the ship-ramp-ship axis. Linear and quadratic penalties were used, and with the quadratic penalty the optimal ramp length that minimized the pitch angle was found to be 30 meters. Unfortunately, this method failed to take into account all of the possible wave directions, and was instead demonstrated for a single case. In this section, a method is introduced which considers the wave orientations as well. As such, the optimal values of both the ramp length and ship heading can be determined.

Extending the procedure to optimize over two parameters entails taking the pitch angle surface plot in Graph 5.7 and adding a penalty function that now depends on both ramp length and wave angle. However, in this report the penalty function is allowed to be invariant in the φ direction as there is not enough evidence to permit the penalization of some wave orientations. In fact, the only possibility for penalizing certain wave directions would be if the roll angle vs. wave orientation relationship was fairly smooth and convex, and contained particular regions that were obviously desirable. Instead, it was previously noted that the roll angles are erratic functions of wave orientation and are difficult to deal with for optimization purposes. As a result, the correlation between the roll angle and wave incidence angle cannot be used as a basis for a penalty function. Since the penalty functions are invariant with wave orientation, they are basically identical to those in the previous section except that they are extended along the

φ direction. Graph 6.3 shows the pitch angle vs. ramp length and wave orientation plot for the pitch-only joint with a quadratic penalty function given by

$$P\left(\varphi, L_{ramp}\right) = 0.003L_{ramp}^2 \tag{6.1}$$

In Graph 6.3 the penalty function is represented by a clear mesh grid, the old pitch angle plot by a smooth shaded surface, and the resulting convex plot by a shaded surface with grids. Here, the term convex refers to convexity along the ramp length, as there is never global convexity along the wave orientations (although they can be roughly approximated as locally convex from [90° 0°] and [0° -90°]). The pitch-only joint is the only joint considered for optimization as the pitch angle surface plots are all quite similar for each joint (see Chapter 5).

Graph 6.3: Cost function formed by adding a quadratic penalty function to the pitch angle vs. ramp length and wave orientation surface plot

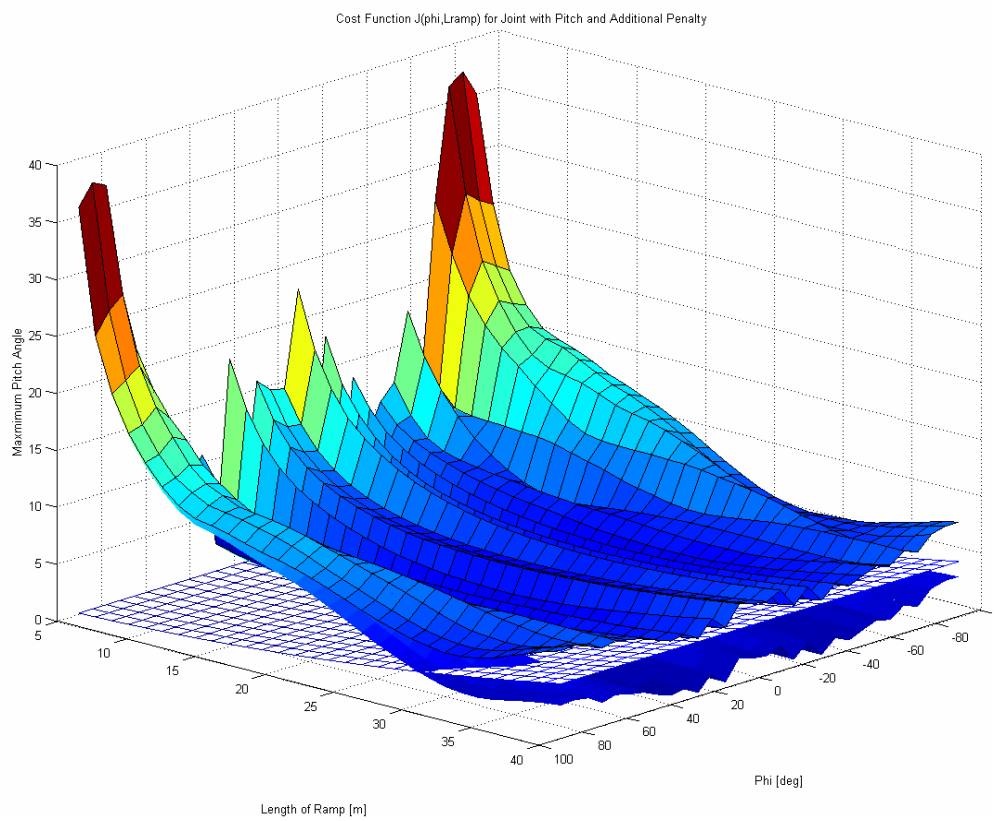

Finding the optimal ramp length and wave orientation from the above graph is a more complex matter than before due to the extra parameter, φ that is being optimized over. In addition, the particular ramp length that minimizes the pitch angle is different for each wave orientation. For example, at φ = 27.93°, the minimum pitch angle occurs when the ramp length is 13 meters, whereas at φ = 90°, the minimum angle is reached for a ramp length of 31.5 meters. Graph 6.4 below shows the convexity along the ramp length of the curves that are generated when adding the penalty function (separate faint blue line). Each non-vertical line in the shaded region represents the relationship of the pitch angle and ramp length for a given wave orientation. It is then obvious from the graph that the minimum values of the various curves occur at different ramp lengths.

Graph 6.4: Cost function formed by adding a quadratic penalty function viewed from a two-dimensional perspective

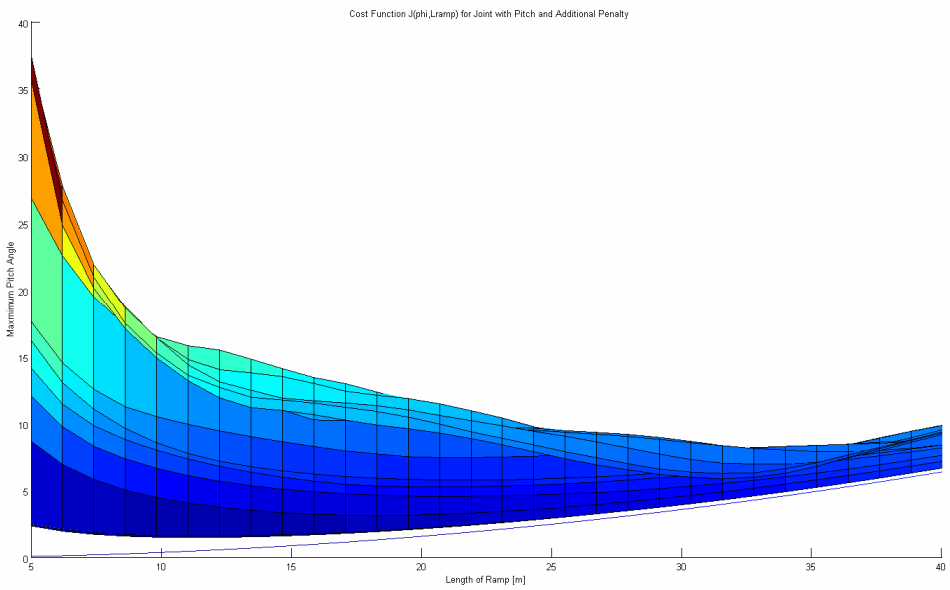

An interesting consequence of the penalty function being invariant with respect to the φ direction is that the pitch angle and wave orientation relationship remains the same as it was before incorporating the penalty. This means that the

wave orientation of $\varphi = \pm 28°$ that was found in Chapter 5 to minimize the pitch angle is still the best direction, even after adding the penalty function. From the surface plots, the optimal ramp length for this particular wave orientation occurs at a value of 13 meters. Therefore, the global minimum of the surface plots after adding a quadratic penalty function occurs at a ramp length of 13 meters and a wave orientation of $\varphi = \pm 28°$. Although the optimal wave direction (which can conversely be thought of as the desired ship heading) is not up for the user to decide, the optimal ramp length is still contingent on the type of penalty used.

The findings in this chapter as well as Chapter 5 can be used by the ship operators of the Sea Base and T-Craft to change the ship heading as well as adjust the ramp length (assuming that the ramp is retractable and capable of length adjustment) in order to minimize the angles between the ramp and the ships. The roll angles, although independent of ramp length, can be reduced by rotating the ship-ramp-ship system such that the waves are 62° removed from the parallel cases (this means that $\varphi = \pm 28°$). Fortunately, it has been found that this wave orientation is also optimal when considering the pitch angles. However, the choice of the best ramp length depends on a user-defined function that penalizes longer ramp lengths as they introduce a prohibitive weight and fail to decrease roll or yaw angles. It can be concluded that selecting a quadratic penalty given by Equation (6.1) results in an optimal ramp length of 13 meters when $\varphi = \pm 28°$. If the ship operates at a different wave orientation for whatever reason, Graphs 6.3 and 6.4 can then be used to find the corresponding optimal ramp length that reduces the pitch angles.

CHAPTER 7: EXREMUM SEEKING

7.1 Introduction to Extremum Seeking

A major limitation of using surface plots that depict the ship-ramp angles as functions of ramp length and ship heading for optimization is that the ship operators would have to obtain large look-up tables which contain the data from these plots. Furthermore, the validity of these plots rests upon many assumptions and simplifications regarding the wave and ship modeling which are necessary for implementation into the computer program. The actual dynamics of the interconnected system out at sea are obviously not fully captured by the spring-mass-damper mathematical construction that has been provided. As such, instead of using results from the surface plots, it would be advantageous to employ a real-time optimization method which would actively update the ramp length and ship heading in order to reduce the ship-ramp angles. This would allow the system to operate at the global minimum of the angles (specifically, the global minimum of the pitch while reducing roll as much as possible) without referring to graphs or tables. One possibility that will be briefly explored here is to incorporate the method of extremum seeking. This method was a popular tool in controls as early as the 1940's. However, it has been recent advances that have led to a well-defined theory discussed in the text of Ariyur and Krstic [1].

Extremum seeking is a method of adaptive control that has the objective of selecting an operating set point that keeps the output at an extremum

(maximum or minimum) value. Typically, adaptive control methods are model based and deal with the stabilization of a known set point or reference. However, extremum seeking can be distinguished from such methods in that it is not model based and works even with an uncertainty in the set point which extremizes the output. These characteristics of extremum seeking are precisely catered to the problem at hand since a rigorous mathematical model of the system has not been developed. Furthermore, even though the input-to-output map is unknown (assuming we cannot use the surface plots of the previous chapters), extremum seeking can still be applied to find the optimal ramp length and ship heading that reaches the unknown extremum. In this application, the extremum will be the minimum value of the ship-ramp pitch angles (using measurements from either the pitch displacement, velocity, acceleration, or some combination).

Extremum seeking applies the method of sinusoidal perturbations fed into the plant in an effort to extract the gradient information of the input-to-output map. The particular schemes discussed in [1] permit fast adaptation and achieve convergence to the optimal value on a time scale similar to that of the plant dynamics. Figure 7.1 shows a simple version of the extremum seeking scheme.

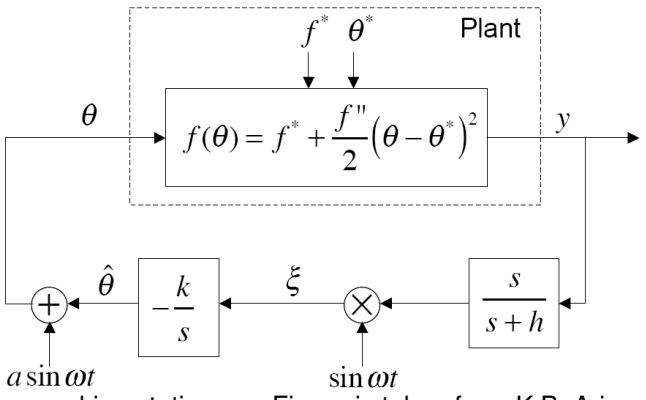

Figure 7.1: Extremum seeking static map. Figure is taken from K.B. Ariyur and M. Krstic in [1]

The purpose of the algorithm represented in the above block diagram is to operate at an unknown parameter, θ* which corresponds to an unknown output extremum, f*. Any function that is continuously differentiable with a continuous second derivative (C^2 function) can be approximated locally by the expansion:

$$f(\theta) = f^* + \frac{f''}{2}\left(\theta - \theta^*\right)^2 \tag{7.1}$$

From Equation (7.1) it is clear that for the output to reach the extremum value of f*, the term θ - θ* must be minimized (i.e. our input must track to the optimal value). As with the case of most tracking problems, this can be viewed as meeting a stabilization objective in which the estimation error $\tilde{\theta} = \theta^* - \hat{\theta}$ must be stabilized to a neighborhood around the origin.

Unfortunately, the algorithm in Figure 7.1 fails to take into account the multiparameter nature of the problem that arises from the need to optimize over both ramp length and ship heading. In addition, the plant dynamics of the ship-ramp-ship system need to be accounted for. Accordingly, a generalized version of the extremum seeking scheme as provided below in Figure 7.2 is necessary.

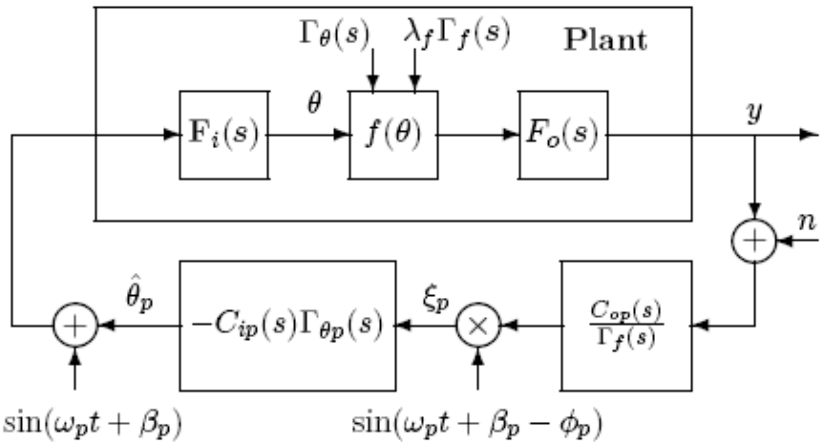

Figure 7.2: Extremum seeking for a plant with dynamics, time varying input and output: θ* and f*, and multiple parameters: p=1, 2,…, n. Figure is taken from K.B. Ariyur and M. Krstic in [1]

In the above block diagram, $\sin(\omega_p t + \beta_p - \theta_p)$ is referred to as the demodulation signal whereas $a_p \sin(\omega_p t + \beta_p)$ is the perturbation signal. The input and output dynamics are provided by the terms $F_i(s)$ and $F_o(s)$. The optimal inputs $\theta^*(t)$, and output $f^*(t)$, are allowed to be time varying and are represented in the frequency domain by $\lambda_{\theta p}\Gamma_{\theta p}(s)$ and $\lambda_f\Gamma_f(s)$ respectively. However, the system in this report does not have time varying optimal inputs or outputs. Thus, $\theta^*(t)$ and $f^*(t)$ can be considered to be step functions: $\lambda_{\theta p}/s$ and λ_f/s, where $\lambda_{\theta p}$ and λ_f represent the unknown desired values. The washout (high pass) filter is designated by the block that contains $C_{op}(s)/\Gamma_f(s)$. The compensators, $C_{op}(s)$ must be chosen such that the necessary stability conditions and convergence rates of the algorithm are satisfied. It is also known that the compensators, $C_{ip}(s)$ in the block containing $-C_{ip}(s)\Gamma_{\theta p}(s)$ should also be chosen to satisfy the stability conditions and desired convergence rates. The stability conditions and compensator design guidelines are not provided here, and can instead be found in a text on extremum seeking. $C_{ip}(s)$ and $C_{op}(s)$ are often chosen such that the following expressions hold:

$$\frac{C_{op}(s)}{\Gamma_f(s)} = \frac{s}{s + h_p} \tag{7.2}$$

$$C_{ip}(s)\Gamma_{\theta p}(s) = \frac{k_p}{s} \tag{7.3}$$

where h_p determines the cutoff frequency and k_p is an adaption gain.

When finding a minimum of the pitch angle, it has already been determined that the parameters to be varied are ramp length and ship heading. This means that a multiparameter extremum seeking scheme with p = 1, 2 must be used. The output is a quantity that characterizes the pitch angle evolution with

time between one of the ships and the ramp. As previously mentioned, possible choices include the pitch angle's displacement, velocity, or acceleration. For clarity, it should be noted that only the pitch angle is being optimized over. This is because the roll is constant with respect to ramp length and difficult to optimize over wave orientation. Furthermore, yaw is fairly unimportant in that it does not hinder cargo transfer. However, the algorithm is quite general, and a combination of all three (or two) angles can be used if desired. The extremum seeking loop tailored to work so far for the ship-ramp-ship system is given in Figure 7.3. Here it is assumed that there is no measurement noise and the same washout filter, adaption gain, and frequencies are used: $h_1 = h_2$, and $k_1 = k_2$, and $\omega_1 = \omega_2$.

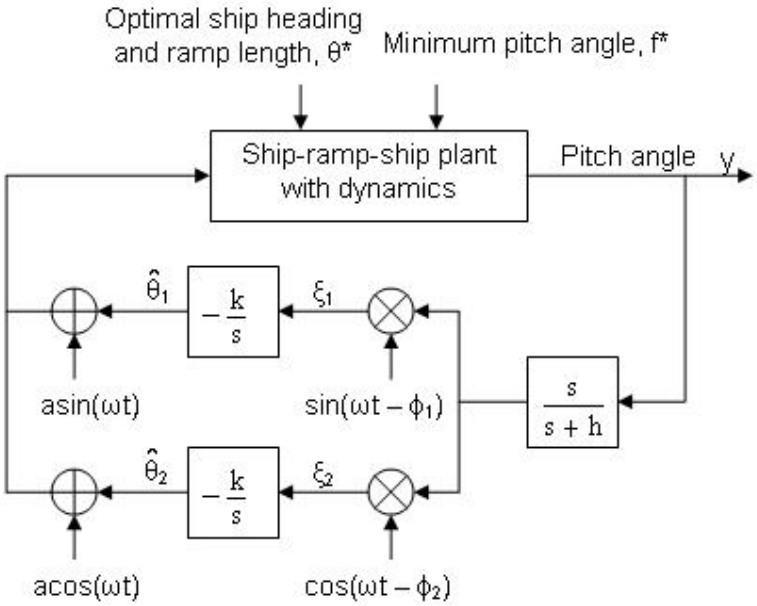

Figure 7.3: Possible extremum seeking loop for ship-ramp-ship system

A more in-depth discussion of how the above extremum seeking loop could be possibly modified and then applied to the ship-ramp-ship system will be provided in Section 7.3. However, before discussing the application of such a scheme, the algorithm is first tested in the next section on a simple multiparameter static map.

7.2 Multiparameter Extremum Seeking Example

The purpose of the example in this section is to illustrate the extremum seeking algorithm on a simple three-dimensional convex map with a well-defined global minimum. Graph 7.1 shows that the static map considered consists of two input parameters, x and y, and an output, z. The input-to-output map is given as:

$$z(x, y) = 5 + (y-2)^2 + (x-3)^2 \tag{7.4}$$

It is clear from Equation (7.4) that the extremum (minimum) of the map at z = 5 occurs when the parameters y and x are equal to 2 and 3 respectively. This fact can also be clearly observed from the surface plot below.

Graph 7.1: Example of a two-parameter convex function for extremum seeking

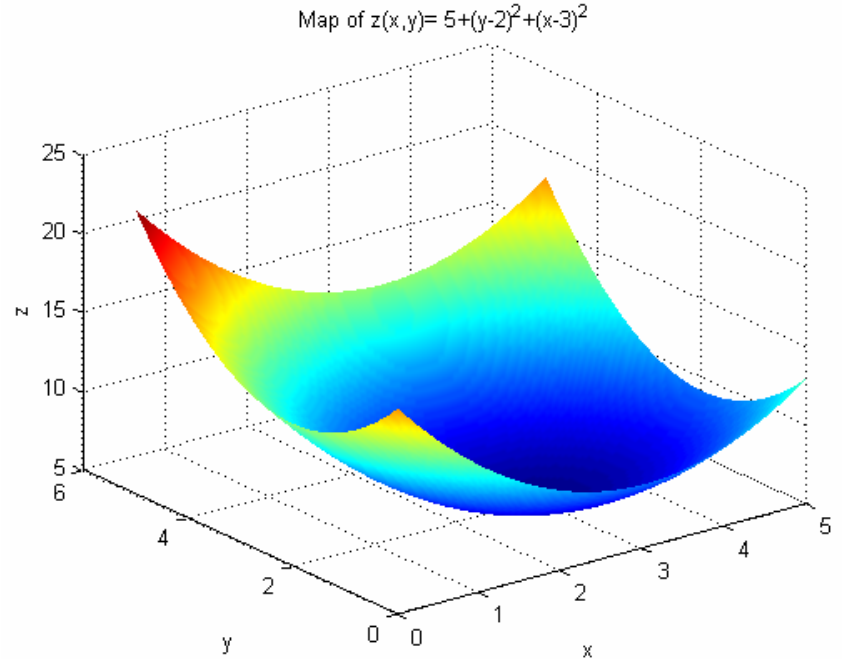

Since the map is smooth and convex everywhere, there are no local minima. Therefore, the method of extremum seeking can be used in order to get a measure of the gradient information of this map and then drive the parameters to

operate at the desired extremum. Figure 7.4 shows the Simulink multiparameter extremum seeking block diagram that is implemented. This diagram is similar to Figure 7.3 except that a static map is used instead of a dynamical system. An x-y plot depicting the trajectory of the parameters is included below in Graph 7.2.

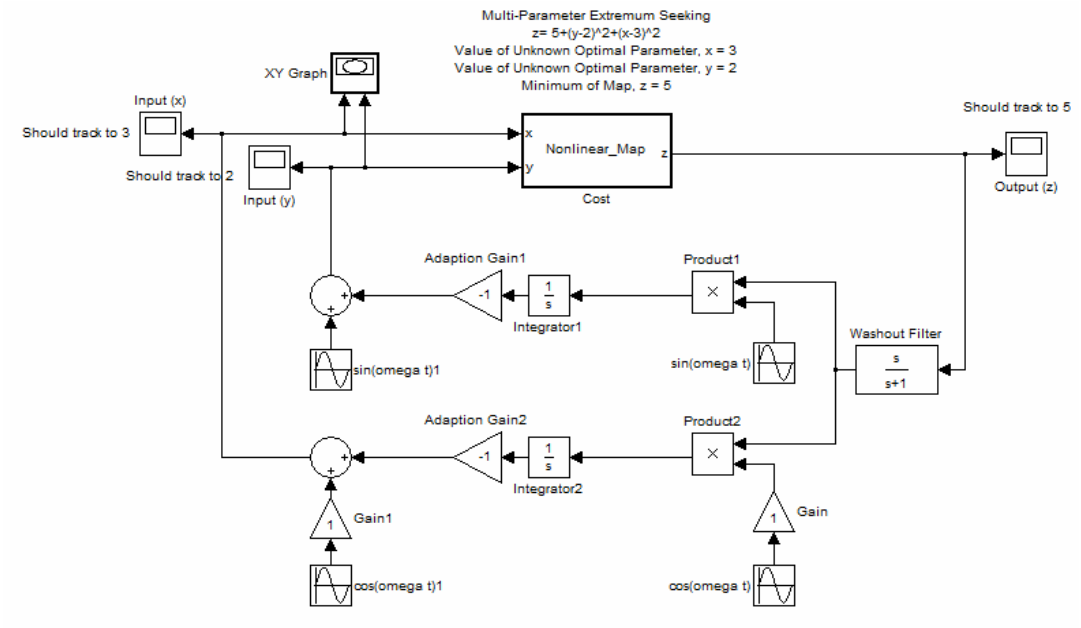

Figure 7.4: Simulink multiparameter extremum seeking block diagram

Graph 7.2: Trajectory of input parameters during extremum seeking

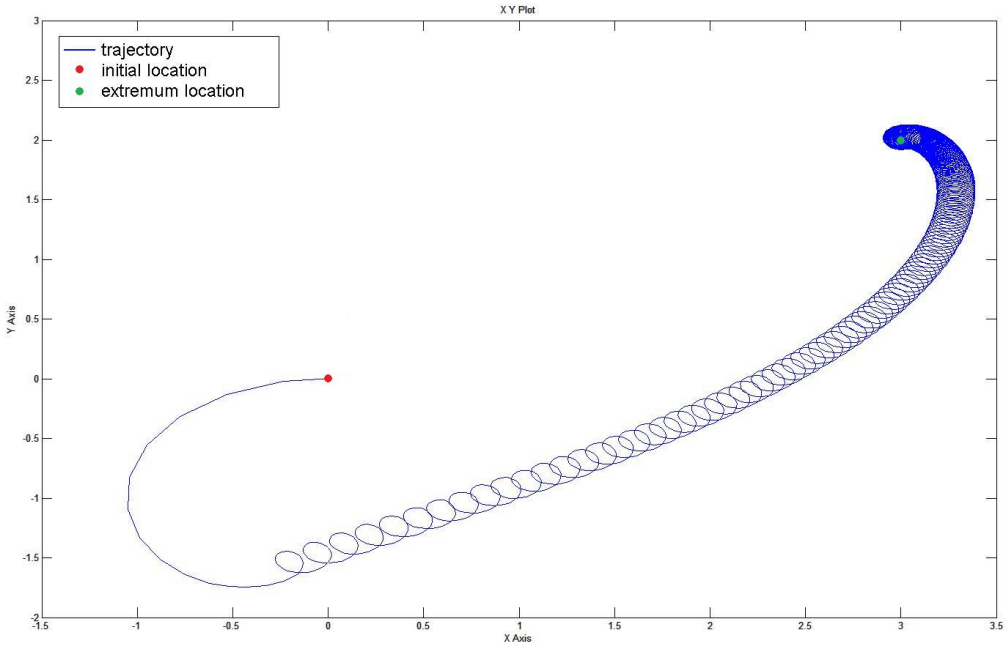

Starting with an initial state at the origin, the trajectory of the system eventually approaches the extremum location. The only irregularity is the initial transient period in which there are large fluctuations in the parameters, and the trajectory starts off in the wrong direction. The adaption gain can be decreased to minimize this transient at the expense of convergence rate. Fortunately, this initial transient is of an extremely small time scale and cannot be detected in the plots below. Graph 7.3 shows that the input parameters reach the optimal values whereas Graph 7.4 proves that convergence to the extremum of the map is obtained.

Graph 7.3: Evolution of input parameters for multiparameter extremum seeking example

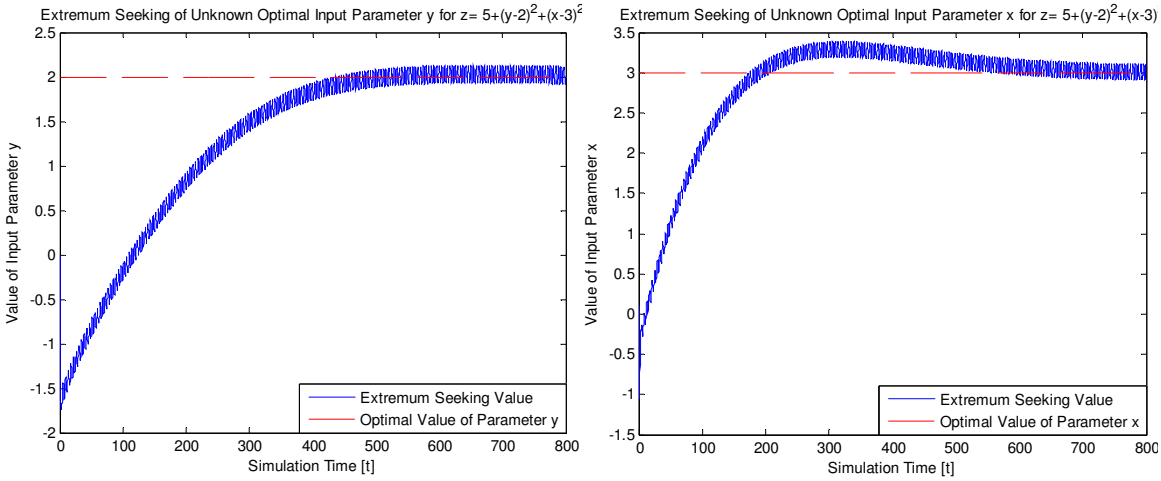

Graph 7.4: Evolution of output. Since the map is static, the large simulation times required for convergence are simply a result of using perturbations of relatively low frequencies.

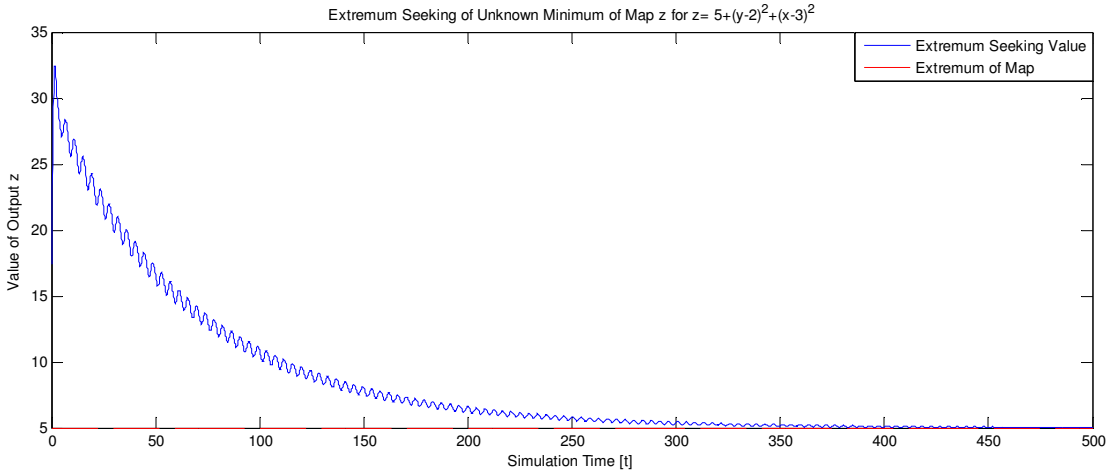

7.3 Applicability of Extremum Seeking to Ship-Ramp-Ship System

It was briefly discussed in Section 7.1 how a general multiparameter extremum seeking scheme with plant dynamics could be tailored to work for the interconnected ship-ramp-ship system at hand. Figure 7.3 contained a possible version of the algorithm for two input parameters: ship heading and ramp length, and a single output: pitch angle (can be from displacement, velocity, or acceleration measurements). The purpose of this section is to further investigate possible modifications that would be necessary in order to utilize a real-time extremum seeking loop for the system while out at sea. Due to ongoing research that is being done in this area, no results will be provided. However, a possible candidate for an extremum seeking scheme will be presented.

The optimization results of Chapter 6 relied on a penalty function which was used to create a global minimum (in the ramp length direction) for the pitch angle surface plots. This penalty was a monotonically increasing function that physically represented the probative weight and wasted effort with respect to the roll and yaw angles when using long ramps. Based on this information, the output of the extremum seeking loop should actually be the addition of the pitch angle with a user-defined penalty. Unfortunately, the resulting cost function, while fairly smooth and convex with a global minimum in the ramp length direction, is full of local minima and maxima in the wave orientation direction. The existence of a “spiky” cost function when using extremum seeking has been previously investigated by E. Schuster et al. on Beam matching adaptive control via

extremum seeking [5]. In the paper it is discussed that local minima can be dealt with by varying the amplitude of the sinusoidal excitation according to the value of the cost function. The amplitude of the probing signal would be reduced as the value of the cost function decreases, thus allowing the algorithm to continuously seek a lower value of the cost function. Future research will have to be conducted to see whether such an approach would be applicable here as well.

In order for the terms asin(ωt) and acos(ωt) to be physically implemented, it would be necessary to introduce periodic perturbations to the ramp length and ship heading. This is a task that is not well suited for the given system due to the relatively large sizes and masses of the two ships. It would entail using the more mobile of the two ships, the T-Craft, to rapidly move back and forth in both the longitudinal direction (ramp length perturbations) and transverse direction (ship heading perturbations). These are unrealistic requirements and would involve a prohibitive amount of effort. Fortunately, it is suggested here that the signals $a_p\sin(\omega_p t + \beta_p)$ are not even necessary. This is because there are perturbations due to the ocean waves that are already inherent to the system. Thus, no active actuation should be required to extract the gradient information, as the ocean waves may be sufficient (although the low wave frequency is a constraint).

The demodulation signals in the extremum seeking algorithm are also problematic in that no open-loop external sine wave signals are available. To solve this issue one could construct an actuator that outputs sine waves. However, it would be more desirable to use a signal that is readily available and internal to the system. In Chapter 2 it was discussed that ocean waves are often

composed of multiple sinusoids with a range of frequencies and one dominant frequency, ω_0. As such, ocean waves can appear to be sine waves of frequency ω_0 with additional low and high frequency components. The simulation results of Chapter 4 showed that quantities such as the pitch and roll angles and heaves of the ships also have a somewhat sinusoidal nature. More precisely, it was found that the dominant frequency of these quantities coincided with the dominant frequency of the exciting wave force. It will be up to future research efforts to determine whether a general signal that is not exactly periodic, but can be approximated as so, may be used as the demodulation signal. Little attention has been devoted to this possibility, and considerable theoretical work would have to first be developed before attempting to introduce such a signal.

Based on the previous discussion, a candidate for an extremum seeking scheme is provided in Figure 7.5. Ongoing research will ultimately determine whether or not such a loop will work, how realistic its physical application would be, and the acceptability of the resulting performance and convergence.

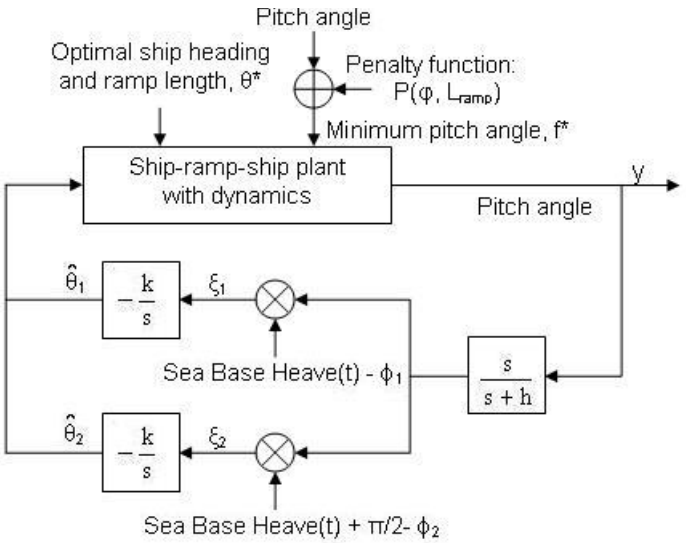

Figure 7.5: Modified extremum seeking loop for ship-ramp-ship system

CHAPTER 8: CONCLUSION

The wave-induced motion of an interconnected ship-ramp-ship system has been simulated using the computer programs of SimMechanics, Simulink, and MATLAB. Due to the overwhelming complexity of the system, it was necessary to utilize a simplified model based on a spring-mass-damper concept that approximated the forces of gravity and buoyancy. Furthermore, the ocean waves were modeled as sine waves with additive noise, and the incoming wavefront was emulated by applying phase formulas derived from simple trigonometry. Simulation results revealed that the dominant frequency of ship motions such as heave and pitch (between the ships and ramp) was equal to the exciting wave frequency. Various joints that enabled different motions between the ships and ramp were then explored, where it was realized that the reduction of such motions is important with regard to cargo transfer between the two ships. Optimization over both ramp length and ship heading showed that for greater ramp lengths and wave angles of about 62° from the ship-ramp-ship axis, the pitch angles between the ships and ramp were minimized. An increasing penalty function was then created to account for the prohibitive weight and wasted effort with respect to the roll and yaw angles when using longer ramps. The addition of such a user-defined function helps introduce a global minimum in a surface plot that is originally not globally convex. For wave angles of 62°, a ramp length of 13 meters minimized the pitch angles. Finally, the possibility of applying an

extremum seeking scheme to the system was discussed with a candidate block diagram.

This report only considered the adjustment of ramp length and ship heading as a means of reducing the ship-ramp angles. The purpose of this minimization procedure is to facilitate the transfer of cargo between the two ships in the absence of direct control over the ramp motions. It should be noted that there are also other methods that can be used to reduce the relative motions between the ships and ramp. For example, a starboard-to-port configuration offers some key advantages. A considerable amount of literature is devoted to roll stabilization for a single ship out at sea. Using fins that extend beyond the hull of the vessel are an active method of reducing the roll experienced while moving. A passive means of roll reduction is provided by anti-roll tanks which allow water to move out of sync with the roll of the ship. In the starboard-to-port configuration, roll reduction of the ships themselves using such methods will result in pitch reduction of the ramp. On the other hand, selecting the bow-to-stern configuration would entail minimizing the ship pitch motions, which is far more difficult, in order to achieve pitch reduction of the ramp. It will be up to future research to determine the feasibility of such methods and whether or not they can be combined with the optimization results and eventual extremum seeking algorithm.

APPENDIX

A.1 Complete List of Phase Formulas

The representation of an approaching wavefront is a complex matter that rests upon various phase formulas. Provided below is a collection of all the phase formulas. This collection includes wave angles of $\varphi \in \left[\frac{\pi}{2} \quad 0\right)$ which represent the waves parallel to the ships (approaching the T-Craft first) up to almost perpendicular. The perpendicular formulas can be derived from application of L'Hôptial's rule and are valid only for φ = 0. In addition, the angles of $\varphi \in \left(0 \quad -\frac{\pi}{2}\right]$ are included which represent the waves parallel to the ships (approaching the Sea Base first) up to almost perpendicular. The derivations of these formulas are not included in this report as they use the same trigonometric process outlined in Chapter 4.

$\varphi \in \left[\frac{\pi}{2} \quad 0\right)$ (Waves parallel to ship axis up to almost perpendicular)

Point 1	Phase:	$\frac{\left(\frac{w_{sb}}{2} - \frac{w_{tc}}{2}\right)\sin\left(\frac{\pi}{2} - \varphi\right)}{\lambda} 2\pi$
Point 2	Phase:	$\frac{\left(w_{tc} + \frac{w_{sb}}{2} - \frac{w_{tc}}{2}\right)\sin\left(\frac{\pi}{2} - \varphi\right)}{\lambda} 2\pi$

Point 3 Phase: $$\frac{\frac{L_{tc}}{\cos\left(\frac{\pi}{2}-\varphi\right)}-\left[L_{tc}\frac{\cos\varphi}{\sin\varphi}-\left(\frac{w_{sb}}{2}-\frac{w_{tc}}{2}\right)\right]\cos\varphi}{\lambda}2\pi$$

Point 4 Phase: $$\frac{\frac{L_{tc}}{\cos\left(\frac{\pi}{2}-\varphi\right)}-\left[L_{tc}\frac{\cos\varphi}{\sin\varphi}-\left(w_{tc}+\frac{w_{sb}}{2}-\frac{w_{tc}}{2}\right)\right]\cos\varphi}{\lambda}2\pi$$

Point 5 Phase: $$\frac{\left(L_{tc}+L_{ramp}\right)\sin\varphi}{\lambda}2\pi$$

Point 6 Phase: $$\frac{\frac{L_{tc}+L_{ramp}}{\cos\left(\frac{\pi}{2}-\varphi\right)}-\left[\left(L_{tc}+L_{ramp}\right)\frac{\cos\varphi}{\sin\varphi}-w_{sb}\right]\cos\varphi}{\lambda}2\pi$$

Point 7 Phase: $$\frac{\left(L_{tc}+L_{ramp}+L_{sb}\right)\sin\varphi}{\lambda}2\pi$$

Point 8 Phase: $$\frac{\frac{L_{tc}+L_{ramp}+L_{sb}}{\cos\left(\frac{\pi}{2}-\varphi\right)}-\left[\left(L_{tc}+L_{ramp}+L_{sb}\right)\frac{\cos\varphi}{\sin\varphi}-w_{sb}\right]\cos\varphi}{\lambda}2\pi$$

$\varphi = 0$ (Waves are perpendicular)

Points 5 and 7 Phase: 0

Points 6 and 8 Phase: $\frac{w_{sb}}{\lambda}2\pi$

Points 1 and 3 Phase: $\frac{\frac{w_{sb}}{2}-\frac{w_{tc}}{2}}{\lambda}2\pi$

Points 2 and 4 Phase: $\frac{\left(\frac{w_{sb}}{2}-\frac{w_{tc}}{2}\right)+w_{tc}}{\lambda}2\pi$

$\varphi \in \left(0 \quad -\frac{\pi}{2} \right]$ (Waves almost perpendicular to parallel from right side)

Point 1 Phase: $$\frac{\frac{L_{sb}+L_{ramp}+L_{tc}}{\cos\left(\frac{\pi}{2}-|\varphi|\right)}-\left[\left(L_{sb}+L_{ramp}+L_{tc}\right)\frac{\cos|\varphi|}{\sin|\varphi|}-\left(\frac{w_{sb}}{2}-\frac{w_{tc}}{2}\right)\right]\cos|\varphi|}{\lambda}2\pi$$

Point 2 Phase: $$\frac{\frac{L_{sb}+L_{ramp}+L_{tc}}{\cos\left(\frac{\pi}{2}-|\varphi|\right)}-\left[\left(L_{sb}+L_{ramp}+L_{tc}\right)\frac{\cos|\varphi|}{\sin|\varphi|}-\left(w_{sb}+\frac{w_{tc}}{2}-\frac{w_{sb}}{2}\right)\right]\cos|\varphi|}{\lambda}2\pi$$

Point 3 Phase: $$\frac{\frac{L_{sb}+L_{ramp}}{\cos\left(\frac{\pi}{2}-|\varphi|\right)}-\left[\left(L_{sb}+L_{ramp}\right)\frac{\cos|\varphi|}{\sin|\varphi|}-\left(\frac{w_{sb}}{2}-\frac{w_{tc}}{2}\right)\right]\cos|\varphi|}{\lambda}2\pi$$

Point 4 Phase: $$\frac{\frac{L_{sb}+L_{ramp}}{\cos\left(\frac{\pi}{2}-|\varphi|\right)}-\left[\left(L_{sb}+L_{ramp}\right)\frac{\cos|\varphi|}{\sin|\varphi|}-\left(w_{sb}+\frac{w_{tc}}{2}-\frac{w_{sb}}{2}\right)\right]\cos|\varphi|}{\lambda}2\pi$$

Point 5 Phase: $$\frac{L_{sb}\sin|\varphi|}{\lambda}2\pi$$

Point 6 Phase: $$\frac{\frac{L_{sb}}{\cos\left(\frac{\pi}{2}-|\varphi|\right)}-\left[L_{sb}\frac{\cos|\varphi|}{\sin|\varphi|}-w_{sb}\right]\cos|\varphi|}{\lambda}2\pi$$

Point 7 Phase: 0

Point 8 Phase: $$\frac{w_{sb}\sin\left(\frac{\pi}{2}-|\varphi|\right)}{\lambda}2\pi$$

Note: Taking absolute values of the angles is necessary as it prevents sign changes from placing the origin of the angles at the right side of the system (see Figure 5.3) instead of the left side.

A.2 MATLAB m-file used in Chapter 4 (Simulation Results)

```
%The following program is a general-purpose m-file to initialize
%variables in the various Simulink/SimMechanics models. User inputs
%Joint type and Case type and variables are entered into the workspace
%accordingly.

%Two-Ship Ramp Data for SimMechanics Model

%Sea Base mass + dimensions
m_sb= 45359237; %kg   50,000 tons
L_sb= 200;  %m
r_sb= 15;   %m
w_sb= 2*r_sb;

%T-craft mass + dimensions
m_tc= 2721554.22; %kg   2,000 t + 1,000 t payload   (3,360 dwt)
L_tc= 40;  %m
r_tc= 8;   %m
w_tc= 2*r_tc;

%Ramp mass + dimensions
%Assume Steel Ramp
rho_steel= 7850;  %kg/m^3 density of steel
L_ramp= 25;       %m   82.021 feet
w_ramp= 4;        %m   13.1234 feet
h_ramp= 0.0508;   %m   2 inches
V_ramp= L_ramp*w_ramp*h_ramp;
m_ramp= rho_steel*V_ramp;

%Moment of Inertia Tensor of Ship
%Assume Ship is modeled as half cylinder
% Ixx= (1/2 - 16/(9pi^2))*mr^2
% Iyy= 1/4*mr^2 + 1/2*(mL^2)
% Izz= (1/4 - 16/(9pi^2))*mr^2 + 1/12*(mL^2)

%Moment of Inertia of SeaBase through CG CS
I_sb= [(1/2- 16/(9*pi^2))*m_sb*r_sb^2 0 0; 0 (1/4)*m_sb*r_sb^2 +
(1/12)*m_sb*L_sb^2 0; ...
    0 0 (1/4-16/(9*pi^2))*m_sb*r_sb^2 + (1/12)*m_sb*L_sb^2];

%Moment of Inertia of T-craft through CG CS
I_tc= [(1/2- 16/(9*pi^2))*m_tc*r_tc^2 0 0; 0 (1/4)*m_tc*r_tc^2 +
(1/12)*m_tc*L_tc^2 0; ...
    0 0 (1/4-16/(9*pi^2))*m_tc*r_tc^2 + (1/12)*m_tc*L_tc^2];

%Moment of Inertia Tensor of Ramp
%Assume Ramp is modeled as a thin rectangular prism
%      [ 1/12mw^2  0       0  ]
%   I= [ 0  1/12m(w^2+L^2) 0  ]
%      [ 0         0 1/12mL^2 ]
```

```
%Moment of Inertia of Ramp through CG CS
I_ramp= [(1/12)*m_ramp*(w_ramp^2) 0 0; 0
(1/12)*m_ramp*((w_ramp^2)+(L_ramp^2)) 0; 0 0 (1/12)*m_ramp*(L_ramp^2)];

%Draught Information
T_tc= 1/4*r_tc;
T_sb= 1/2*r_sb;
%Waterplane Area
Aw_tc= 2*L_tc*sqrt(r_tc^2-(r_tc-T_tc)^2);
Aw_sb= 2*L_sb*sqrt(r_sb^2-(r_sb-T_sb)^2);
%Density of sea water and gravity
rho= 1025;  %kg/m^3
g= 9.81; %m/s^2

%Wave Information
%8 seconds in between waves
time= 8;           %s
f= 1/time;         %linear frequency
omega= 2*pi*f;  %angular frequency
zetaknot=1;     %wave amplitude
A_tc= rho*g*Aw_tc*zetaknot; %Wave for T-Craft
A_sb= rho*g*Aw_sb*zetaknot; %Wave for Sea Base

%Assume there is 125 ft between wave peaks
lambda= 38.1;    %125 ft

%Spring Constants to Simulate Springs in Joints
SpringRoll= 500000;
SpringRollYaw= 50000; %different only in these simulations, not for
optimization

%Metacentric Heights

%Roll Motions
GMrsb=(r_sb-(2/3*r_sb^3*((sin(acos((r_sb-
T_sb)/r_sb))^3))/(r_sb^2*acos((r_sb-T_sb)/r_sb)-(r_sb-
T_sb)*sqrt(r_sb^2-(r_sb-T_sb)^2)))+...
    (((L_sb*w_sb^3)/12)/(L_sb*(r_sb^2*acos((r_sb-T_sb)/r_sb)-(r_sb-
T_sb)*sqrt(r_sb^2-(r_sb-T_sb)^2))))-(r_sb-((4*r_sb)/(3*pi))));

GMrtc=(r_tc-(2/3*r_tc^3*((sin(acos((r_tc-
T_tc)/r_tc))^3))/(r_tc^2*acos((r_tc-T_tc)/r_tc)-(r_tc-
T_tc)*sqrt(r_tc^2-(r_tc-T_tc)^2)))+...
    (((L_tc*w_tc^3)/12)/(L_tc*(r_tc^2*acos((r_tc-T_tc)/r_tc)-(r_tc-
T_tc)*sqrt(r_tc^2-(r_tc-T_tc)^2))))-(r_tc-((4*r_tc)/(3*pi))));

%Pitch Motions
GMpsb=(0.5*T_sb+(((w_sb*L_sb^3)/12)/(L_sb*(r_sb^2*acos((r_sb-
T_sb)/r_sb)-(r_sb-T_sb)*sqrt(r_sb^2-(r_sb-T_sb)^2))))-r_sb/2);

GMptc=(0.5*T_tc+(((w_tc*L_tc^3)/12)/(L_tc*(r_tc^2*acos((r_tc-
T_tc)/r_tc)-(r_tc-T_tc)*sqrt(r_tc^2-(r_tc-T_tc)^2))))-r_tc/2);
```

```
%Account for the difference in forces
eta_rolltc= (rho*Aw_tc)/(m_tc);
eta_rollsb= (rho*Aw_sb)/(m_sb);

eta_pitchtc= (rho*Aw_tc)/(m_tc);
eta_pitchsb= (rho*Aw_sb)/(m_sb);

%Spring Contstant to Simulate Gravity and Buoyancy
P3tc= rho*g*Aw_tc;  %Heave Motions
P3sb= rho*g*Aw_sb;

R1sb= g*m_sb*GMrsb*eta_rollsb; %Roll Motions
R1tc= g*m_tc*GMrtc*eta_rolltc;

R2sb= g*m_sb*GMpsb*eta_pitchsb; %Pitch Motions
R2tc= g*m_tc*GMptc*eta_pitchtc;

%Damping Coefficients
b=0.01;
BP3tc= b;        %Heave
BP3sb= b;
BR1tc= 2*m_tc*((w_tc/(2*sqrt(3)))^2)*b;  %Roll
BR1sb= 2*m_sb*((w_sb/(2*sqrt(3)))^2)*b;
BR2tc= 2*m_tc*((L_tc/(2*sqrt(3)))^2)*b;  %Pitch
BR2sb= 2*m_sb*((L_sb/(2*sqrt(3)))^2)*b;

%JOINT CHOICE
Joint= input('Enter Joint type (1 for Pitch-Only, 2 for Pitch-Roll, 3
for Pitch-Roll-Spring, and 4 for Pitch-Roll-Yaw-Spring: ');

%WAVE ORIENTATION CHOICE
Case= input('Enter Case type (1 for phi= 90 (Case 1), 2 for phi= 45
(Case 2), 3 for phi= 0 (Case 3): ');

if (Case==1)
    %Case 1 Phase Values
    Phase1= 0;
    Phase2= 0;
    Phase3= (L_tc)*(2*pi/lambda);
    Phase4= (L_tc)*(2*pi/lambda);
    Phase5= (L_tc+L_ramp)*(2*pi/lambda);
    Phase6= (L_tc+L_ramp)*(2*pi/lambda);
    Phase7= (L_tc+L_ramp+L_sb)*(2*pi/lambda);
    Phase8= (L_tc+L_ramp+L_sb)*(2*pi/lambda);
end

if (Case==3)
    %Case 3 Phase Values
    Phase1= (w_sb/2-w_tc/2)*(2*pi/lambda);
    Phase2= (w_sb/2-w_tc/2+w_tc)*(2*pi/lambda);
    Phase3= (w_sb/2-w_tc/2)*(2*pi/lambda);
    Phase4= (w_sb/2-w_tc/2+w_tc)*(2*pi/lambda);
    Phase5= 0;
```

```
    Phase6= (w_sb)*(2*pi/lambda);
    Phase7= 0;
    Phase8= (w_sb)*(2*pi/lambda);
end

if (Case==2)
    %Case 2 Phase Values
    phi= pi/4; %45 degree angle
    Phase1= (w_sb/2-w_tc/2)*sin(pi/2-phi)*(2*pi/lambda);
    Phase2= (w_tc+w_sb/2-w_tc/2)*sin(pi/2-phi)*(2*pi/lambda);
    Phase3= ((L_tc/cos(pi/2-phi))-(L_tc*(cos(phi)/sin(phi))-(w_sb/2-
w_tc/2))*cos(phi))*(2*pi/lambda);
    Phase4= ((L_tc/cos(pi/2-phi))-(L_tc*(cos(phi)/sin(phi))-
(w_tc+w_sb/2-w_tc/2))*cos(phi))*(2*pi/lambda);
    Phase5= (L_tc+L_ramp)*sin(phi)*(2*pi/lambda);
    Phase6= (((L_tc+L_ramp)/cos(pi/2-phi))-
((L_tc+L_ramp)*(cos(phi)/sin(phi))-w_sb)*cos(phi))*(2*pi/lambda);
    Phase7= (L_tc+L_ramp+L_sb)*sin(phi)*(2*pi/lambda);
    Phase8= (((L_tc+L_ramp+L_sb)/cos(pi/2-phi))-
((L_tc+L_ramp+L_sb)*(cos(phi)/sin(phi))-w_sb)*cos(phi))*(2*pi/lambda);
end

%Input Signals
for i=1:400
    t= linspace(0,100,400); %up to simulation time
    u_sb(i)= zetaknot*sin(omega*t(i))-4*w_sb/(6*pi);
    u_ramp(i)= zetaknot*sin(omega*t(i));
    u_tc(i)= zetaknot*sin(omega*t(i))-4*w_tc/(6*pi);
end

%Joint Types
if (Joint==1)
    sim Simulation_3D_Pitch_Only
end

if (Joint==2)
    sim Simulation_3D_Pitch_Roll

    %Additional Plotting Commands
    plot(RampAngleRR(:,1),RampAngleRR(:,2))
    title('Roll Ramp Angle Between Sea Base vs. Time');
    xlabel('Simulation Time [s]');
    ylabel('Angle [deg]');
    max_angle_RR= max(abs(RampAngleRR(:,2))) %Maximum Angle
    hold on;
    plot(RampAngleRR(:,1),u_ramp,'r--')
    legend('Roll Angle','Input Signal');
    figure;
end

if (Joint==3)
    sim Simulation_3D_Pitch_Roll_Spring

    %Additional Plotting Commands
```

```
    plot(RampAngleRR(:,1),RampAngleRR(:,2))
    title('Roll Ramp Angle Between Sea Base vs. Time');
    xlabel('Simulation Time [s]');
    ylabel('Angle [deg]');
    max_angle_RR= max(abs(RampAngleRR(:,2))) %Maximum Angle
    hold on;
    plot(RampAngleRR(:,1),u_ramp,'r--')
    legend('Roll Angle','Input Signal');
    figure;
end

if (Joint==4)
    sim Simulation_3D_Pitch_Roll_Yaw_Spring

    %Additional Plotting Commands for Roll
    plot(RampAngleRR(:,1),RampAngleRR(:,2))
    title('Roll Ramp Angle Between Sea Base vs. Time');
    xlabel('Simulation Time [s]');
    ylabel('Angle [deg]');
    max_angle_RR= max(abs(RampAngleRR(:,2))) %Maximum Angle
    hold on;
    plot(RampAngleRR(:,1),u_ramp,'r--')
    legend('Roll Angle','Input Signal');
    figure;

    %Additional Plotting Commands for Yaw
    plot(RampAngleRY(:,1),RampAngleRY(:,2))
    title('Yaw Ramp Angle Between Sea Base vs. Time');
    xlabel('Simulation Time [s]');
    ylabel('Angle [deg]');
    max_angle_RY= max(abs(RampAngleRY(:,2))) %Maximum Angle
    figure;

    %Additional Plotting Commands for Yaw
    plot(RampAngleLY(:,1),RampAngleLY(:,2))
    title('Yaw Ramp Angle Between T-Craft vs. Time');
    xlabel('Simulation Time [s]');
    ylabel('Angle [deg]');
    max_angle_LY= max(abs(RampAngleLY(:,2))) %Maximum Angle
    figure;
end

%Plotting Commands
plot(SeaBaseX(:,1),SeaBaseX(:,2))
title('Sea Base Center of Gravity Surge');
xlabel('Simulation Time [s]');
ylabel('X Position [m]');
figure;

plot(SeaBaseY(:,1),SeaBaseY(:,2))
title('Sea Base Center of Gravity Sway');
xlabel('Simulation Time [s]');
ylabel('Y Position [m]');
figure;
```

```
plot(SeaBaseZ(:,1),SeaBaseZ(:,2))
title('Sea Base Center of Gravity Heave');
xlabel('Simulation Time [s]');
ylabel('Z Position [m]');
hold on;
plot(SeaBaseX(:,1),u_sb,'r--')
legend('Sea Base Heave','Input Signal');
figure;

plot(TCraftX(:,1),TCraftX(:,2))
title('T-Craft Center of Gravity Surge');
xlabel('Simulation Time [s]');
ylabel('X Position [m]');
figure;

plot(TCraftY(:,1),TCraftY(:,2))
title('T-Craft Center of Gravity Sway');
xlabel('Simulation Time [s]');
ylabel('Y Position [m]');
figure;

plot(TCraftZ(:,1),TCraftZ(:,2))
title('T-Craft Center of Gravity Heave');
xlabel('Simulation Time [s]');
ylabel('Z Position [m]');
hold on;
plot(SeaBaseX(:,1),u_tc,'r--')
legend('T-Craft Heave','Input Signal');
figure;

plot(RampAngleR(:,1),RampAngleR(:,2))
title('Pitch Ramp Angle Between Sea Base vs. Time');
xlabel('Simulation Time [s]');
ylabel('Angle [deg]');
max_angle_R= max(abs(RampAngleR(:,2))) %Maximum Angle
hold on;
plot(RampAngleR(:,1),u_ramp,'r--')
legend('Pitch Angle','Input Signal');

%plot(RampAngleL(:,1),RampAngleL(:,2))
%title('Pitch Ramp Angle Between T-Craft vs. Time');
%xlabel('Simulation Time [s]');
%ylabel('Angle [deg]');
max_angle_L= max(abs(RampAngleL(:,2))) %Maximum Angle
```

A.3 MATLAB m-file used in Chapter 5.1 (Angles vs. Ramp Length)

```
%2D Ramp Optimization: The following program explores the 3 different
%wave orientations explored in the simulations (0 deg, 45 deg, and 90
%deg) as well as the various ramp lengths. The resulting maximum
%angles: pitch, roll, and yaw are then given with respect to the ramp
%lengths. All joint types are explored at once

%Sea Base mass + dimensions
m_sb= 45359237; %kg   50,000 tons
L_sb= 200;  %m
r_sb= 15;   %m
w_sb= 2*r_sb;

%T-craft mass + dimensions
m_tc= 2721554.22; %kg   2,000 t + 1,000 t payload   (3,360 dwt)
L_tc= 40;  %m
r_tc= 8;   %m
w_tc= 2*r_tc;

%Moment of Inertia Tensor of Ship
%Assume Ship is modeled as half cylinder
% Ixx= (1/2 - 16/(9pi^2))*mr^2
% Iyy= 1/4*mr^2 + 1/2*(mL^2)
% Izz= (1/4 - 16/(9pi^2))*mr^2 + 1/12*(mL^2)

%Moment of Inertia of SeaBase through CG CS
I_sb= [(1/2- 16/(9*pi^2))*m_sb*r_sb^2 0 0; 0 (1/4)*m_sb*r_sb^2 +
(1/12)*m_sb*L_sb^2 0; ...
    0 0 (1/4-16/(9*pi^2))*m_sb*r_sb^2 + (1/12)*m_sb*L_sb^2];

%Moment of Inertia of T-craft through CG CS
I_tc= [(1/2- 16/(9*pi^2))*m_tc*r_tc^2 0 0; 0 (1/4)*m_tc*r_tc^2 +
(1/12)*m_tc*L_tc^2 0; ...
    0 0 (1/4-16/(9*pi^2))*m_tc*r_tc^2 + (1/12)*m_tc*L_tc^2];

%Draught Information
T_tc= 1/4*r_tc;
T_sb= 1/2*r_sb;
%Waterplane Area
Aw_tc= 2*L_tc*sqrt(r_tc^2-(r_tc-T_tc)^2);
Aw_sb= 2*L_sb*sqrt(r_sb^2-(r_sb-T_sb)^2);
%Density of sea water and gravity
rho= 1025;  %kg/m^3
g= 9.81; %m/s^2

%Wave Information
%8 seconds in between waves
time= 8;           %s
f= 1/time;         %linear frequency
omega= 2*pi*f;  %angular frequency
```

```
zetaknot=1;
A_tc= rho*g*Aw_tc*zetaknot; %Wave for T-Craft
A_sb= rho*g*Aw_sb*zetaknot; %Wave for Sea Base

%Assume there is 125 ft between wave peaks
lambda= 38.1;    %125 ft

%Spring Constants to Simulate Springs in Joints
SpringRoll= 500000;
SpringRollYaw= 500000;

%Metacentric Heights

%Roll Motions
GMrsb=(r_sb-(2/3*r_sb^3*((sin(acos((r_sb-
T_sb)/r_sb))^3))/(r_sb^2*acos((r_sb-T_sb)/r_sb)-(r_sb-
T_sb)*sqrt(r_sb^2-(r_sb-T_sb)^2)))+...
    (((L_sb*w_sb^3)/12)/(L_sb*(r_sb^2*acos((r_sb-T_sb)/r_sb)-(r_sb-
T_sb)*sqrt(r_sb^2-(r_sb-T_sb)^2))))-(r_sb-((4*r_sb)/(3*pi))));

GMrtc=(r_tc-(2/3*r_tc^3*((sin(acos((r_tc-
T_tc)/r_tc))^3))/(r_tc^2*acos((r_tc-T_tc)/r_tc)-(r_tc-
T_tc)*sqrt(r_tc^2-(r_tc-T_tc)^2)))+...
    (((L_tc*w_tc^3)/12)/(L_tc*(r_tc^2*acos((r_tc-T_tc)/r_tc)-(r_tc-
T_tc)*sqrt(r_tc^2-(r_tc-T_tc)^2))))-(r_tc-((4*r_tc)/(3*pi))));

%Pitch Motions
GMpsb=(0.5*T_sb+(((w_sb*L_sb^3)/12)/(L_sb*(r_sb^2*acos((r_sb-
T_sb)/r_sb)-(r_sb-T_sb)*sqrt(r_sb^2-(r_sb-T_sb)^2))))-r_sb/2);

GMptc=(0.5*T_tc+(((w_tc*L_tc^3)/12)/(L_tc*(r_tc^2*acos((r_tc-
T_tc)/r_tc)-(r_tc-T_tc)*sqrt(r_tc^2-(r_tc-T_tc)^2))))-r_tc/2);

%Account for the difference in forces
eta_rolltc= (rho*Aw_tc)/(m_tc);
eta_rollsb= (rho*Aw_sb)/(m_sb);

eta_pitchtc= (rho*Aw_tc)/(m_tc);
eta_pitchsb= (rho*Aw_sb)/(m_sb);

%Spring Contstant to SImulate Gravity and Buoyancy
P3tc= rho*g*Aw_tc;  %Heave Motions
P3sb= rho*g*Aw_sb;

R1sb= g*m_sb*GMrsb*eta_rollsb; %Roll Motions
R1tc= g*m_tc*GMrtc*eta_rolltc;

R2sb= g*m_sb*GMpsb*eta_pitchsb; %Pitch Motions
R2tc= g*m_tc*GMptc*eta_pitchtc;

%Damping Coefficients
b=0.01;
BP3tc= b;        %Heave
```

```
BP3sb= b;
BR1tc= 2*m_tc*((w_tc/(2*sqrt(3)))^2)*b;  %Roll
BR1sb= 2*m_sb*((w_sb/(2*sqrt(3)))^2)*b;
BR2tc= 2*m_tc*((L_tc/(2*sqrt(3)))^2)*b;  %Pitch
BR2sb= 2*m_sb*((L_sb/(2*sqrt(3)))^2)*b;

%Relationship Between Ramp Length and Pitch Angle for 3 Cases
for k=1:4 %JOINT LOOP

    %k=1 Simulation_3D_Pitch_Only
    %k=2 Simulation_3D_Pitch_Roll
    %k=3 Simulation_3D_Pitch_Roll_Spring
    %k=4 Simulation_3D_Pitch_Roll_Yaw_Spring

    for j=1:3  %CASE LOOP

        %j=1 Case 1
        %j=2 Case 3
        %j=3 Case 2

        for i=1:25 %RAMP LENGTH LOOP 5 m to 125 m

            %Ramp mass + dimensions
            %Assume Steel Ramp
            rho_steel= 7850;  %kg/m^3 density of steel
            L_ramp= 5*i; %This changes with the iterations
            w_ramp= 4;        %meters   13.1234 feet
            h_ramp= 0.0508;   %meters   2 inches
            V_ramp= L_ramp*w_ramp*h_ramp;
            m_ramp= rho_steel*V_ramp;

            %Moment of Inertia of Ramp through CG CS
            I_ramp= [(1/12)*m_ramp*(w_ramp^2) 0 0; 0
(1/12)*m_ramp*((w_ramp^2)+(L_ramp^2)) 0; 0 0 (1/12)*m_ramp*(L_ramp^2)];


            if (j==1)
                %Case 1 Phase Values
                Phase1= 0;
                Phase2= 0;
                Phase3= (L_tc)*(2*pi/lambda);
                Phase4= (L_tc)*(2*pi/lambda);
                Phase5= (L_tc+L_ramp)*(2*pi/lambda);
                Phase6= (L_tc+L_ramp)*(2*pi/lambda);
                Phase7= (L_tc+L_ramp+L_sb)*(2*pi/lambda);
                Phase8= (L_tc+L_ramp+L_sb)*(2*pi/lambda);
            end

            if (j==2)
                %Case 3 Phase Values
                Phase1= (w_sb/2-w_tc/2)*(2*pi/lambda);
                Phase2= (w_sb/2-w_tc/2+w_tc)*(2*pi/lambda);
                Phase3= (w_sb/2-w_tc/2)*(2*pi/lambda);
```

```
                Phase4= (w_sb/2-w_tc/2+w_tc)*(2*pi/lambda);
                Phase5= 0;
                Phase6= (w_sb)*(2*pi/lambda);
                Phase7= 0;
                Phase8= (w_sb)*(2*pi/lambda);
            end

            if (j==3)
                %Case 2 Phase Values
                phi= pi/4; %45 degree angle
                Phase1= (w_sb/2-w_tc/2)*sin(pi/2-phi)*(2*pi/lambda);
                Phase2= (w_tc+w_sb/2-w_tc/2)*sin(pi/2-
phi)*(2*pi/lambda);
                Phase3= ((L_tc/cos(pi/2-phi))-
(L_tc*(cos(phi)/sin(phi))-(w_sb/2-w_tc/2))*cos(phi))*(2*pi/lambda);
                Phase4= ((L_tc/cos(pi/2-phi))-
(L_tc*(cos(phi)/sin(phi))-(w_tc+w_sb/2-
w_tc/2))*cos(phi))*(2*pi/lambda);
                Phase5= (L_tc+L_ramp)*sin(phi)*(2*pi/lambda);
                Phase6= (((L_tc+L_ramp)/cos(pi/2-phi))-
((L_tc+L_ramp)*(cos(phi)/sin(phi))-w_sb)*cos(phi))*(2*pi/lambda);
                Phase7= (L_tc+L_ramp+L_sb)*sin(phi)*(2*pi/lambda);
                Phase8= (((L_tc+L_ramp+L_sb)/cos(pi/2-phi))-
((L_tc+L_ramp+L_sb)*(cos(phi)/sin(phi))-w_sb)*cos(phi))*(2*pi/lambda);
            end

            %Spring Constants to Simulate Gravity and Buoyancy
            if (k==1)
                sim('Simulation_3D_Pitch_Only');
            end

            if (k==2)
                sim('Simulation_3D_Pitch_Roll');
            end

            if (k==3)
                sim('Simulation_3D_Pitch_Roll_Spring');
            end

            if (k==4)
                sim('Simulation_3D_Pitch_Roll_Yaw_Spring');
            end

            %Extract data for the various ramp angles
            %Pitch Only Joint
            if (k==1) && (j==1) %Case 1
                pitchJ1C1(i)= max(abs(RampAngleR(:,2))); %Maximum Pitch
            end

            if (k==1) && (j==2) %Case 3
                pitchJ1C3(i)= max(abs(RampAngleR(:,2))); %Maximum Pitch
            end

            if (k==1) && (j==3) %Case 2
```

```
    pitchJ1C2(i)= max(abs(RampAngleR(:,2))); %Maximum Pitch
end

%Pitch Roll Joint
if (k==2) && (j==1) %Case 1
    pitchJ2C1(i)= max(abs(RampAngleR(:,2))); %Maximum Pitch
    rollJ2C1(i)= max(abs(RampAngleRR(:,2))); %Maximum Roll
end

if (k==2) && (j==2) %Case 3
    pitchJ2C3(i)= max(abs(RampAngleR(:,2))); %Maximum Pitch
    rollJ2C3(i)= max(abs(RampAngleRR(:,2))); %Maximum Roll
end

if (k==2) && (j==3) %Case 2
    pitchJ2C2(i)= max(abs(RampAngleR(:,2))); %Maximum Pitch
    rollJ2C2(i)= max(abs(RampAngleRR(:,2))); %Maximum Roll
end

%Pitch Roll Joint w/ Spring On Roll
if (k==3) && (j==1) %Case 1
    pitchJ3C1(i)= max(abs(RampAngleR(:,2))); %Maximum Pitch
    rollJ3C1(i)= max(abs(RampAngleRR(:,2))); %Maximum Roll
end

if (k==3) && (j==2) %Case 3
    pitchJ3C3(i)= max(abs(RampAngleR(:,2))); %Maximum Pitch
    rollJ3C3(i)= max(abs(RampAngleRR(:,2))); %Maximum Roll
end

if (k==3) && (j==3) %Case 2
    pitchJ3C2(i)= max(abs(RampAngleR(:,2))); %Maximum Pitch
    rollJ3C2(i)= max(abs(RampAngleRR(:,2))); %Maximum Roll
end

%Pitch Roll Yaw Joint w/ Springs on Roll and Yaw
if (k==4) && (j==1) %Case 1
    pitchJ4C1(i)= max(abs(RampAngleR(:,2))); %Maximum Pitch
    rollJ4C1(i)= max(abs(RampAngleRR(:,2))); %Maximum Roll
    yawJ4C1(i)= max(abs(RampAngleRY(:,2)));  %Maximum Yaw
end

if (k==4) && (j==2) %Case 3
    pitchJ4C3(i)= max(abs(RampAngleR(:,2))); %Maximum Pitch
    rollJ4C3(i)= max(abs(RampAngleRR(:,2))); %Maximum Roll
    yawJ4C3(i)= max(abs(RampAngleRY(:,2)));  %Maximum Yaw
end

if (k==4) && (j==3) %Case 2
    pitchJ4C2(i)= max(abs(RampAngleR(:,2))); %Maximum Pitch
    rollJ4C2(i)= max(abs(RampAngleRR(:,2))); %Maximum Roll
    yawJ4C2(i)= max(abs(RampAngleRY(:,2)));  %Maximum Yaw
end
```

```
            xaxis(i)= 5*i;

        end
    end

    if (k==1) %Simulation_3D_Pitch_Only
        figure;
        plot(xaxis,pitchJ1C1);
        hold on;
        grid on;
        plot(xaxis,pitchJ1C3, 'r');
        plot(xaxis,pitchJ1C2, 'g');
        xlabel('Ramp Length [m]');
        ylabel('Ramp Angle w/ Sea Base [deg]');
        title('Ramp Angle vs Ramp Length (Wavelength= 38.1 m) using
Pitch-Only Joint');
        legend('Pitch Angles for Case 1','Pitch Angles for Case
3','Pitch Angles for Case 2');
    end

    if (k==2) %k=2 Simulation_3D_Pitch_Roll
        figure;
        plot(xaxis,pitchJ2C1);
        hold on;
        grid on;
        plot(xaxis,pitchJ2C3, 'r');
        plot(xaxis,pitchJ2C2, 'g');
        plot(xaxis,rollJ2C1, 'y')
        plot(xaxis,rollJ2C3, 'c');
        plot(xaxis,rollJ2C2, 'm');
        xlabel('Ramp Length [m]');
        ylabel('Ramp Angle w/ Sea Base [deg]');
        title('Ramp Angle vs Ramp Length (Wavelength= 38.1 m) using
Pitch and Roll Joint');
        legend('Pitch Angles for Case 1','Pitch Angles for Case
3','Pitch Angles for Case 2','Roll Angles for Case 1','Roll Angles for
Case 3','Roll Angles for Case 2');
    end

    if (k==3) %k=3 Simulation_3D_Pitch_Roll_Spring
        figure;
        plot(xaxis,pitchJ3C1);
        hold on;
        grid on;
        plot(xaxis,pitchJ3C3, 'r');
        plot(xaxis,pitchJ3C2, 'g');
        plot(xaxis,rollJ3C1, 'y')
        plot(xaxis,rollJ3C3, 'c');
        plot(xaxis,rollJ3C2, 'm');
        xlabel('Ramp Length [m]');
        ylabel('Ramp Angle w/ Sea Base [deg]');
        title('Ramp Angle vs Ramp Length (Wavelength= 38.1 m) using
Pitch and Roll Joint w/ Spring on Roll');
```

```
        legend('Pitch Angles for Case 1','Pitch Angles for Case
3','Pitch Angles for Case 2','Roll Angles for Case 1','Roll Angles for
Case 3','Roll Angles for Case 2');
    end

    if (k==4) %k=4 Simulation_3D_Pitch_Roll_Yaw_Spring
        figure;
        plot(xaxis,pitchJ4C1);
        hold on;
        grid on;
        plot(xaxis,pitchJ4C3, 'r');
        plot(xaxis,pitchJ4C2, 'g');
        plot(xaxis,rollJ4C1, 'y')
        plot(xaxis,rollJ4C3, 'c');
        plot(xaxis,rollJ4C2, 'm');
        plot(xaxis,yawJ4C1, 'k')
        plot(xaxis,yawJ4C3, 'k:');
        plot(xaxis,yawJ4C2, 'k-.');
        xlabel('Ramp Length [m]');
        ylabel('Ramp Angle w/ Sea Base [deg]');
        title('Ramp Angle vs Ramp Length using Pitch, Roll, and Yaw
Joint w/ Springs on Roll and Yaw');
        legend('Pitch Angles for Case 1','Pitch Angles for Case
3','Pitch Angles for Case 2','Roll Angles for Case 1','Roll Angles for
Case 3','Roll Angles for Case 2','Yaw Angles for Case 1','Yaw Angles
for Case 3', 'Yaw Angles for Case 2');
    end
end
```

A.4 MATLAB m-file used in Chapter 5.1 (Time Dependent Angles)

```
%The following m-file describes the evolution of the ramp-ship
%pitch angle for various ramp lengths given phi=90 (theta=0)
%meaning the parallel orientation, Case 1 with the waves
%approaching the T-Craft first. Also examined is when phi=-90
%which means the same case but when waves approach the Sea Base
%first. The pitch-only joint is used in this m-file

%Sea Base mass + dimensions
m_sb= 45359237; %kg   50,000 tons
L_sb= 200;  %m
r_sb= 15;   %m
w_sb= 2*r_sb;

%T-craft mass + dimensions
m_tc= 2721554.22; %kg   2,000 t + 1,000 t payload   (3,360 dwt)
L_tc= 40;  %m
r_tc= 8;   %m
w_tc= 2*r_tc;

%Moment of Inertia Tensor of Ship
%Assume Ship is modeled as half cylinder
% Ixx= (1/2 - 16/(9pi^2))*mr^2
% Iyy= 1/4*mr^2 + 1/2*(mL^2)
% Izz= (1/4 - 16/(9pi^2))*mr^2 + 1/12*(mL^2)

%Moment of Inertia of SeaBase through CG CS
I_sb= [(1/2- 16/(9*pi^2))*m_sb*r_sb^2 0 0; 0 (1/4)*m_sb*r_sb^2 +
(1/12)*m_sb*L_sb^2 0; ...
    0 0 (1/4-16/(9*pi^2))*m_sb*r_sb^2 + (1/12)*m_sb*L_sb^2];

%Moment of Inertia of T-craft through CG CS
I_tc= [(1/2- 16/(9*pi^2))*m_tc*r_tc^2 0 0; 0 (1/4)*m_tc*r_tc^2 +
(1/12)*m_tc*L_tc^2 0; ...
    0 0 (1/4-16/(9*pi^2))*m_tc*r_tc^2 + (1/12)*m_tc*L_tc^2];

%Draught Information
T_tc= 1/4*r_tc;
T_sb= 1/2*r_sb;
%Waterplane Area
Aw_tc= 2*L_tc*sqrt(r_tc^2-(r_tc-T_tc)^2);
Aw_sb= 2*L_sb*sqrt(r_sb^2-(r_sb-T_sb)^2);
%Density of sea water and gravity
rho= 1025;  %kg/m^3
g= 9.81; %m/s^2

%Wave Information
%8 seconds in between waves
time= 8;           %s
f= 1/time;         %linear frequency
```

```
omega= 2*pi*f;  %angular frequency
zetaknot=1;
A_tc= rho*g*Aw_tc*zetaknot; %Wave for T-Craft
A_sb= rho*g*Aw_sb*zetaknot; %Wave for Sea Base

%Assume there is 125 ft between wave peaks
lambda= 38.1;    %125 ft

%Spring Constants to Simulate Springs in Joints
SpringRoll= 500000;

%Metacentric Heights

%Roll Motions
GMrsb=(r_sb-(2/3*r_sb^3*((sin(acos((r_sb-
T_sb)/r_sb))^3))/(r_sb^2*acos((r_sb-T_sb)/r_sb)-(r_sb-
T_sb)*sqrt(r_sb^2-(r_sb-T_sb)^2)))+...
    (((L_sb*w_sb^3)/12)/(L_sb*(r_sb^2*acos((r_sb-T_sb)/r_sb)-(r_sb-
T_sb)*sqrt(r_sb^2-(r_sb-T_sb)^2))))-(r_sb-((4*r_sb)/(3*pi))));

GMrtc=(r_tc-(2/3*r_tc^3*((sin(acos((r_tc-
T_tc)/r_tc))^3))/(r_tc^2*acos((r_tc-T_tc)/r_tc)-(r_tc-
T_tc)*sqrt(r_tc^2-(r_tc-T_tc)^2)))+...
    (((L_tc*w_tc^3)/12)/(L_tc*(r_tc^2*acos((r_tc-T_tc)/r_tc)-(r_tc-
T_tc)*sqrt(r_tc^2-(r_tc-T_tc)^2))))-(r_tc-((4*r_tc)/(3*pi))));

%Pitch Motions
GMpsb=(0.5*T_sb+(((w_sb*L_sb^3)/12)/(L_sb*(r_sb^2*acos((r_sb-
T_sb)/r_sb)-(r_sb-T_sb)*sqrt(r_sb^2-(r_sb-T_sb)^2))))-r_sb/2);

GMptc=(0.5*T_tc+(((w_tc*L_tc^3)/12)/(L_tc*(r_tc^2*acos((r_tc-
T_tc)/r_tc)-(r_tc-T_tc)*sqrt(r_tc^2-(r_tc-T_tc)^2))))-r_tc/2);

%Account for the difference in forces
eta_rolltc= (rho*Aw_tc)/(m_tc);
eta_rollsb= (rho*Aw_sb)/(m_sb);

eta_pitchtc= (rho*Aw_tc)/(m_tc);
eta_pitchsb= (rho*Aw_sb)/(m_sb);

%Spring Contstant to Simulate Gravity and Buoyancy
P3tc= rho*g*Aw_tc;  %Heave Motions
P3sb= rho*g*Aw_sb;

R1sb= g*m_sb*GMrsb*eta_rollsb; %Roll Motions
R1tc= g*m_tc*GMrtc*eta_rolltc;

R2sb= g*m_sb*GMpsb*eta_pitchsb; %Pitch Motions
R2tc= g*m_tc*GMptc*eta_pitchtc;

%Damping Coefficients
b=0.01;
BP3tc= b;        %Heave
```

```
BP3sb= b;
BR1tc= 2*m_tc*((w_tc/(2*sqrt(3)))^2)*b;  %Roll
BR1sb= 2*m_sb*((w_sb/(2*sqrt(3)))^2)*b;
BR2tc= 2*m_tc*((L_tc/(2*sqrt(3)))^2)*b;  %Pitch
BR2sb= 2*m_sb*((L_sb/(2*sqrt(3)))^2)*b;


a1=1;  %Penalty on Pitch
a2=1;  %Penalty on Roll
n=30;  %Number of data points

phi_range = linspace(-pi/2,pi/2,n);
L_ramp_range = linspace(5,40,n);


phi=pi/2;   %approach T-Craft first
%RAMP LENGTH CHANGES
for j=1:n         %VARY RAMP LENGTH

    L_ramp = L_ramp_range(j); %This changes with the iterations

        %Ramp mass + dimensions
        %Assume Steel Ramp
        rho_steel= 7850;  %kg/m^3 density of steel
        w_ramp= 4;        %meters   13.1234 feet
        h_ramp= 0.0508;   %meters   2 inches
        V_ramp= L_ramp*w_ramp*h_ramp;
        m_ramp= rho_steel*V_ramp;

        %Moment of Inertia of Ramp through CG CS
        I_ramp= [(1/12)*m_ramp*(w_ramp^2) 0 0; 0
(1/12)*m_ramp*((w_ramp^2)+(L_ramp^2)) 0; 0 0 (1/12)*m_ramp*(L_ramp^2)];

        %Cases 1 and 2: Aligned with axis (Case 1) , Angled
Wavefront(Case 2)
        if (phi>0 && phi<=pi/2)

            Phase1= (w_sb/2-w_tc/2)*sin(pi/2-phi)*(2*pi/lambda);
            Phase2= (w_tc+w_sb/2-w_tc/2)*sin(pi/2-phi)*(2*pi/lambda);
            Phase3= ((L_tc/cos(pi/2-phi))-(L_tc*(cos(phi)/sin(phi))-
(w_sb/2-w_tc/2))*cos(phi))*(2*pi/lambda);
            Phase4= ((L_tc/cos(pi/2-phi))-(L_tc*(cos(phi)/sin(phi))-
(w_tc+w_sb/2-w_tc/2))*cos(phi))*(2*pi/lambda);
            Phase5= (L_tc+L_ramp)*sin(phi)*(2*pi/lambda);
            Phase6= (((L_tc+L_ramp)/cos(pi/2-phi))-
((L_tc+L_ramp)*(cos(phi)/sin(phi))-w_sb)*cos(phi))*(2*pi/lambda);
            Phase7= (L_tc+L_ramp+L_sb)*sin(phi)*(2*pi/lambda);
            Phase8= (((L_tc+L_ramp+L_sb)/cos(pi/2-phi))-
((L_tc+L_ramp+L_sb)*(cos(phi)/sin(phi))-w_sb)*cos(phi))*(2*pi/lambda);
        end

        %Run Program
        sim Simulation_3D_Pitch_Only;
```

```
        R_Pitch_time(:,j)=RampAngleR(:,2);
        L_Pitch_time(:,j)=RampAngleL(:,2);

end

phi=-pi/2;   %approach Sea Base first
for j=1:n         %VARY RAMP LENGTH

    L_ramp = L_ramp_range(j); %This changes with the iterations

        %Ramp mass + dimensions
        %Assume Steel Ramp
        rho_steel= 7850;  %kg/m^3 density of steel
        w_ramp= 4;        %meters   13.1234 feet
        h_ramp= 0.0508;   %meters   2 inches
        V_ramp= L_ramp*w_ramp*h_ramp;
        m_ramp= rho_steel*V_ramp;

        %Moment of Inertia of Ramp through CG CS
        I_ramp= [(1/12)*m_ramp*(w_ramp^2) 0 0; 0
(1/12)*m_ramp*((w_ramp^2)+(L_ramp^2)) 0; 0 0 (1/12)*m_ramp*(L_ramp^2)];

        %Cases 1 and 2 but coming from the Sea Base side
        if (phi<0 && phi>=-pi/2)

            phia= abs(phi); %To prevent -1's from appearing
            Phase1= (((L_sb+L_ramp+L_tc)/cos(pi/2-phia))-
((L_sb+L_ramp+L_tc)*(cos(phia)/sin(phia))-(w_sb/2-
w_tc/2))*cos(phia))*(2*pi/lambda);
            Phase2= (((L_sb+L_ramp+L_tc)/cos(pi/2-phia))-
((L_sb+L_ramp+L_tc)*(cos(phia)/sin(phia))-(w_sb+w_tc/2-
w_sb/2))*cos(phia))*(2*pi/lambda);
            Phase3= (((L_sb+L_ramp)/cos(pi/2-phia))-
((L_sb+L_ramp)*(cos(phia)/sin(phia))-(w_sb/2-
w_tc/2))*cos(phia))*(2*pi/lambda);
            Phase4= (((L_sb+L_ramp)/cos(pi/2-phia))-
((L_sb+L_ramp)*(cos(phia)/sin(phia))-(w_sb+w_tc/2-
w_sb/2))*cos(phia))*(2*pi/lambda);
            Phase5= L_sb*sin(phia)*(2*pi/lambda);
            Phase6= ((L_sb/cos(pi/2-phia))-(L_sb*(cos(phia)/sin(phia))-
w_sb)*cos(phia))*(2*pi/lambda);
            Phase7= 0;
            Phase8= w_sb*sin(pi/2-phia)*(2*pi/lambda);
        end

        %Run Program
        sim Simulation_3D_Pitch_Only;

        R_Pitch_time_negpi2(:,j)=RampAngleR(:,2);
        L_Pitch_time_negpi2(:,j)=RampAngleL(:,2);

end
```

```
t=linspace(0,100,400); %for meshgrid
L=linspace(0,30,400);

%T-Craft Pitch Angle for phi= pi/2
[L,to]=meshgrid(L_ramp_range,t);
subplot(2,1,1); plot3(to,L,L_Pitch_time.^2)
xlabel('time [sec]');
ylabel('Ramp Length [m]');
zlabel('(Pitch Angle)^2 [deg]');
title('T-Craft-Ramp Pitch Angle for \phi = \pi/2');

%Sea Base Pitch Angle for phi= pi/2
[L,to]=meshgrid(L_ramp_range,t);
subplot(2,1,2); plot3(to,L,R_Pitch_time.^2)
xlabel('time [sec]');
ylabel('Ramp Length [m]');
zlabel('(Pitch Angle)^2 [deg]');
title('Sea Base-Ramp Pitch Angle for \phi = \pi/2');

figure;

%T-Craft Pitch Angle for phi= -pi/2
[L,to]=meshgrid(L_ramp_range,t);
subplot(2,1,1); plot3(to,L,L_Pitch_time_negpi2.^2)
xlabel('time [sec]');
ylabel('Ramp Length [m]');
zlabel('(Pitch Angle)^2 [deg]');
title('T-Craft-Ramp Pitch Angle for \phi = -\pi/2');

%Sea Base Pitch Angle for phi= -pi/2
[L,to]=meshgrid(L_ramp_range,t);
subplot(2,1,2); plot3(to,L,R_Pitch_time_negpi2.^2)
xlabel('time [sec]');
ylabel('Ramp Length [m]');
zlabel('(Pitch Angle)^2 [deg]');
title('Sea Base-Ramp Pitch Angle for \phi = -\pi/2');
```

A.5 MATLAB m-file used in Chapters 5.2 and 6.1 (3-D Surface Plots)

```
%The following program explores the dependence of the roll and pitch
%angles between the ships and the ramp on the wave orientation and ramp
%length. For wave orientations varying from phi = [-pi/2,pi/2] and ramp
%lengths varying from [5 40] surface plots are generated in which the z
%axis indicates the ramp angle (individual or a composite function)

%Sea Base mass + dimensions
m_sb= 45359237; %kg   50,000 tons
L_sb= 200;  %m
r_sb= 15;   %m
w_sb= 2*r_sb;

%T-craft mass + dimensions
m_tc= 2721554.22; %kg   2,000 t + 1,000 t payload   (3,360 dwt)
L_tc= 40;  %m
r_tc= 8;   %m
w_tc= 2*r_tc;

%Moment of Inertia Tensor of Ship
%Assume Ship is modeled as half cylinder
% Ixx= (1/2 - 16/(9pi^2))*mr^2
% Iyy= 1/4*mr^2 + 1/2*(mL^2)
% Izz= (1/4 - 16/(9pi^2))*mr^2 + 1/12*(mL^2)

%Moment of Inertia of SeaBase through CG CS
I_sb= [(1/2- 16/(9*pi^2))*m_sb*r_sb^2 0 0; 0 (1/4)*m_sb*r_sb^2 +
(1/12)*m_sb*L_sb^2 0; ...
    0 0 (1/4-16/(9*pi^2))*m_sb*r_sb^2 + (1/12)*m_sb*L_sb^2];

%Moment of Inertia of T-craft through CG CS
I_tc= [(1/2- 16/(9*pi^2))*m_tc*r_tc^2 0 0; 0 (1/4)*m_tc*r_tc^2 +
(1/12)*m_tc*L_tc^2 0; ...
    0 0 (1/4-16/(9*pi^2))*m_tc*r_tc^2 + (1/12)*m_tc*L_tc^2];

%Draught Information
T_tc= 1/4*r_tc;
T_sb= 1/2*r_sb;
%Waterplane Area
Aw_tc= 2*L_tc*sqrt(r_tc^2-(r_tc-T_tc)^2);
Aw_sb= 2*L_sb*sqrt(r_sb^2-(r_sb-T_sb)^2);
%Density of sea water and gravity
rho= 1025;  %kg/m^3
g= 9.81; %m/s^2

%Wave Information
%8 seconds in between waves
time= 8;           %s
f= 1/time;         %linear frequency
omega= 2*pi*f;  %angular frequency
```

```
zetaknot=0.95;
%zetaknot=1;
A_tc= rho*g*Aw_tc*zetaknot; %Wave for T-Craft
A_sb= rho*g*Aw_sb*zetaknot; %Wave for Sea Base

%Assume there is 125 ft between wave peaks
lambda= 38.1;    %125 ft

%Spring Constants to Simulate Springs in Joints
SpringRoll= 500000;
SpringRollYaw= 500000;

%Metacentric Heights

%Roll Motions
GMrsb=(r_sb-(2/3*r_sb^3*((sin(acos((r_sb-
T_sb)/r_sb))^3))/(r_sb^2*acos((r_sb-T_sb)/r_sb)-(r_sb-
T_sb)*sqrt(r_sb^2-(r_sb-T_sb)^2)))+...
    (((L_sb*w_sb^3)/12)/(L_sb*(r_sb^2*acos((r_sb-T_sb)/r_sb)-(r_sb-
T_sb)*sqrt(r_sb^2-(r_sb-T_sb)^2))))-(r_sb-((4*r_sb)/(3*pi))));

GMrtc=(r_tc-(2/3*r_tc^3*((sin(acos((r_tc-
T_tc)/r_tc))^3))/(r_tc^2*acos((r_tc-T_tc)/r_tc)-(r_tc-
T_tc)*sqrt(r_tc^2-(r_tc-T_tc)^2)))+...
    (((L_tc*w_tc^3)/12)/(L_tc*(r_tc^2*acos((r_tc-T_tc)/r_tc)-(r_tc-
T_tc)*sqrt(r_tc^2-(r_tc-T_tc)^2))))-(r_tc-((4*r_tc)/(3*pi))));

%Pitch Motions
GMpsb=(0.5*T_sb+(((w_sb*L_sb^3)/12)/(L_sb*(r_sb^2*acos((r_sb-
T_sb)/r_sb)-(r_sb-T_sb)*sqrt(r_sb^2-(r_sb-T_sb)^2))))-r_sb/2);

GMptc=(0.5*T_tc+(((w_tc*L_tc^3)/12)/(L_tc*(r_tc^2*acos((r_tc-
T_tc)/r_tc)-(r_tc-T_tc)*sqrt(r_tc^2-(r_tc-T_tc)^2))))-r_tc/2);

%Account for the difference in forces
eta_rolltc= (rho*Aw_tc)/(m_tc);
eta_rollsb= (rho*Aw_sb)/(m_sb);

eta_pitchtc= (rho*Aw_tc)/(m_tc);
eta_pitchsb= (rho*Aw_sb)/(m_sb);

%Spring Contstant to SImulate Gravity and Buoyancy
P3tc= rho*g*Aw_tc;  %Heave Motions
P3sb= rho*g*Aw_sb;

R1sb= g*m_sb*GMrsb*eta_rollsb; %Roll Motions
R1tc= g*m_tc*GMrtc*eta_rolltc;

R2sb= g*m_sb*GMpsb*eta_pitchsb; %Pitch Motions
R2tc= g*m_tc*GMptc*eta_pitchtc;

%Damping Coefficients
b=0.01;
```

```
BP3tc= b;        %Heave
BP3sb= b;
BR1tc= 2*m_tc*((w_tc/(2*sqrt(3)))^2)*b;  %Roll
BR1sb= 2*m_sb*((w_sb/(2*sqrt(3)))^2)*b;
BR2tc= 2*m_tc*((L_tc/(2*sqrt(3)))^2)*b;  %Pitch
BR2sb= 2*m_sb*((L_sb/(2*sqrt(3)))^2)*b;


a1=1;  %Penalty on Pitch
a2=1;  %Penalty on Roll
n=30;  %Number of data points

%Range for ramp length and wave orientations
phi_range = linspace(-pi/2,pi/2,n);
L_ramp_range = linspace(5,40,n);

%Initialize Cost Function
for j=1:n
    for i=1:n
        J_L(i,j)=0;
    end
end

%JOINT CHOICE
Joint= input('Enter Joint type (1 for Pitch-Only, 2 for Pitch-Roll, 3
for Pitch-Roll-Spring, and 4 for Pitch-Roll-Yaw-Spring: ');

%RAMP LENGTH OPTIMIZATION
for j=1:n         %VARY RAMP LENGTH

    L_ramp = L_ramp_range(j); %This changes with the iterations

    for i=1:n     %VARY PHI

        phi = phi_range(i); %This changes with the iterations

        %Ramp mass + dimensions
        %Assume Steel Ramp
        rho_steel= 7850;  %kg/m^3 density of steel
        w_ramp= 4;        %meters   13.1234 feet
        h_ramp= 0.0508;   %meters   2 inches
        V_ramp= L_ramp*w_ramp*h_ramp;
        m_ramp= rho_steel*V_ramp;

        %Moment of Inertia of Ramp through CG CS
        I_ramp= [(1/12)*m_ramp*(w_ramp^2) 0 0; 0
(1/12)*m_ramp*((w_ramp^2)+(L_ramp^2)) 0; 0 0 (1/12)*m_ramp*(L_ramp^2)];

        %Cases 1 and 2: Aligned with axis (Case 1) , Angled
Wavefront(Case 2)
        if (phi>0 && phi<=pi/2)

            Phase1= (w_sb/2-w_tc/2)*sin(pi/2-phi)*(2*pi/lambda);
```

```
            Phase2= (w_tc+w_sb/2-w_tc/2)*sin(pi/2-phi)*(2*pi/lambda);
            Phase3= ((L_tc/cos(pi/2-phi))-(L_tc*(cos(phi)/sin(phi))-
(w_sb/2-w_tc/2))*cos(phi))*(2*pi/lambda);
            Phase4= ((L_tc/cos(pi/2-phi))-(L_tc*(cos(phi)/sin(phi))-
(w_tc+w_sb/2-w_tc/2))*cos(phi))*(2*pi/lambda);
            Phase5= (L_tc+L_ramp)*sin(phi)*(2*pi/lambda);
            Phase6= (((L_tc+L_ramp)/cos(pi/2-phi))-
((L_tc+L_ramp)*(cos(phi)/sin(phi))-w_sb)*cos(phi))*(2*pi/lambda);
            Phase7= (L_tc+L_ramp+L_sb)*sin(phi)*(2*pi/lambda);
            Phase8= (((L_tc+L_ramp+L_sb)/cos(pi/2-phi))-
((L_tc+L_ramp+L_sb)*(cos(phi)/sin(phi))-w_sb)*cos(phi))*(2*pi/lambda);
        end

        %Case 3: perpendicular wavefront (phi = 0)
        if (phi==0)

            Phase1= (w_sb/2-w_tc/2)*(2*pi/lambda);
            Phase2= (w_sb/2-w_tc/2+w_tc)*(2*pi/lambda);
            Phase3= (w_sb/2-w_tc/2)*(2*pi/lambda);
            Phase4= (w_sb/2-w_tc/2+w_tc)*(2*pi/lambda);
            Phase5= 0;
            Phase6= (w_sb)*(2*pi/lambda);
            Phase7= 0;
            Phase8= (w_sb)*(2*pi/lambda);
        end

        %Cases 1 and 2 but coming from the Sea Base side
        if (phi<0 && phi>=-pi/2)

            phia= abs(phi); %To prevent -1's from appearing
            Phase1= (((L_sb+L_ramp+L_tc)/cos(pi/2-phia))-
((L_sb+L_ramp+L_tc)*(cos(phia)/sin(phia))-(w_sb/2-
w_tc/2))*cos(phia))*(2*pi/lambda);
            Phase2= (((L_sb+L_ramp+L_tc)/cos(pi/2-phia))-
((L_sb+L_ramp+L_tc)*(cos(phia)/sin(phia))-(w_sb+w_tc/2-
w_sb/2))*cos(phia))*(2*pi/lambda);
            Phase3= (((L_sb+L_ramp)/cos(pi/2-phia))-
((L_sb+L_ramp)*(cos(phia)/sin(phia))-(w_sb/2-
w_tc/2))*cos(phia))*(2*pi/lambda);
            Phase4= (((L_sb+L_ramp)/cos(pi/2-phia))-
((L_sb+L_ramp)*(cos(phia)/sin(phia))-(w_sb+w_tc/2-
w_sb/2))*cos(phia))*(2*pi/lambda);
            Phase5= L_sb*sin(phia)*(2*pi/lambda);
            Phase6= ((L_sb/cos(pi/2-phia))-(L_sb*(cos(phia)/sin(phia))-
w_sb)*cos(phia))*(2*pi/lambda);
            Phase7= 0;
            Phase8= w_sb*sin(pi/2-phia)*(2*pi/lambda);
        end

        %Case Scenarios
        if (Joint==1)
            sim('Simulation_3D_Pitch_Only');
            MaxPitch_R(j,i)= max(abs(RampAngleR(:,2)));  %Maximum Pitch
Angle w/ Sea Base
```

```
            MaxPitch_L(j,i)= max(abs(RampAngleL(:,2)));  %Maximum Pitch
Angle w/ T-Craft
            J_L(j,i)= a1*MaxPitch_R(j,i); %Cost Function
            RampAngleR=0; %Set back to zero for next simulation
            RampAngleL=0;
        end

        if (Joint==2)
            sim('Simulation_3D_Pitch_Roll');
            MaxPitch_R(j,i)= max(abs(RampAngleR(:,2)));  %Maximum Pitch
Angle w/ Sea Base
            MaxRoll_R(j,i)= max(abs(RampAngleRR(:,2))); %Maximum Roll
Angle w/ Sea Base
            MaxPitch_L(j,i)= max(abs(RampAngleL(:,2)));  %Maximum Pitch
Angle w/ T-Craft
            MaxRoll_L(j,i)= max(abs(RampAngleLR(:,2))); %Maximum Roll
Angle w/ T-Craft
            J_L(j,i)= a1*MaxPitch_R(j,i) + a2*MaxRoll_R(j,i); %Add
together the two angles
            RampAngleR=0; %Set back to zero for next simulation
            RampAngleRR=0;
            RampAngleL=0;
            RampAngleLR=0;
        end

        if (Joint==3)
            sim('Simulation_3D_Pitch_Roll_Spring');
            MaxPitch_R(j,i)= max(abs(RampAngleR(:,2)));  %Maximum Pitch
Angle w/ Sea Base
            MaxRoll_R(j,i)= max(abs(RampAngleRR(:,2))); %Maximum Roll
Angle w/ Sea Base
            MaxPitch_L(j,i)= max(abs(RampAngleL(:,2)));  %Maximum Pitch
Angle w/ T-Craft
            MaxRoll_L(j,i)= max(abs(RampAngleLR(:,2))); %Maximum Roll
Angle w/ T-Craft
            J_L(j,i)= a1*MaxPitch_R(j,i) + a2*MaxRoll_R(j,i); %Add
together the two angles
            RampAngleR=0; %Set back to zero for next simulation
            RampAngleRR=0;
            RampAngleL=0;
            RampAngleLR=0;
        end

        if (Joint==4)
            sim('Simulation_3D_Pitch_Roll_Yaw_Spring');
            MaxPitch_R(j,i)= max(abs(RampAngleR(:,2)));  %Maximum Pitch
Angle w/ Sea Base
            MaxRoll_R(j,i)= max(abs(RampAngleRR(:,2))); %Maximum Roll
Angle w/ Sea Base
            MaxPitch_L(j,i)= max(abs(RampAngleL(:,2)));  %Maximum Pitch
Angle w/ T-Craft
            MaxRoll_L(j,i)= max(abs(RampAngleLR(:,2))); %Maximum Roll
Angle w/ T-Craft
            J_L(j,i)= a1*MaxPitch_R(j,i) + a2*MaxRoll_R(j,i); %Add
together the two angles
```

```
            RampAngleR=0; %Set back to zero for next simulation
            RampAngleRR=0;
            RampAngleL=0;
            RampAngleLR=0;
        end
    end
end

%PENALTY
for j=1:n          %VARY RAMP LENGTH

    L_ramp = L_ramp_range(j); %This changes with the iterations

    for i=1:n      %VARY PHI

        phi = phi_range(i); %This changes with the iterations

        P(j,i)=0.004*L_ramp^2; %Quadratic Penalty

    end
end

%PLOT DATA AND INCLUDE PENALTIES FOR OPTIMIZATION

if (Joint==1)

    %----------------Pitch Only Joint-------------------
    %Maxmum Pitch Angle Curve
    phi_range_deg= phi_range*(180/pi); %Convert to deg
    surf(phi_range_deg,L_ramp_range,J_L);
    title('Cost Function J(phi,Lramp) for Joint with Pitch Only');
    xlabel('Phi [deg]')
    ylabel('Length of Ramp [m]');
    zlabel('Maximum Pitch Angle [deg]');
    figure;
    %-------------Pitch Only Joint with Penalty-----------------
    phi_range_deg= phi_range*(180/pi); %Convert to deg
    surf(phi_range_deg,L_ramp_range,J_L);
    shading flat
    hold on;
    mesh(phi_range_deg,L_ramp_range,P);
    hold on;
    surf(phi_range_deg,L_ramp_range,P+J_L);
    title('Cost Function J(phi,Lramp) for Joint with Pitch and
Additional Penalty');
    xlabel('Phi [deg]')
    ylabel('Length of Ramp [m]');
    zlabel('Maxmimum Pitch Angle');
    legend('Cost Function J(phi,Lramp)','Penalty on Ramp
Length','J(phi,Lramp)+Penalty for Optimal Length');
    figure;
end
```

```
if (Joint==2)

    %----------------Pitch and Roll----------------------
    %Maxmum Pitch Angle Curve
    phi_range_deg= phi_range*(180/pi); %Convert to deg
    surf(phi_range_deg,L_ramp_range,MaxPitch_R);
    title('Cost Function J(phi,Lramp) for Joint with Pitch and Roll');
    xlabel('Phi [deg]')
    ylabel('Length of Ramp [m]');
    zlabel('Maximum Pitch Angle [deg]');
    figure;
    %Maximum Roll Angle Curve
    phi_range_deg= phi_range*(180/pi); %Convert to deg
    surf(phi_range_deg,L_ramp_range,MaxRoll_R);
    title('Cost Function J(phi,Lramp) for Joint with Pitch and Roll');
    xlabel('Phi [deg]')
    ylabel('Length of Ramp [m]');
    zlabel('Maximum Roll Angle [deg]');
    figure;
%     %Curve without odd peak at phi= -77 and Lramp=5
%     %Maxmum Roll Angle Curve
%     L_ramp_range_mod= linspace(10,40,n-5);
%     for i=1:25
%         for j=1:30
%             MaxRoll_R_new(i,j)= MaxRoll_R(i+5,j);
%         end
%     end
%     surf(phi_range_deg,L_ramp_range_mod,MaxRoll_R_new);
%     title('Cost Function J(phi,Lramp) for Joint with Pitch and
Roll');
%     xlabel('Phi [deg]')
%     ylabel('Length of Ramp [m]');
%     zlabel('Maximum Roll Angle [deg]');
%     figure;
    %Composite Curve
    phi_range_deg= phi_range*(180/pi); %Convert to deg
    surf(phi_range_deg,L_ramp_range,J_L);
    title('Cost Function J(phi,Lramp) for Joint with Pitch and Roll');
    xlabel('Phi [deg]')
    ylabel('Length of Ramp [m]');
    zlabel('Linear Combination of Pitch and Roll Angles [deg]');
    figure;
end

if (Joint==3)

    %-------------Pitch and Roll w/Spring-----------------
    %Maxmum Pitch Angle Curve
    phi_range_deg= phi_range*(180/pi); %Convert to deg
    surf(phi_range_deg,L_ramp_range,MaxPitch_R);
    title('Cost Function J(phi,Lramp) for Joint with Pitch and Roll w/
Spring on Roll');
    xlabel('Phi [deg]')
    ylabel('Length of Ramp [m]');
    zlabel('Maximum Pitch Angle [deg]');
```

```
    figure;
    %Maxmum Roll Angle Curve
    phi_range_deg= phi_range*(180/pi); %Convert to deg
    surf(phi_range_deg,L_ramp_range,MaxRoll_R);
    title('Cost Function J(phi,Lramp) for Joint with Pitch and Roll w/
Spring on Roll');
    xlabel('Phi [deg]')
    ylabel('Length of Ramp [m]');
    zlabel('Maximum Roll Angle [deg]');
    figure;
    %Composite Curve
    phi_range_deg= phi_range*(180/pi); %Convert to deg
    surf(phi_range_deg,L_ramp_range,J_L);
    title('Cost Function J(phi,Lramp) for Joint with Pitch and Roll w/
Spring on Roll');
    xlabel('Phi [deg]')
    ylabel('Length of Ramp [m]');
    zlabel('Linear Combination of Pitch and Roll Angles [deg]');
    figure;
end

if (Joint==4)

    %----------------Pitch, Roll, and Yaw-----------------
    %Maxmum Pitch Angle Curve
    phi_range_deg= phi_range*(180/pi); %Convert to de
    surf(phi_range_deg,L_ramp_range,MaxPitch_R);
    title('Cost Function J(phi,Lramp) for Joint with Pitch, Roll, and
Yaw  w/ Spring on Roll and Yaw');
    xlabel('Phi [deg]')
    ylabel('Length of Ramp [m]');
    zlabel('Maximum Pitch Angle [deg]');
    figure;
    %Maxmum Roll Angle Curve
    phi_range_deg= phi_range*(180/pi); %Convert to deg
    surf(phi_range_deg,L_ramp_range,MaxRoll_R);
    title('Cost Function J(phi,Lramp) for Joint with Pitch, Roll, and
Yaw  w/ Spring on Roll and Yaw');
    xlabel('Phi [deg]')
    ylabel('Length of Ramp [m]');
    zlabel('Maximum Roll Angle [deg]');
    figure;
    %Composite Curve
    phi_range_deg= phi_range*(180/pi); %Convert to deg
    surf(phi_range_deg,L_ramp_range,J_L);
    title('Cost Function J(phi,Lramp) for Joint with Pitch, Roll, and
Yaw  w/ Spring on Roll and Yaw');
    xlabel('Phi [deg]')
    ylabel('Length of Ramp [m]');
    zlabel('Linear Combination of Pitch and Roll Angles [deg]');
    figure;
end
```

A.6 MATLAB m-file used in Chapter 7 (Multiparameter Extremum Seeking)

```
%-------------Multi-Parameter Extremum Seeking------------------
%The following program finds the extremum value of the following
%map z= 5+(y-2)^2+(x-3)^2 which has a minimum value of z=5 for
%parameter values of x=3 and y=2
x=linspace(0,5,100);   y=linspace(0,5,100);
[X,Y]=meshgrid(x,y);
Z=5+(Y-2).^2+(X-3).^2;
surf(X,Y,Z)
shading interp
xlabel('x');
ylabel('y');
zlabel('z');
title('Map of z(x,y)= 5+(y-2)^2+(x-3)^2')
sim MultiParameter_Extremum_Seeking;
figure;
plot(ExtremumInput_y(:,1),ExtremumInput_y(:,2));
hold on;
for i=1:length(tout)
    thetay(i)=2;
end
plot(tout,thetay,'r--');
xlabel('Simulation Time [t]');
ylabel('Value of Input Parameter y');
title('Extremum Seeking of Unknown Optimal Input Parameter y for z=
5+(y-2)^2+(x-3)^2');
legend('Extremum Seeking Value','Optimal Value of Parameter y');
figure;
plot(ExtremumInput_x(:,1),ExtremumInput_x(:,2));
hold on;
for i=1:length(tout)
    thetax(i)=3;
end
plot(tout,thetax,'r--');
xlabel('Simulation Time [t]');
ylabel('Value of Input Parameter x');
title('Extremum Seeking of Unknown Optimal Input Parameter x for z=
5+(y-2)^2+(x-3)^2');
legend('Extremum Seeking Value','Optimal Value of Parameter x');
figure;
plot(ExtremumOutput_z(:,1),ExtremumOutput_z(:,2));
hold on;
for i=1:length(tout)
    extremum(i)=5;
end
plot(tout,extremum,'r--');
xlabel('Simulation Time [t]');
ylabel('Value of Output z');
title('Extremum Seeking of Unknown Minimum of Map z for z= 5+(y-
2)^2+(x-3)^2');
legend('Extremum Seeking Value','Extremum of Map');
```

A.7 SimMechanics Block Diagram (Pitch-Roll-Yaw Joint)

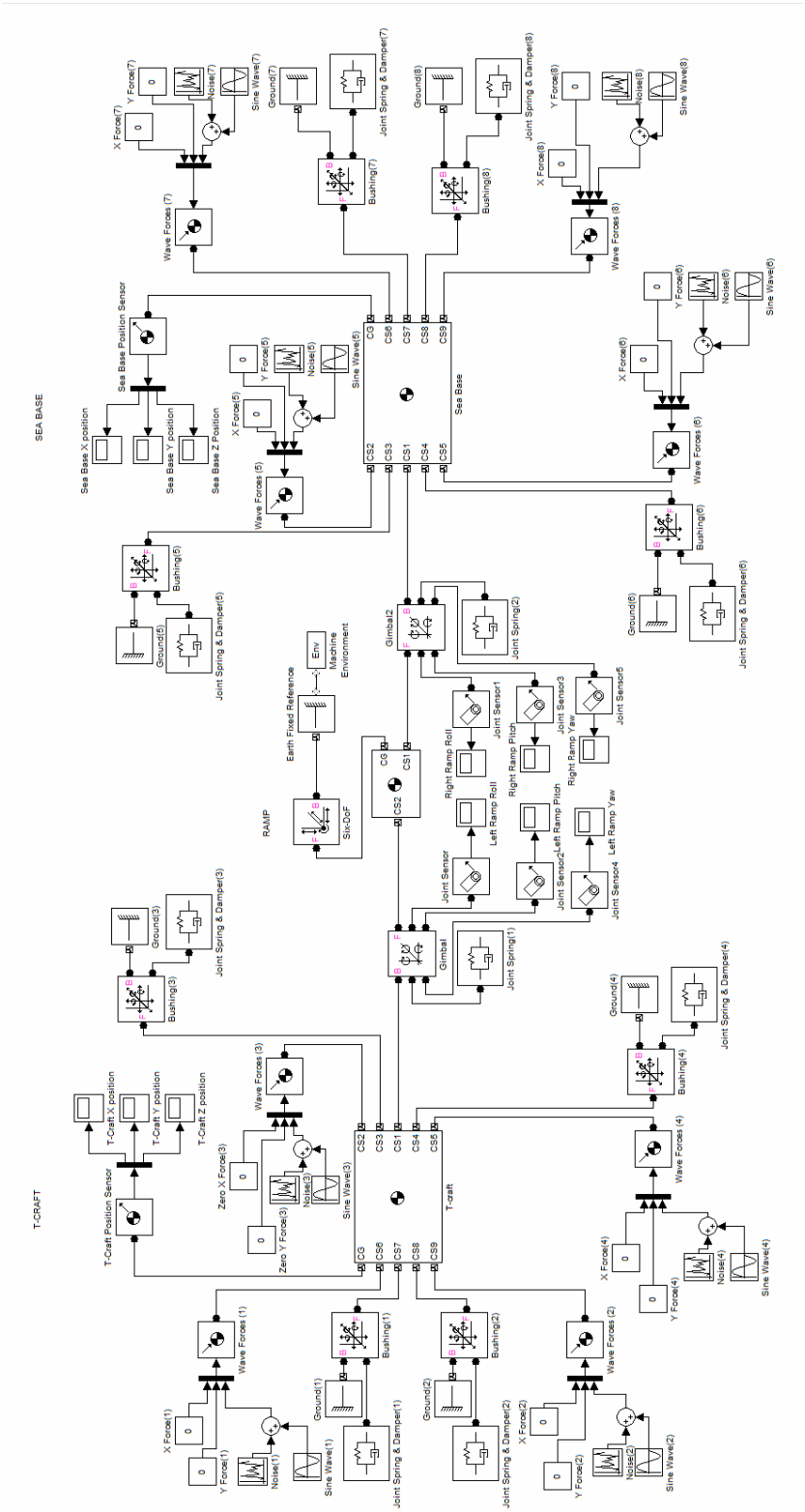

BIBLIOGRAPHY

[1] K. B. Ariyur, M Krstic. *Real-Time Optimization by Extremum-Seeking Control*. John Wiley & Sons, New York, 2003

[2] A. Biran. *Ship Hydrostatics and Stability*. Oxford: Butterworth-Heinemann, MA, 2003

[3] T. I. Fossen. *Guidance and Control of Ocean Vehicles*. John Wiley & Sons, New York, 1994

[4] L. Ljung. *System Identification: Theory for the User*. PTR Prentice Hall, New Jersey, second edition, 1999

[5] E. Schuster, C. Xu, N. Torres, E. Morinaga, C. Allen, M. Krstic. “Beam matching adaptive control via extremum seeking”. Nuclear Instruments and Methods in Physics Research Section A: Accelerators, Spectrometers, Detectors and Associated Equipment, vol. 581, no. 3, pp. 799–815, 2007

[6] J. Stewart. *Calculus: Early Transcendentals*. Brooks/Cole – Thomsan Learning, CA, fifth edition, 2003